AN ABSTRACT OF THE DISSERTATION OF

Maoya Bassiouni for the degree of Doctor of Philosophy in Water Resources Engineering presented on October 25, 2019.

Title: Soil Moisture Encodes Plant Water Use Strategies

Abstract approved

Chad W. Higgins Stephen P. Good

Resilient water, food, and energy management strategies for an ever-growing population and changing environment depends on our understanding of water and carbon cycles from local to global scales. Fluxes of water and carbon are coupled by photosynthesis and plant transpiration cycles the largest fraction of terrestrial water from the land back to the atmosphere. Our limited ability to characterize interactions between hydrology and climate, regulated by plants' response to stress, contributes to the greatest source of uncertainty in climate and carbon projections. Parameterized models need to represent the complexity and diversity of plant water use strategies, but hydrologically relevant model inputs are difficult to measure at ecosystem scales. Soil moisture integrates landscape fluxes and the spatial and temporal variability in soil moisture reflects dynamics of dominant land-surface processes. Diagnosing variability in soil moisture observations from point to landscape scales can thus quantify characteristics which are not measured directly. The central hypothesis of this dissertation is: soil moisture observations encode valuable ecohydrological information, and this information can be extracted to quantify plant water use strategies. This dissertation develops: (1) an inverse modeling framework to estimate scale-specific ecohydrological thresholds from probability distributions of soil moisture observations; (2) a global dataset of thresholds of soil water uptake, which are consistent with satellite soil moisture; and (3) relations between evapotranspiration and soil moisture at a range of biomes, based on the energy spectrum and probability distribution of soil moisture and information theory metrics. This work provides data driven methods that leverage new global observations and quantify ecohydrological relations which are critical to a variety of open climate, water, and ecosystem research questions and modeling endeavors.

Soil Moisture Encodes Plant Water Use Strategies

by
Maoya Bassiouni

A DISSERTATION

submitted to

Oregon State University

in partial fulfillment of
the requirements for the
degree of

Doctor of Philosophy

Presented October 25, 2019
Commencement June 2020

Doctor of Philosophy dissertation of Maoya Bassiouni presented on October 25, 2019

APPROVED:

Co-major Professor, representing Water Resources Engineering

Co-major Professor, representing Water Resources Engineering

Director of the Water Resources Graduate Program

Dean of the Graduate School

I understand that my dissertation will become part of the permanent collection of Oregon State University libraries. My signature below authorizes release of my dissertation to any reader upon request.

Maoya Bassiouni, Author

ACKNOWLEDGEMENTS

The author expresses sincere appreciation toward Major Professors Chad Higgins and Stephen Good; committee members Christopher Still and Dominique Bachelet; graduate council representative John Sessions; and Water Resources Graduate Program Director, Mary Santelmann. The author acknowledges financial support from the Ron Minor Bioengineering Scholarship and the National Science Foundation Graduate Research Fellowship Program. The author is grateful for everyone's inspiration, it has made this journey a pleasure.

TABLE OF CONTENTS

TABLE OF CONTENTS (Continued)

TABLE OF CONTENTS (Continued)

LIST OF FIGURES

LIST OF TABLES

DEDICATION

May all beings everywhere be happy, free from suffering, and at peace, and may my thoughts, words, and actions contribute to that happiness, freedom and peace for all.

1 General Introduction

Resilient water, food, and energy management strategies for an ever-growing population and changing environment depends on our understanding of water and carbon cycles from local to global scales. Fluxes of water and carbon are coupled by photosynthesis and plant transpiration cycles the largest fraction of terrestrial water from the land back to the atmosphere (Good et al., 2015).Vegetation regulates the terrestrial water cycle as it adapts to water availability and climatic conditions. A plant's resilience and response to environmental stress is governed by a set of complex and diverse traits, which vary along a continuum from drought avoidant to drought tolerant and determine vegetation strategies when faced with the tradeoff between carbon assimilation and water conservations (Anderegg et al., 2016; Fu & Meinzer, 2019; Skelton et al., 2015). Our limited ability to characterize interactions between hydrology and climate, regulated by plants' response to stress (Xu et al., 2013), contributes to one of the greatest source of uncertainty in climate and carbon projections (Friedlingstein et al., 2014; Trugman et al., 2018). Parameterized models need to represent the complexity and diversity of plant water use strategies, but hydrologically relevant model inputs are difficult to measure at ecosystem scales.

Soil moisture integrates landscape fluxes and the spatial and temporal variability in soil moisture reflects dynamics of dominant land-surface processes (Rodríguez-Iturbe & Porporato, 2007). Diagnosing variability in soil moisture from point to landscape scales can thus quantify characteristics which are not measured directly. The central hypothesis of this dissertation is: soil moisture observations encode valuable ecohydrological information, and this information can be extracted to quantify plant water use strategies. Soil moisture observations from point- to landscape-scales are available through sensor networks (Baldocchi et al., 2001) and satellite missions (Entekhabi et al., 2010; Wagner et al., 2012) and offer new opportunities to diagnose ecohydrological processes globally. Detecting significant relations about processes which are spatially and temporally heterogeneous, driven by correlated variables, and inherently noisy is a major challenge, especially when using satellite data. Novel statistical methods, based on simple physical principles, are needed to relate the variability in soil moisture observations to plant water use strategies and derive metrics that improve hydrologic flux estimates.

This dissertation develops: (1) an inverse modeling framework to estimate scale-specific ecohydrological thresholds from probability distribution functions of soil moisture observations; (2) a global dataset of thresholds of soil water uptake, which are consistent with satellite soil moisture estimates; and (3) relations between evapotranspiration and soil moisture at a range of biomes, based on the energy spectrum and probability distribution of soil moisture and information theory metrics. This work provides data driven methods that leverage new global observations and quantify ecohydrological relations which are critical to a variety of open climate, water, and ecosystem research questions and modeling endeavors.

2 Probabilistic Inference of Ecohydrological Parameters Using Observations from Point to Satellite Scales

Maoya Bassiouni[1], Chad W Higgins[1], Christopher J Still[2], and Stephen P Good[1]

[1]Department of Biological and Ecological Engineering, Oregon State University, Corvallis, OR 97333, USA. [2]Department of Forest Ecosystems & Society, Oregon State University, Corvallis, OR 97333, USA

Hydrology and Earth System Science
Volume 23, issue 6, pages 3807–3821, 2019

2.1 Abstract

Vegetation controls on soil moisture dynamics are challenging to measure and translate into scale and site-specific ecohydrological parameters for simple soil water balance models. We hypothesize that empirical probability density functions (pdfs) of relative soil moisture or soil saturation encodes sufficient information to determine these ecohydrological parameters. Further, these parameters can be estimated through inverse modelling of the analytical equation for soil saturation pdfs, derived from the commonly used stochastic soil water balance framework. We developed a generalizable Bayesian inference framework to estimate ecohydrological parameters consistent with empirical soil saturation pdfs derived from observations at point, footprint, and satellite scales. We applied the inference method to four sites with different land cover and climate assuming i) an annual rainfall pattern and ii) a wet season rainfall pattern with a dry season of negligible rainfall. The Nash-Sutcliffe efficiencies of the analytical model's fit to soil observations ranged from 0.89 to 0.99. The coefficient of variation of posterior parameter distributions ranged from <1 to 15 %. The parameter identifiability was not significantly improved in the more complex seasonal model; however, small differences in parameter values indicate that the annual model may have absorbed dry season dynamics. Parameter estimates were most constrained for scales and locations at which soil water dynamics are more sensitive to the fitted ecohydrological parameters of interest. In these cases, model inversion converged more slowly but ultimately provided better goodness of fit and lower uncertainty. Results were robust using as little few as 100 daily observations randomly sampled from the full records, demonstrating the advantage of analyzing soil saturation pdfs instead of time series to estimate ecohydrological parameters from sparse records. Our work combines modelling and empirical approaches in ecohydrology and provides a simple framework to obtain scale- and site-specific analytical descriptions of soil moisture dynamics consistent with soil moisture observations.

2.2 Introduction

The movement of water from soils, through plants, and back to the atmosphere via transpiration is a critical component of local and global hydrologic cycles and is the largest surface-to-atmosphere water pathway (Good et al., 2015). A realistic analytical description of soil moisture dynamics is key to understanding ecohydrological processes that regulate the productivity of natural and managed ecosystems. (Rodriguez-Iturbe et al., 1999) introduced a simple framework using a bucket model of soil-column hydrology forced with stochastic precipitation inputs where soil water losses are only a function of relative soil moisture or soil saturation. Given this ecohydrological framework, the analytical equation for the probability density function (pdf) of soil saturation depends on simple abiotic characteristics such as average climate and soil texture, and biotic characteristics including soil saturation thresholds at which vegetation can influence soil water losses. However, the shapes of analytical soil saturation pdfs are generally not consistent with observations when literature values for model parameters are used (Miller et al., 2007). Some parameters such as field capacity and wilting point do not correspond to conventional definitions, because of simplifications made to describe soil water loss processes in the model, and need to be calibrated (Dralle & Thompson, 2016). To our knowledge, parameters of the analytical soil saturation pdfs have not been directly calibrated to empirical pdfs derived from measurements beyond the point scale. Observation networks provide freely available point scale, spatially integrated soil moisture observations, while remotely sensed soil moisture observations are available through satellite products. These data sources create an opportunity to: i) evaluate whether analytical soil saturation pdfs are consistent with observations across a range of scales, and ii) determine average ecohydrological parameters relevant to each scale.

Estimates of ecohydrological parameters are used in a large range of applications for which the stochastic soil water balance framework has been used and adapted, including: the effects of climate, soil and vegetation on soil moisture dynamics (Laio et al., 2001a; Porporato et al., 2004; Rodriguez-Iturbe et al., 2001); ecohydrological factors driving spatial and structural characteristics of vegetation (Caylor et al., 2006; Manfreda et al., 2017); soil salinization dynamics (Suweis et al., 2010); biological soil crusts (Whitney et al., 2017); vegetation stress; optimum plant water use strategies and plant hydraulic failure (Laio, et al., 2001b; Manzoni et al., 2014; Feng et al., 2017); vertical root distributions (Laio et al., 2006); plant pathogen risk (Thompson et al., 2013); streamflow persistence in seasonally dry landscapes (Dralle et al., 2016); and soil water balance partitioning (Good et al., 2014, 2017). A survey of nearly 400 ecohydrology publications revealed that 40% of studies relied heavily on simulation, rarely integrated empirical measurements, and were almost never coupled with experimental studies, suggesting a critical need to combine modelling and empirical approaches in ecohydrology (King & Caylor, 2011). Only a few studies have directly confronted the governing equations of the stochastic soil water balance model with observed soil moisture data, and even fewer studies have attempted to optimize model parameters

to best fit soil moisture observations. Miller et al. (2007) calibrated soil saturation pdfs to project vegetation stress in a changing climate. Dralle & Thompson (2016) developed an analytical expression for annually integrated soil saturation pdfs under seasonal climates and then calibrated soil saturation thresholds between which evapotranspiration is maximum and zero to compare the model to soil moisture observations at a savanna site. Chen et al. (2008) related evapotranspiration observations at the stand scale to soil moisture values using a Bayesian inversion approach, and Volo et al. (2014) calibrated the soil moisture loss curve to investigate effects of irrigation scheduling and precipitation on soil moisture dynamics and plant stress. The functional form of the soil moisture losses was approximated using conditionally averaged precipitation (Saleem & Salvucci, 2002; Salvucci, 2001) and remotely sensed data (Tuttle & Salvucci, 2014). The time scale of soil moisture dry-downs, derived from the soil moisture loss equations, were parameterized using evapotranspiration measured at micro-meteorological stations (Teuling et al., 2006) and space-borne near-surface soil moisture observations (McColl et al., 2017). These studies indicate that the ecohydrological soil water balance framework is consistent with ground and larger scale remotely sensed measurements.

Parameters representative of larger scale observations are necessary to characterize ecohydrological processes at ecosystem scales and are more relevant to ecohydrological modelling. These larger scale parameters integrate a range of ecohydrological interactions that are poorly understood and difficult to measure. Abiotic controlling factors of soil water balance including rainfall and soil texture can generally be assessed from readily available data, including site measurements, regionalized maps, and satellite observations, but vegetation controls on soil water dynamics are largely unknown and difficult to measure at hydrologically meaningful scales (Li et al., 2017). Vegetation water-use traits are generally observed at the species level and are not easily translated to the simple parameters necessary in soil-water balance models. The rate of soil water losses from the near-surface soil layer, where soil moisture measurements are generally made, do not precisely correspond to evapotranspiration observed or calculated from meteorological stations. We thus focused on estimating parameters that are not directly observable, particularly the soil saturation thresholds at which vegetation controls soil water losses and the maximum rate of evapotranspiration from a near-surface soil layer. We use an inverse modelling approach and data that are commonly collected at environmental monitoring sites or measured from satellites. We present an inference framework that provides a means to quantify and compare the sensitivity of soil moisture dynamics at varying scales through estimates of simple ecohydrological parameters.

A number of studies have combined inverse modelling approaches with ground and remotely sensed soil moisture data to extract meaningful hydrologic information(Xu et al., 2006; Miller et al., 2007; Chen et al., 2008; Volo et al., 2014; Wang et al., 2016; Baldwin et al., 2017). Bayesian inference methods are effective in relating prior pdfs of observations to posterior estimates of model parameters (Baldwin et al., 2017; Chen et al., 2008; Xu et al., 2006). The soil water balance model provides a direct analytical

equation for soil saturation pdfs that is convenient to use with the Bayesian paradigm because it is a low parameter model with few data inputs. We selected a Bayesian inversion approach instead of a least-squares or maximum likelihood approach because it quantifies the inference uncertainty and improves upon the work of Miller et al. (2007), which used a least-squares approach to calibrate soil saturation pdfs. Measures of inference uncertainty and parameter convergence diagnostics provided by the Bayesian approach can be used to evaluate the validity of model inversion and develop criteria to generalize the presented framework.

We assume that if a sufficient range of soil moisture values are observed at a site, the shape of the empirical soil saturation pdf is constrained by the ecohydrological factors driving soil moisture dynamics. We hypothesize that key information required to determine these ecohydrological factors is encoded in empirical soil saturation pdfs and that this information can be extracted by calculating the inverse of the commonly used stochastic soil water balance. The analysis of soil saturation pdfs is a more robust and integrated approach to investigate ecohydrological factors of soil water dynamics than is time series analysis. Soil saturation pdfs are less sensitive to the many sources of uncertainty, sensor noise, and common gaps in soil moisture observations and do not require high-quality, co-located and concurrent hydrologic measurements that are often lacking. We tested three key assumptions embedded in the proposed method. (i) The analytical soil saturation pdfs properly describe empirical soil saturation pdfs observed in annual data. Annual soil moisture records can be affected by transitional dynamics between wet and dry seasons, and the appropriate level of model complexity must be used. We compare parameter identifiability using an annual and a seasonal formulation of the analytical soil saturation pdfs. (ii) Parameter estimates and their uncertainty at point-, footprint-, and satellite- scales are different and reflect variability in soil water dynamics. We determine whether the inference approach can be applied at point-, footprint-, and satellite-scales to provide appropriate scale-specific parameters for ecohydrological modelling. (iii) The range of realizable soil moistures values is captured by the selected time series and the soil saturation pdf determined from these observations is not truncated. We determine whether the inference method based on soil saturation pdfs is robust against reduced data availability by repeating the model inversions on subsets of the soil moisture time series and show that the method can be applied to sparse datasets.

Our goal was to match empirical soil saturation pdfs derived from point-, footprint-, and satellite-scale observations to a commonly used analytical model. We demonstrate the use of a Bayesian inversion framework to calibrate the ecohydrological parameters of a simple stochastic soil water balance model that best fit empirical soil saturation pdfs. We first present data sources, define the analytical model for soil saturation pdfs including parameter assumptions, and detail the algorithm used in the Bayesian inversion. Then, we present a summary of the goodness of fit of optimal analytical soil saturation pdfs and estimated parameter uncertainty. We evaluated results to test key method assumptions including model complexity and data availability. Finally, we discuss the potential of the approach to provide a

simple means to investigate variability in ecohydrological controlling factors at varying spatial scales. Our work combines modelling and empirical approaches in ecohydrology to provide more realistic analytical descriptions of soil moisture dynamics. Estimates of ecohydrological parameters consistent with observed soil saturation pdfs, from point- to ecosystem-scales, are needed to better characterize site-specific ecohydrological processes.

2.3 Data and methods

2.3.1 Data

We used daily soil moisture observations from three data products at three spatial scales. We used point-scale soil moisture data at a depth of 10 cm from the FLUXNET2015 data product (http://fluxnet.fluxdata.org/data/fluxnet2015-dataset/). We used footprint-scale soil moisture data from the Cosmic-ray Soil Moisture Observing System (COSMOS) (http://cosmos.hwr.arizona.edu/Probes/probelist.html). The COSMOS soil moisture footprint measures soil moisture at an average depth of 20 cm with a radius ranging from 130 to 240 m, depending on site characteristics (Köhli et al., 2015). Near-surface soil moisture observations at a spatial resolution of 0.25˚ were taken from the European Space Agency's (ESA) Climate change Initiative (CCI) project. We used the combined soil moisture product (ECV-SM, version 0.2.2) that merges soil moisture retrievals from four passive (SMMR, SMM/I, TMI, and ASMR-E) and two active (AMI and ASCAT) coarse resolution microwave sensors (Liu et al., 2011, 2012; Wagner et al., 2012). Although the ECV-SM sensing depth is <5 centimetres, it has been shown to have a close relation to ground-based observations of soil moisture in the upper 10 centimetres (Dorigo et al., 2015). We compiled daily rainfall time series from the FLUXNET2015 dataset for the point- and footprint-scale analysis, and National Aeronautics and Space Administration's (NASA) Tropical Rainfall Measuring Mission (TRMM) dataset (Huffman et al., 2007) for the satellite-scale analysis.

We selected 4 sites with soil moisture and rainfall data available for the 2012 calendar year (Figure 2.1, Table 2.1). Selected sites spanned a range of land cover types including crop and grasslands, oak savanna, deciduous forest and pine forest. We determined dominant soil texture of the upper soil layer from the Harmonized World Soil Database (HWSD) (version 1.2) (FAO/IIASA/ISRIC/ISS-CAS/JRC, 2012) for each site. We used soil porosity values, derived from the HWSD available as ancillary data through the ESA-CCI data product, for the satellite-scale analysis. We used the maximum soil moisture observation during the year 2012 as a site-specific soil porosity estimate for point- and footprint-scale data products. We used soil porosity for each site to calculate soil saturation s ($0 \leq s \leq 1$) from each observed soil moisture value. We do not expect the differences in data quality between data sources and sites to significantly affect empirical soil saturation pdfs and resulting parameter estimates. All sites had

full records of daily point- and footprint-scale observations except for US-Me2, which had 55 missing footprint-scale observations during winter when the ground was saturated and frozen. The number of daily satellite-scale observations in the 2012 records ranged from 202 to 283.

2.3.2 Analytical model for soil saturation probability density functions

Model definition

Our framework is based on a standard bucket model of soil column hydrology at a point forced with stochastic precipitation inputs and in which soil water losses are a function of soil saturation. We followed the simple formulation of soil water losses in (Laio et al., 2001a). We applied two associated analytical formulations for the soil saturation pdf detailed below and derived under the assumption of steady state, wherein parameters are constant for a given period of time. The annual model assumed an annual rainfall pattern and the seasonal model accounted for a wet season rainfall pattern and a dry season of negligible rainfall.

The soil water balance model is defined at a point and a daily time step, for a soil with porosity n, and assuming that soil saturation is uniform in the considered soil column of depth Z. Rainfall, the only input to the soil water balance, is treated as a Poisson distribution characterized by an average event frequency λ and average event intensity α. For simplicity, we assumed that the rainfall applied was equal to the amount that reached the ground surface and that interception by vegetation was negligible. Interception may be a significant component of the soil water balance at forested sites and may need to be considered in future extensions of this work. The daily soil water balance is the difference between the rate of rainfall infiltration φ and the rate of soil moisture losses χ:

$$nZ\frac{ds(t)}{dt} = \varphi[s(t);t] - \chi[s(t)] \quad (1)$$

$\varphi[s(t);t]$ is both a stochastic process controlled by rainfall and also a state-dependent process because excess rainfall relative to available soil storage is converted to surface runoff. the soil moisture loss curve, $\chi[s(t)]$, includes leakage losses due to gravity and evapotranspiration and is described in stages determined by five soil saturation thresholds (Laio et al., 2001a). These stages are: (i) the saturation point ($s = 1$), at which all pores are filled with water; (ii) the field capacity (s_{fc}), at which soil-gravity drainage becomes negligible compared to evaporation; (iii) the point of incipient stomata closure (s^*), at which plants begin to reduce transpiration from water stress; (iv) the wilting point (s_w), at which plants cease to transpire; and (v) the hydroscopic point (s_h), at which water is bound to the soil matrix. Soil water losses are controlled by physical soil properties for saturation states above s_{fc}. The rate of leakage due to gravity is assumed maximum when soil is saturated (K_s) and decays exponentially to zero at s_{fc}

(Brooks & Corey, 1964). Soil water losses are controlled by micro-meteorological conditions for saturation states between s_{fc} and s^*. The rate of evapotranspiration is assumed to occur at a maximum rate (E_{max}), independent of the saturation state. Soil water losses are controlled primarily by vegetation for saturation states between s^* and s_w. Plants close their stomata in response to soil water deficits that drive leaf water potential gradients, as well as to atmospheric vapor pressure deficits, and evapotranspiration decreases linearly from E_{max} to E_w at s_w. Soil water losses are controlled by soil diffusivity for soil saturation states below s_w, and soil evaporation decreases linearly from E_w to zero at s_h. Soil water losses are negligible for soil saturation states below s_h. For this simplified theoretical description of the soil water loss curve and stochastic rainfall forcing, the analytical solution of the steady state probability distributions of soil saturation, $p(s)$, was given by (Laio et al., 2001a):

$$p(s)=\begin{cases}0, & 0<s\le s_h,\\ \frac{C}{\eta_w}\left(\frac{s-s_h}{s_w-s_h}\right)^{\frac{\lambda(s_w-s_h)}{\eta_w}-1}e^{-\gamma s}, & s_h<s\le s_w,\\ \frac{C}{\eta_w}\left[1+\left(\frac{\eta}{\eta_w}-1\right)\left(\frac{s-s_w}{s^*-s_w}\right)\right]^{\frac{\lambda(s^*-s_w)}{\eta-\eta_w}-1}e^{-\gamma s}, & s_w<s\le s^*,\\ \frac{C}{\eta}e^{-\gamma s+\frac{\lambda}{\eta}(s-s^*)}\frac{\eta}{\eta_w}^{\frac{\lambda(s^*-s_w)}{\eta-\eta_w}}, & s^*<s\le s_{fc},\\ \frac{C}{\eta}e^{-(\beta+\gamma)s+\beta s_{fc}}\left(\frac{\eta e^{\beta s}}{(\eta-m)e^{\beta s_{fc}}+me^{\beta s}}\right)^{\frac{\lambda}{\beta(\eta-m)}+1}\frac{\eta}{\eta_w}^{\frac{\lambda(s^*-s_w)}{\eta-\eta_w}}e^{\frac{\lambda}{\eta}\left(s_{fc}-s^*\right)}, & s_{fc}<s\le 1,\end{cases} \quad (2)$$

where

$\frac{1}{\gamma}=\frac{\alpha}{nZ}$,

$\eta_w=\frac{E_w}{nZ}$,

$\eta=\frac{E_{max}}{nZ}$,

$m=\frac{K_s}{nZ(e^{\beta\left(1-s_{fc}\right)}-1)}$,

$\beta=2b-4$.

where b, is an experimentally determined parameter used in the Clapp & Hornberger (1978) soil water retention curve, and the constant C can be obtained numerically to ensure the integral of $p(s)$ = 1. We used a simplifying relation $E_w=0.05E_{max}$ to reduce the number of parameters.

We adopted Dralle & Thompson (2016) framework to account for transient dynamics between wet and dry seasons. We defined the dry season as a period of duration t_d in which precipitation was negligible

and assumed to not contribute to soil moisture. During that period, we assumed soil saturation decayed from an initial value s_0 to $s(t_d, s_0)$, given by Laio et al. (2001a). For simplicity, we determined t_d using rainfall records at a monthly step and s_0 was the soil saturation value on the last day of the wet season. Note that we did not define s_0 as the soil saturation following the last significant storm of the wet season as was done in prior studies (Dralle & Thompson, 2016). We then calculated the annual soil saturation pdf ($p_{wd}(\mathrm{s})$) as the weighted sum of the wet and dry season pdfs, $p_w(s)$ and $p_d(s)$, respectively.

$$p_{wd}(\mathrm{s}) = \left(1 - \frac{t_d}{365}\right) p_w(s) + \frac{t_d}{365} p_d(s) \tag{3}$$

The steady state solution in Eq. (2) was used for the wet season pdf and the dry season pdf is numerically determined by

$$p_d(s) = \int_{s_0}^{1} p_{S_d|S_0}(s, s_0) p_0(s_0) ds_0 \tag{4}$$

where $p_0(s_0)$ is the pdf of the initial dry season soil saturation, equal to $p_w(s)$, and $p_{S_d|S_0}(s, s_0)$ is the pdf of dry season soil saturation given an initial condition s_0.

$$p_{S_d|S_0}(s, s_0) = \frac{C_d}{t_d} \begin{cases} \frac{e^{\beta(s_0 - s)}}{(\eta^d - m)e^{\beta(s_0 - s)} - \eta^d + m + m e^{\beta\left(s_0 - s_{fc}\right)}}, & s_{fc} < \mathrm{s} \leq 1, \\ \frac{1}{\eta^d}, & s^* < \mathrm{s} \leq s_{fc}, \\ \frac{1}{\eta^d - {\eta_w}^d}\left(\frac{s^* - s_w}{(\eta^d - {\eta_w}^d)(s - s_w) + {\eta_w}^d(s^* - s_w)}\right), & s_w < \mathrm{s} \leq s^* \\ \frac{1}{{\eta_w}^d}\left(\frac{s_w - s_h}{s - s_h}\right), & s_h < \mathrm{s} \leq s_w \\ 0, & s_0 \leq \mathrm{s}, \\ 0, & \mathrm{s} \leq s_h, \\ 0, & \mathrm{s} \leq s(t_d, s_0) \end{cases} \tag{5}$$

where η^d and ${\eta_w}^d$ are equivalent to η and η_w relative to ${E_{max}}^d$, the maximum evapotranspiration rate during the dry season, and C_d is a normalization constant. We used the analytical expression for soil saturation decay, $s(t, s_0)$, in absence of rainfall given by Laio et al. (2001a) to derive $p_{S_d|S_0}(s, s_0)$.

Climate, soil and vegetation parameter characterization

We chose readily available data for rainfall characteristics (λ and α), length of the dry period (t_d), and physical soil parameters (s_{fc}, s_h, K_s, and) b needed in the analytical models of soil saturation pdfs (Eq. (2) and Eq. (3)). We focused on estimating the ecohydrological parameters s^*, s_w, and E_{max}, which describe vegetation control on soil water losses and are not easily observable.

We calculated rainfall characteristics λ and α for the year and wet season months for each site from FLUXNET2015 and TRMM rainfall records following Rodriguez-Iturbe et al., (1984) (Table 2.1). We used FLUXNET2015 rainfall characteristics for point- and footprint-scale analyses, and we used TRMM rainfall characteristics for the satellite-scale analysis. TRMM rainfall records were generally consistent with ground-based measurements. For each location, we evaluated monthly FLUXNET2015 rainfall depth and categorized consecutive months contributing <5 % of the site's annual rainfall as dry season months (Figure 2.1). We then calculated length of the dry period (t_d) as the number of days in those dry months. We used physical soil characteristics for soil textures at each site (s_h, K_s, and *b)* from Rawls et al. (1982) (Table 2.1). We estimated s_{fc} from each soil saturation record (Table 2.1) to be consistent with the assumption that drainage losses are insignificant compared to evapotranspiration losses the day following a rain event. We identified all days in the 2012 record following an observed decrease in soil saturation and estimated s_{fc} as the 95th percentile of the soil saturation value of the selected days. Daily soil saturation below s_w and above s_{fc} are rare (Laio et al., 2001a), so we did not expect the average soil texture values for s_h and K_s to significantly affect the results. Soil depths Z are 10, 20, and 5 cm for the point-, footprint-, and satellite-scales, respectively. E_{max} is only a fraction of the atmospheric moisture demand (or potential evapotranspiration) contributed by that soil depth because we used a soil depth that is shallower than the rooting depth. Consequently, our framework includes 4 (or 3 if seasonality is ignored) unknown soil water balance parameters, s^*, s_w, E_{max}, and ${E_{max}}^d$. We estimated these parameters over the following intervals:

$$\begin{cases} s_h \le s^* \le s_{fc}, \\ s_h \le s_w \le s_{fc}, \\ 0 \le E_{max} \le 10, \\ 0 \le {E_{max}}^d \le 10 \end{cases} \tag{6}$$

where 10 mm day^{-1} is the pre-defined upper possible boundary for potential evapotranspiration.

2.3.3 Bayesian inversion approach

Application of the Bayes theorem

We related $p(S)$, the empirical soil saturation pdf of the $j = [1, \dots, m]$ soil saturation observations (s_j) and the analytical soil saturation pdfs in Eq. (2) or Eq. (3) derived from the simple soil water balance model in Eq. (1) with up to four unknown soil water balance parameters $\theta = [s^*, s_w, E_{max}, {E_{max}}^d]$ using the Bayes' theorem defined as:

$$p(\theta|S) = \frac{p(S|\theta)\, p(\theta)}{p(S)} \tag{7}$$

where the posterior distribution, $p(\theta|S)$, is the solution of the inverse problem and describes the probability of model parameters θ given the set $S = [s_1, s_2, \dots s_m]$ of soil saturation observations. Assuming uninformed prior knowledge, the prior distribution of model parameters θ, $p(\theta)$, were defined by uniform distributions over the intervals (Eq. (6)). The conditional probability of observations S given model parameters θ, $p(\mathrm{S}|\theta)$, is the likelihood function of model parameters θ.

Parameter estimation

We used the Metropolis-Hasting Markov chain Monte Carlo (MH-MCMC) technique to estimate the posterior distribution of $p(\theta|S)$ by drawing random model samples θ_i from $p(\theta)$ and evaluating $p(\mathrm{S}|\theta_i)$ (Hastings, 1970; Metropolis et al., 1953; Xu et al., 2006). We defined the likelihood function of a model i, $p(S|\theta_i)$ as:

$$p(S|\theta_i) = \prod_{j=1}^{m} p\left(s_j\middle|\theta_i\right) \tag{8}$$

where $p\left(s_j\middle|\theta_i\right)$ is the probability of observation s_j given Eq. (2) or Eq. (3) using parameters θ_i.

The MH-MCMC technique converges to a stationary distribution according to the ergodicity theorem in Markov chain theory. The sampling algorithm consisted of repeating two steps: (i) a proposing step, in which the algorithm generates a new model $\theta_i{}'$ using a random function that is symmetric about the previously accepted model θ_i, and (ii) a moving step, to determine if the model should be accepted or rejected, in which, $\theta_i{}'$ is tested against the Metropolis criterion (a) defined as:

$$a = \frac{p\left(S\middle|\theta_i{}'\right)}{p(S|\theta_i)} \tag{9}$$

If $a > 1$, θ_i was accepted and $\theta_{i+1} = \theta_i{}'$ was used for the next sample. If $a < 1$, a random number $p_* \in [0,1]$ was drawn from a uniform distribution and compared to a. If $p_* < a$, $\theta_i{}'$ was accepted and $\theta_{i+1} = \theta_i{}'$ was used for the next sample. If $p_* > a$, $\theta_i{}'$ was rejected and $\theta_{i+1} = \theta_i$ was used for the next sample. If $\theta_i{}'$ was an inconsistent model in which soil saturation thresholds (s_w, s_*) were ranked incorrectly or any of the soil water balance parameters (s^*, s_w, E_{max}, ${E_{max}}^d$) were outside of their defined physical bounds, the model likelihood was zero and $\theta_i{}'$ was never accepted. The log-likelihood was more convenient to compute than the likelihood. The symmetric function used in the proposing step was a Gaussian distribution with a mean value equal to the accepted model θ_i and a standard deviation of 1 % of interval range for which each parameter is defined in Eq. (6). We selected this value of the standard deviation of each model parameter after a number of test runs to generally ensure an acceptance rate between 20 and 50% (Roberts & Rosenthal, 1998). We obtained statistics of the estimated parameters in θ from the union of three run samples of 20,000 simulations each. The burn-in period is

the number of simulations after which the running mean and standard deviation are stabilized. We considered a burn-in period of 10,000 simulations, which were discarded for each run sample. If the acceptance rate of a run sample was <1% or >90% after the burn-in period, we discarded the run and concluded that the algorithm was stuck in a local minimum that might be physically impossible. We evaluated convergence by the Gelman-Rubin (GR) diagnostic (Gelman & Rubin, 1992) on the run samples. The GR diagnostic determines that the algorithm reaches convergence when the within-run variability (σ_w) is roughly equal to the between-run variability (σ_b), that is, when σ_w/σ_b approaches one. We verified that the GR diagnostic for each estimated parameter was <1.1. If the GR diagnostic did not indicate that the three run samples converged, we discarded the run with the lowest likelihood and re-initiated a new run sample until convergence was attained. We counted the number of attempts to quantify how rapidly convergence occurred. We computed mean and standard deviation for each parameter from a total of 30,000 simulations of θ resulting from the three converging run samples. A mean analytical model of soil saturation pdf was determined by applying Eq. (2) or Eq. (3) with the mean values of the 30,000 posterior parameter estimates

2.3.4 Model evaluation criteria

We did not have direct measurement to validate the parameters s^*, s_w, and E_{max} estimated through the Bayesian inversion methods. We therefore analyzed convergence and uncertainty metrics of the model inversion and goodness of fit between empirical and analytical soil saturation pdfs to evaluate the identifiability of the ecohydrological parameters. We compared the optimum analytical pdf derived from the mean parameter estimates and the empirical pdfs derived from observations. We evaluated the model inversion using the following criteria:

(i) Convergence of the Bayesian inversion: a GR diagnostic <1.1 for all unknown parameters is obtained from the union of three run samples and within ≤10 sample runs.

(ii) Low uncertainty in parameter estimates: the posterior distributions of parameter estimates are physically plausible and have coefficients of variations <20%.

(iii) Goodness of fit: a quantile-level Nash-Sutcliffe efficiency (NSE) (Müller et al., 2014) > 0.85 and a Kolmogorov-Smirnov statistic <0.2.

2.3.5 Method assessment

Major assumptions and limitations embedded in the proposed inference framework were tested through the analysis detailed below. We assume, for each scale and location, that the shape of empirical the soil saturation pdfs is controlled by the physical constraints used to parameterize the analytical model of soil

saturation pdfs, these parameters can be determined with some certainty and reflect variability in soil water dynamics. We expect that estimated soil saturation thresholds have greater certainty when the empirical soil saturation pdf is defined around those values and greater uncertainty when fewer soil saturation values are observed around the thresholds. We acknowledge that pre-defined rainfall characteristics and physical soil parameters based on observations or literature values may not be exactly representative of the processes at each location or scale and could also create biases and uncertainties in the fitted parameters of interest. We used model evaluation criteria (Section 2.3.4) to investigate the applicability of the inference framework with varying model complexities, scales, locations and data availability.

(i) Analytical expressions for soil saturation pdfs were derived under the assumption of steady state. Annual soil moisture records can be affected by transitional dynamics between wet and dry seasons, and the appropriate level of model complexity must be used. We applied the inversion framework to annual soil saturation using variations of the analytical model for soil saturation pdfs of increasing complexity: (i) the annual model in Eq. (2) and (ii) the seasonal model in Eq. (3). We determined whether the added complexity of the dry season pdf increases the identifiability of ecohydrological parameters or if the simpler annual model is sufficiently consistent with annual empirical soil saturation pdfs.

(ii) We compared co-located parameter estimates and their uncertainty at point-, footprint-, and satellite- scales for each site. We determine whether the inference approach can provide appropriate scale-specific parameters for ecohydrological modelling at each location.

(iii) We assumed that the whole range of realizable soil saturation values was captured within the selected time series at each scale and that the resulting soil saturation pdf was not truncated. If the range of observed values is not representative of the soil saturation pdf because it is truncated or affected by noise in the data, parameter estimates may be biased. Minimum and maximum observed soil saturation values during 2012 (Table 2.1) indicate the range of observed soil saturation values we used to estimate ecohydrological parameters. We determine whether the inference method based on soil saturation pdfs is robust against reduced data availability by repeating the model inversions on subsets of the soil saturation time series and show that the method can be applied to sparse datasets. We performed the model inversion using subsets of each soil saturation record by randomly resampling fractions of the data down to 10 % of the annual timeseries and computed goodness of fit statistics between the resulting analytical models and the empirical models based on the full annual record. We determined the number of data points necessary to infer converging model parameters that best match observations and whether the proposed inference method based on soil saturation pdf can be reliably used to identify ecohydrological parameters from sparse datasets.

2.4 Results and discussion

2.4.1 Level of model complexity

For each of the four locations (Table2.1), we obtained optimal analytical soil saturation pdfs consistent with the empirical pdfs derived from soil saturation observations using the Bayesian inversion framework and a MH-MCMC algorithm. Model inversions for each site and scale and for both annual and seasonal models met the evaluation criteria (see Sec 2.2.4). Our results indicated that the framework of (Dralle & Thompson, 2016) can be applied to sites with low (US-MMS) and high (US-TON) seasonality in rainfall patterns. Posterior probability distributions of soil water balance parameters (s_w, s^*, E_{max}) were well-constrained overall. The parameter estimates and their coefficient of variation as well as the model goodness of fit statistics are summarized in Table 2.2. Figures 2.2 through 2.5 present a comparison between empirical as well as analytical pdfs and associated quantile-quantile plots for point-, footprint-, and satellite-scales at the four study sites and for both annual and seasonal models. The goodness of fit between empirical pdfs and analytical models was only slightly better for the seasonal model than for the annual model. However, the coefficient of variation of the posterior parameter distributions was smaller for the annual model and it converged more rapidly. The Bayesian inversion of the annual model is therefore more computationally efficient. The parameter identifiability was not greatly improved by the more complex seasonal model. The estimated soil saturation threshold $s_w$was consistently smaller for the annual model than for the seasonal model and s^* was often higher, which may indicate that s_w and s^* in the annual model could be biased and may have absorbed dry season dynamics. Previous studies calibrating soil saturation pdf models found ecohydrological parameters values comparable to ours (Table 2.2). For example, using point-scale observations at US-Ton, best fit values of s_w and s_{fc} were 0.26 and 0.82, respectively (Dralle & Thompson, 2016), and best-fit values of s^* and E_{max} were 0.3 and 1.9 mm d^{-1}, respectively (Miller et al., 2007). We did not compare soil saturation thresholds s^* and s_w with literature values of soil water potential at which stomata are fully open or closed because the conversion of soil saturation to soil matrix potential is non-linear (Clapp & Hornberger, 1978) and site and scale specific soil water retention parameters were unknown. Average parameters derived from soil texture (Rawls et al., 1982) were not compatible with soil moisture data from each scale and site.

2.4.2 Site and scale considerations

Parameter estimates were most constrained for scales and locations at which soil water dynamics are more sensitive to the fitted ecohydrological parameters of interest. In these cases, convergence of the model inversion was attained less rapidly but ultimately provided better goodness of fit. Soil saturation

states at drier sites may be more controlled by soil water loss parameters, while soil saturation states at wetter sites may also be controlled by rainfall characteristics. Estimated soil saturation thresholds had greater certainty if the empirical soil saturation pdf were defined around those values and had greater uncertainty if there were fewer soil saturation values observed around the thresholds. For example, uncertainty of s_w was greater for the humid subtropical deciduous forest site (US-MMS) than for the Mediterranean savanna sites (US-Ton), and uncertainty of s^* was greater for US-Ton than US-MMS. Similarly, soil saturation states representing larger spatial scales were less sensitive to specific site characteristics.

Parameter uncertainty for satellite- and footprint-scales was greater than for the point-scale. Estimates of larger scale soil water balance parameters are more relevant to regional ecohydrological dynamics. Differences in parameter estimates among scales within a site may be associated with differences in soil texture properties, such as porosity and field capacity, that were determined separately for each record. Co-located and concurrent soil saturation pdfs are different at each scale (Figure 2.2-2.5) and suggest variability in observed soil water dynamics at each scale. Differences in driving processes among scales were specifically determined from the model inversion for each scale and provided robust scale-specific parameters for ecohydrological modelling.

2.4.3 Data availability

For each spatial scale and site, the annual model was inversed, using random subsamples of 100 to 10 % of the 2012 time series (Figure 2.6). For all sites and scales the number of observations did not significantly impact model inference. The NSE, Kolmogorov-Smirnov statistic and parameter estimates were stable down to about 100 observations. Fitted model parameter values and the variability of parameter estimates among the 10 repetitions in each subsample category were not sensitive to the number of observations used. Results indicate the identifiability of ecohydrological parameters through the inversion of the analytical model of soil saturation pdfs was robust because the mean and standard deviation of the randomly selected subsets of annual data were representative of the full record. There was no correlation between the small differences in the mean and standard deviations of the subsamples and the model goodness of fit. The proposed inference method based on soil saturation pdfs can therefore reliably be used to identify ecohydrological parameters from sparse datasets. Inference methods, which do not require continuous data are particularly relevant to large scale soil moisture measurements, such as satellite products, that are not continuous.

2.5 Conclusions

We document a generalizable Bayesian inversion framework to infer parameter values of the stochastic soil water balance model and their associated uncertainty using freely available rainfall and soil moisture observations at point-, footprint- and satellite-scales. Empirical pdfs derived from soil saturation observations provided key information to determine unknown ecohydrological parameters s^*, s_w, and E_{max}. Model assumptions were appropriately met, and optimal analytical soil saturation pdfs were consistent with empirical pdfs. Uncertainty in parameter estimates were small and reflected the sensitivity of the soil water balance model to ecohydrological parameters at varying scales and locations. We demonstrate that the form of the simple ecohydrological model for soil saturation pdfs was consistent with observations from point-, footprint-, and satellite-scales. However, optimal parameters were different at each scale because co-located and concurrent soil saturation pdfs are different at each scale, which may result from spatial heterogeneity in soil water dynamics. We demonstrate the advantage of analyzing soil saturation pdfs instead of time series. We obtained stable results using sparse subsets of the datasets, indicating that the proposed framework is robust and can be used with non-continuous data. Although the seasonal model was conceptually more consistent with our physical understanding of annual soil water dynamics, the annual model provided satisfactory results matching annual empirical pdf sites we analyzed. We were not able to determine if some differences in parameters estimated using the seasonal model are physically meaningful because wet and dry season dynamics were better characterized in this more complex model. Our methodology can be customized to characterize site-specific parameters and to test consistency between observed and analytical soil saturation pdfs for any other adaptation of the stochastic ecohydrological framework with more or less complexity depending on the study objectives.

We provide a method based on a parsimonious soil water balance model, requiring a minimum level of data inputs to estimate ecohydrological characteristics that are not directly observable and for which established estimation methods are not available. Our methods can be applied in future studies to better understand differences in soil water dynamics at different scales and to improve scaling of ecohydrological processes. Results demonstrate the value of large scale near-surface soil moisture observations to improve characterization of soil water dynamics at ecosystem scales. Relations between the soil saturation threshold values inferred from the near surface soil moisture data and dynamics in the full active rooting zone are unknown. The datasets we used are freely available from sensor networks and global satellite products, and methods can therefore be applied to a large range of sites or to global analyses to improve understanding of spatial patterns in ecohydrological parameters relevant for local and global water cycle analyses.

2.6 Data and code

We downloaded all datasets from publicly available sources. Point-scale soil moisture and rainfall data are available through FLUXNET2015 (http://fluxnet.fluxdata.org/data/fluxnet2015-dataset/); footprint-scale soil moisture data are available through COSMOS (http://cosmos.hwr.arizona.edu/Probes/probelist.html); remotely-sensed soil moisture data are available through ESA CCI (http://www.esa-soilmoisture-cci.org/node/145); remotely sensed rainfall data are available through NASA TRMM (https://pmm.nasa.gov/data-access/downloads/trmm); global soil texture data are available through FAO HWSD (http://www.fao.org/soils-portal/soil-survey/soil-maps-and-databases/harmonized-world-soil-database-v12/en/). Custom scripts in the Python computing language associated with our analysis are available upon request through a private gitHub repository are publicly available (Bassiouni, 2018, https://doi.org/10.5281/zenodo.1283371)

2.7 Acknowledgments

We thank Minghui Zhang, Marc Müller, David Dralle, Xue Feng and Editor Sally Thomspon for their thoughtful reviews and useful feedback on an earlier draft of this manuscript. This material is based upon work supported by the National Science Foundation Graduate Research Fellowship under Grant No. 1314109-DGE. S.P.G. acknowledges the financial support of the United States National Aeronautics and Space Administration (NNX16AN13G). This work used the Extreme Science and Engineering Discovery Environment (XSEDE) via allocation DEB160018, supported by National Science Foundation grant number ACI-1548562. This work used data acquired and shared by the FLUXNET community, including these networks: AmeriFlux, AfriFlux, AsiaFlux, CarboAfrica, CarboEuropeIP, CarboItaly, CarboMont, ChinaFlux, Fluxnet-Canada, GreenGrass, ICOS, KoFlux, LBA, NECC, OzFlux-TERN, TCOS-Siberia, and USCCC. The FLUXNET eddy covariance data processing and harmonization was carried out by the European Fluxes Database Cluster, AmeriFlux Management Project, and Fluxdata project of FLUXNET, with the support of CDIAC and ICOS Ecosystem Thematic Center and the OzFlux, ChinaFlux and AsiaFlux offices.

2.8 References

Baldwin, D., Manfreda, S., Keller, K., & Smithwick, E. A. H. (2017). Predicting root zone soil moisture with soil properties and satellite near-surface moisture data across the conterminous United States. Journal of Hydrology, 546, 393–404. https://doi.org/10.1016/j.jhydrol.2017.01.020

Brooks, R., & Corey, T. (1964). Hydraulic Properties of Porous Media. Hydrology Papers, Colorado State University.

Caylor, K. K., D'Odorico, P., & Rodriguez-Iturbe, I. (2006). On the ecohydrology of structurally heterogeneous semiarid landscapes. Water Resources Research, 42(7). https://doi.org/10.1029/2005WR004683

Chen, X., Rubin, Y., Ma, S., & Baldocchi, D. (2008). Observations and stochastic modeling of soil moisture control on evapotranspiration in a Californian oak savanna: SOIL MOISTURE CONTROL ON ET. Water Resources Research, 44(8). https://doi.org/10.1029/2007WR006646

Clapp, R. B., & Hornberger, G. M. (1978). Empirical equations for some soil hydraulic properties. Water Resources Research, 14(4), 601–604.

Dorigo, W. A., Gruber, A., De Jeu, R. A. M., Wagner, W., Stacke, T., Loew, A., et al. (2015). Evaluation of the ESA CCI soil moisture product using ground-based observations. Remote Sensing of Environment, 162, 380–395. https://doi.org/10.1016/j.rse.2014.07.023

Dralle, D. N., & Thompson, S. E. (2016). A minimal probabilistic model for soil moisture in seasonally dry climates. Water Resources Research, 52(2), 1507–1517.

Dralle, D. N., Karst, N. J., & Thompson, S. E. (2016). Dry season streamflow persistence in seasonal climates. Water Resources Research, 52(1), 90–107. https://doi.org/10.1002/2015WR017752

Feng, X., Dawson, T. E., Ackerly, D. D., Santiago, L. S., & Thompson, S. E. (2017). Reconciling seasonal hydraulic risk and plant water use through probabilistic soil-plant dynamics. Global Change Biology, 23(9), 3758–3769. https://doi.org/10.1111/gcb.13640

Gelman, A., & Rubin, D. B. (1992). Inference from iterative simulation using multiple sequences. Statistical Science, 457–472.

Good, S. P., Soderberg, K., Guan, K., King, E. G., Scanlon, T. M., & Caylor, K. K. (2014). δ 2 H isotopic flux partitioning of evapotranspiration over a grass field following a water pulse and subsequent dry down. Water Resources Research, 50(2), 1410–1432. https://doi.org/10.1002/2013WR014333

Good, S. P., Noone, D., & Bowen, G. (2015). Hydrologic connectivity constrains partitioning of global terrestrial water fluxes. Science, 349(6244), 175–177.

Good, S. P., Moore, G. W., & Miralles, D. G. (2017). A mesic maximum in biological water use demarcates biome sensitivity to aridity shifts. Nature Ecology & Evolution, 1(12), 1883.

Hastings, W. K. (1970). Monte Carlo Sampling Methods Using Markov Chains and Their Applications. Biometrika, 57(1), 97. https://doi.org/10.2307/2334940

Huffman, G. J., Bolvin, D. T., Nelkin, E. J., Wolff, D. B., Adler, R. F., Gu, G., et al. (2007). The TRMM Multisatellite Precipitation Analysis (TMPA): Quasi-Global, Multiyear, Combined-Sensor Precipitation Estimates at Fine Scales. Journal of Hydrometeorology, 8(1), 38–55. https://doi.org/10.1175/JHM560.1

King, E. G., & Caylor, K. K. (2011). Ecohydrology in practice: strengths, conveniences, and opportunities. Ecohydrology, 4(4), 608–612. https://doi.org/10.1002/eco.248

Köhli, M., Schrön, M., Zreda, M., Schmidt, U., Dietrich, P., & Zacharias, S. (2015). Footprint characteristics revised for field-scale soil moisture monitoring with cosmic-ray neutrons. Water Resources Research, 51(7), 5772–5790. https://doi.org/10.1002/2015WR017169

Laio, F., Porporato, A., Ridolfi, L., & Rodriguez-Iturbe, I. (2001a). Plants in water-controlled ecosystems: active role in hydrologic processes and response to water stress: II. Probabilistic soil moisture dynamics. Advances in Water Resources, 24(7), 707–723.

Laio, F., Porporato, A., Fernandez-Illescas, C. P., & Rodriguez-Iturbe, I. (2001b). Plants in water-controlled ecosystems: active role in hydrologic processes and response to water stress: IV. Discussion of real cases. Advances in Water Resources, 24(7), 745–762.

Laio, F., D'Odorico, P., & Ridolfi, L. (2006). An analytical model to relate the vertical root distribution to climate and soil properties: VERTICAL ROOT DISTRIBUTION. Geophysical Research Letters, 33(18), n/a-n/a. https://doi.org/10.1029/2006GL027331

Li, Y., Guan, K., Gentine, P., Konings, A. G., Meinzer, F. C., Kimball, J. S., et al. (2017). Estimating global ecosystem iso/anisohydry using active and passive microwave satellite data: Estimate global ecosystem iso/anisohydry. Journal of Geophysical Research: Biogeosciences. https://doi.org/10.1002/2017JG003958

Liu, Y. Y., Parinussa, R. M., Dorigo, W. A., De Jeu, R. A. M., Wagner, W., van Dijk, A. I. J. M., et al. (2011). Developing an improved soil moisture dataset by blending passive and active microwave satellite-based retrievals. Hydrology and Earth System Sciences, 15(2), 425–436. https://doi.org/10.5194/hess-15-425-2011

Liu, Y. Y., Dorigo, W. A., Parinussa, R. M., de Jeu, R. A. M., Wagner, W., McCabe, M. F., et al. (2012). Trend-preserving blending of passive and active microwave soil moisture retrievals. Remote Sensing of Environment, 123, 280–297. https://doi.org/10.1016/j.rse.2012.03.014

Manfreda, S., Caylor, K. K., & Good, S. P. (2017). An ecohydrological framework to explain shifts in vegetation organization across climatological gradients: Vegetation pattern in dry environments. Ecohydrology, 10(3), e1809. https://doi.org/10.1002/eco.1809

Manzoni, S., Vico, G., Katul, G., Palmroth, S., & Porporato, A. (2014). Optimal plant water-use strategies under stochastic rainfall. Water Resources Research, 50(7), 5379–5394. https://doi.org/10.1002/2014WR015375

McColl, K. A., Wang, W., Peng, B., Akbar, R., Short Gianotti, D. J., Lu, H., et al. (2017). Global characterization of surface soil moisture drydowns: Geophysical Research Letters, 44(8), 3682–3690. https://doi.org/10.1002/2017GL072819

Metropolis, N., Rosenbluth, A. W., Rosenbluth, M. N., Teller, A. H., & Teller, E. (1953). Equation of State Calculations by Fast Computing Machines. The Journal of Chemical Physics, 21(6), 1087–1092. https://doi.org/10.1063/1.1699114

Miller, G. R., Baldocchi, D. D., Law, B. E., & Meyers, T. (2007). An analysis of soil moisture dynamics using multi-year data from a network of micrometeorological observation sites. Advances in Water Resources, 30(5), 1065–1081. https://doi.org/10.1016/j.advwatres.2006.10.002

Porporato, A., Daly, E., & Rodriguez-Iturbe, I. (2004). Soil water balance and ecosystem response to climate change. The American Naturalist, 164(5), 625–632.

Rawls, W. J., Brakensiek, D. L., & Saxtonn, K. E. (1982). Estimation of soil water properties. Transactions of the ASAE, 25(5), 1316–1320.

Roberts, G. O., & Rosenthal, J. S. (n.d.). Optimal Scaling for Various Metropolis–Hastings Algorithms.

Rodriguez-Iturbe, I., Gupta, V. K., & Waymire, E. (1984). Scale considerations in the modeling of temporal rainfall. Water Resources Research, 20(11), 1611–1619. https://doi.org/10.1029/WR020i011p01611

Rodriguez-Iturbe, I., Porporato, A., Ridolfi, L., Isham, V., & Coxi, D. R. (1999). Probabilistic modelling of water balance at a point: the role of climate, soil and vegetation. In Proceedings of the Royal Society of London A: Mathematical, Physical and Engineering Sciences (Vol. 455, pp. 3789–3805). The Royal Society.

Rodriguez-Iturbe, I., Porporato, A., Laio, F., & Ridolfi, L. (2001). Intensive or extensive use of soil moisture: plant strategies to cope with stochastic water availability. Geophysical Research Letters, 28(23), 4495–4497.

Saleem, J. A., & Salvucci, G. D. (2002). Comparison of soil wetness indices for inducing functional similarity of hydrologic response across sites in Illinois. Journal of Hydrometeorology, 3(1), 80–91.

Salvucci, G. D. (2001). Estimating the moisture dependence of root zone water loss using conditionally averaged precipitation. Water Resources Research, 37(5), 1357–1365.

Suweis, S., Rinaldo, A., Van der Zee, S. E. A. T. M., Daly, E., Maritan, A., & Porporato, A. (2010). Stochastic modeling of soil salinity. Geophysical Research Letters, 37(7), n/a-n/a. https://doi.org/10.1029/2010GL042495

Teuling, A. J., Seneviratne, S. I., Williams, C., & Troch, P. A. (2006). Observed timescales of evapotranspiration response to soil moisture. Geophysical Research Letters, 33(23). https://doi.org/10.1029/2006GL028178

Thompson, S., Levin, S., & Rodriguez-Iturbe, I. (2013). Linking Plant Disease Risk and Precipitation Drivers: A Dynamical Systems Framework. The American Naturalist, 181(1), E1–E16. https://doi.org/10.1086/668572

Tuttle, S. E., & Salvucci, G. D. (2014). A new approach for validating satellite estimates of soil moisture using large-scale precipitation: Comparing AMSR-E products. Remote Sensing of Environment, 142, 207–222. https://doi.org/10.1016/j.rse.2013.12.002

Volo, T. J., Vivoni, E. R., Martin, C. A., Earl, S., & Ruddell, B. L. (2014). Modelling soil moisture, water partitioning, and plant water stress under irrigated conditions in desert urban areas. Ecohydrology, n/a-n/a. https://doi.org/10.1002/eco.1457

Wagner, W., Dorigo, W., de Jeu, R., Fernandez, D., Benveniste, J., Haas, E., & Ertl, M. (2012). Fusion of active and passive microwave observations to create an essential climate variable data record on soil moisture. ISPRS Annals of the Photogrammetry, Remote Sensing and Spatial Information Sciences (ISPRS Annals), 7, 315–321.

Wang, T., Franz, T. E., Yue, W., Szilagyi, J., Zlotnik, V. A., You, J., et al. (2016). Feasibility analysis of using inverse modeling for estimating natural groundwater recharge from a large-scale soil moisture monitoring network. Journal of Hydrology, 533, 250–265. https://doi.org/10.1016/j.jhydrol.2015.12.019

Whitney, K. M., Vivoni, E. R., Duniway, M. C., Bradford, J. B., Reed, S. C., & Belnap, J. (2017). Ecohydrological role of biological soil crusts across a gradient in levels of development. Ecohydrology, 10(7), e1875. https://doi.org/10.1002/eco.1875

Xu, T., White, L., Hui, D., & Luo, Y. (2006). Probabilistic inversion of a terrestrial ecosystem model: Analysis of uncertainty in parameter estimation and model prediction. Global Biogeochemical Cycles, 20(2), n/a-n/a. https://doi.org/10.1029/2005GB002468

2.9 Figures

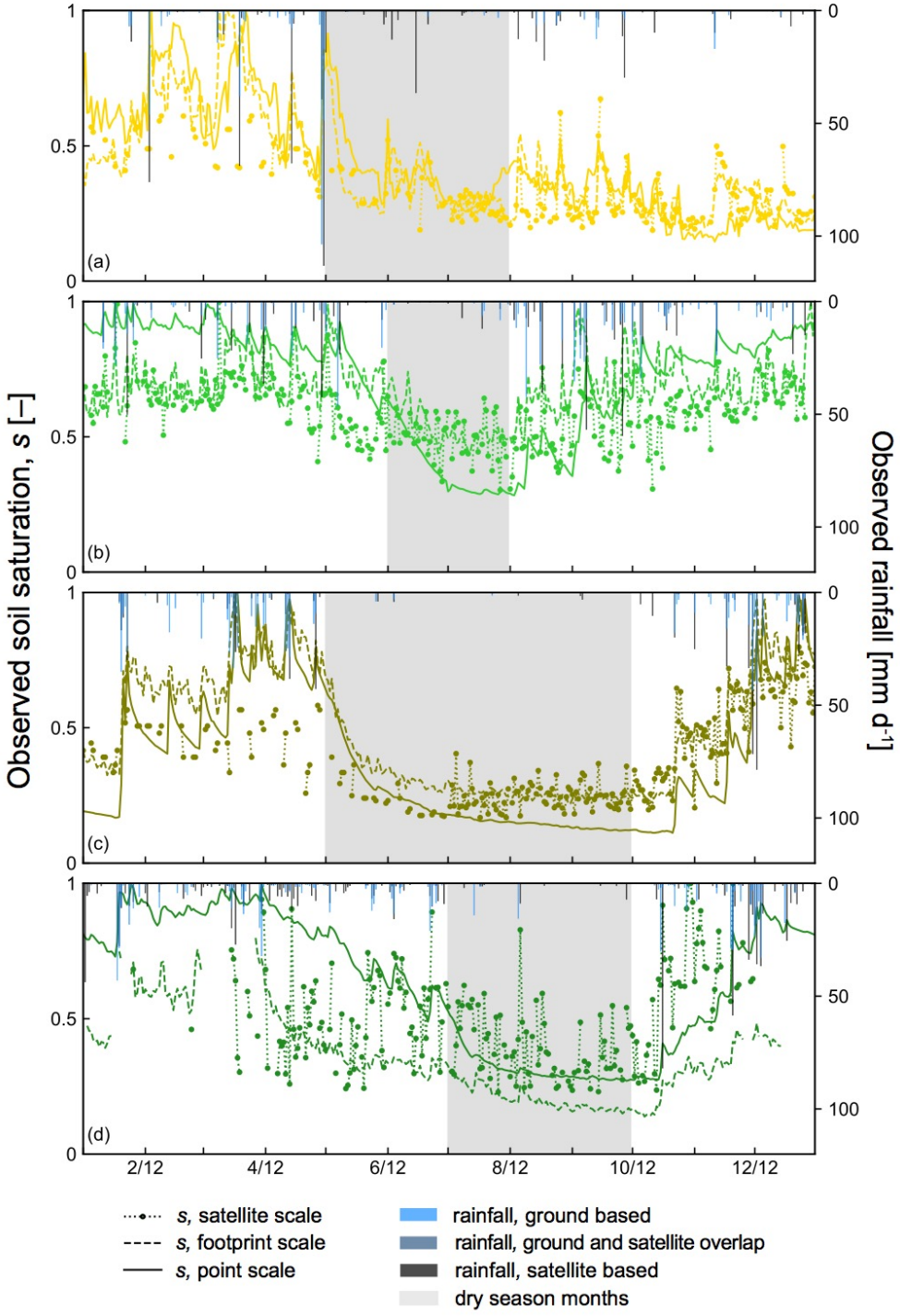

Figure 2.1 Soil saturation and rainfall time series (a) US-ARM, (b) US-MMS, (c) US-Ton, and (d) US-Me2.

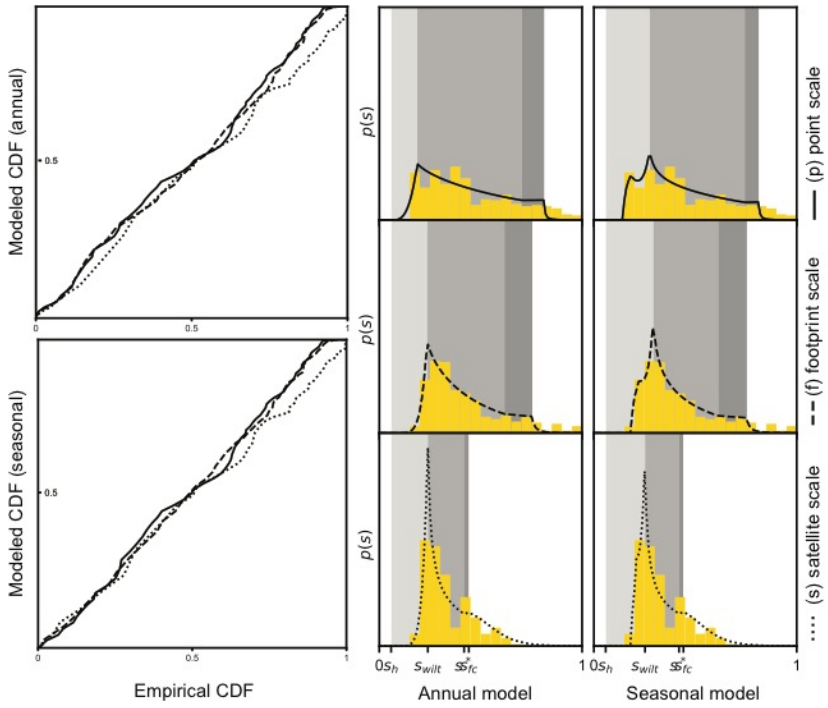

Figure 2.2 Empirical versus modelled cumulative density functions (CDF) and soil saturation probability distribution (p(s)) for US-ARM. The mean values of the posterior parameter distributions were used with the analytical model in Eq (3) in the annual model and Eq (6) in the seasonal model. The grey shaded areas correspond to the soil saturation thresholds (s_h, s_w, s^*, s_{fc}) in the water balance model.

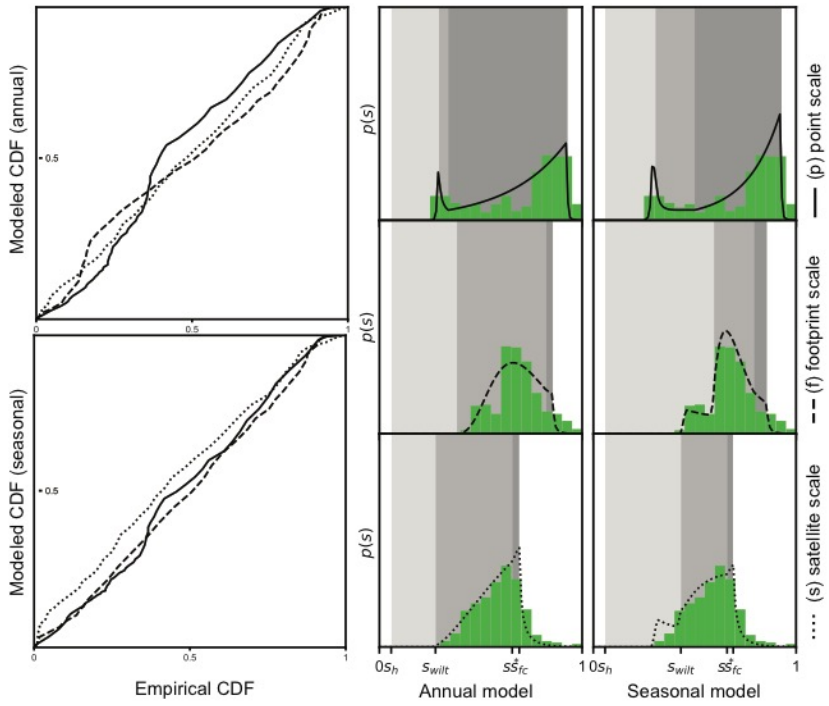

Figure 2.3 Empirical versus modelled cumulative density functions (CDF) and soil saturation probability distribution (p(s)) for US-MMS. The mean values of the posterior parameter distributions were used with the analytical model in Eq. (3) in the annual model and Eq. (6) in the seasonal model. The grey shaded areas correspond to the soil saturation thresholds (s_h, s_w, s^*, s_{fc}) in the water balance model.

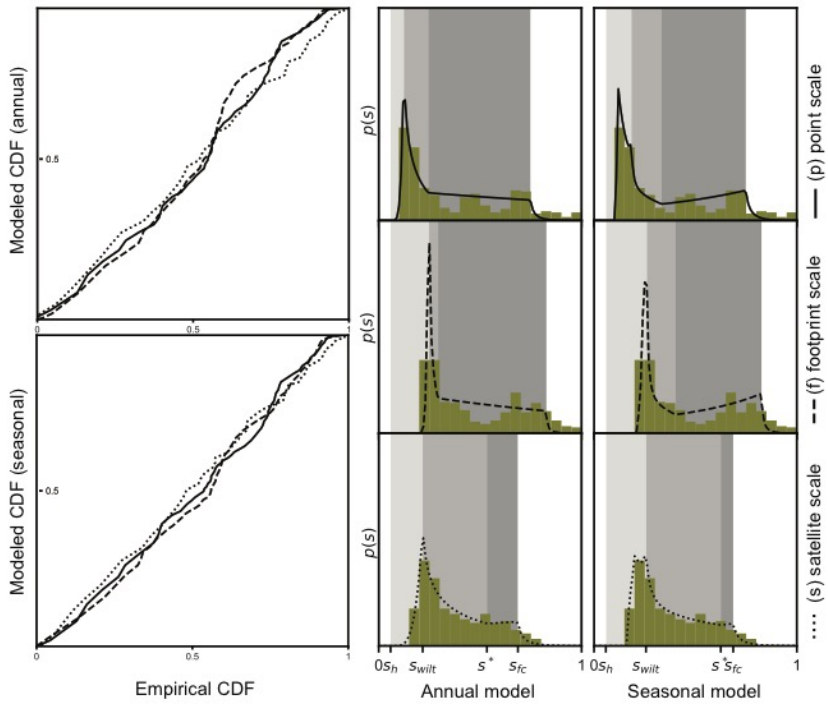

Figure 2.4 Empirical versus modelled cumulative density functions (CDF) and soil saturation probability distribution (p(s)) for US-Ton. The mean values of the posterior parameter distributions were used with the analytical model in Eq (3) in the annual model and Eq (6) in the seasonal model. The grey shaded areas correspond to the soil saturation thresholds (s_h, s_w, s^*, s_{fc}) in the water balance model.

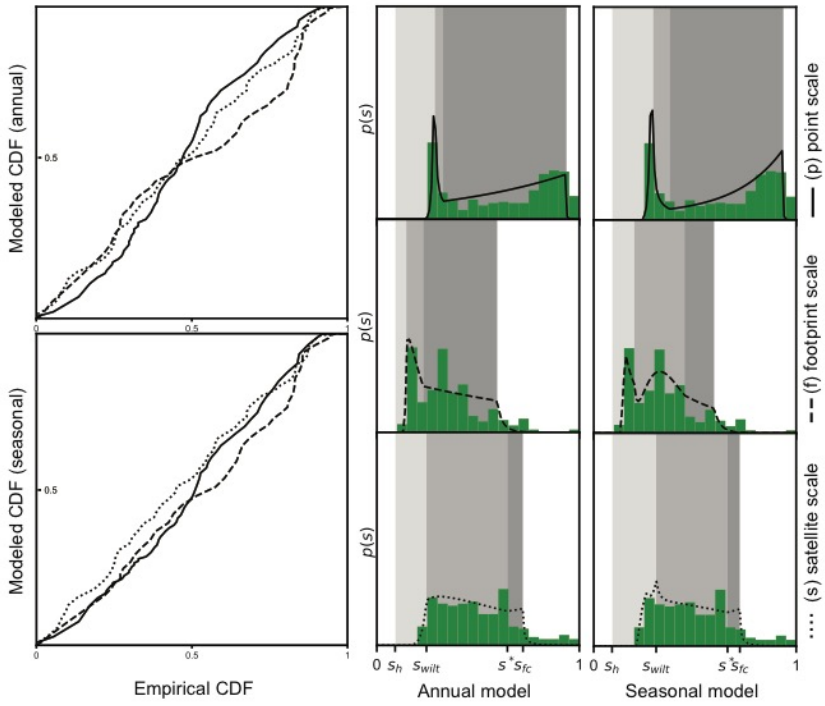

Figure 2.5 Empirical versus modelled cumulative density functions (CDF) and soil saturation probability distribution (p(s)) for US-Me2. The mean values of the posterior parameter distributions were used with the analytical model in Eq (3) in the annual model and Eq (6) in the seasonal model. The grey shaded areas correspond to the soil saturation thresholds (s_h, s_w, s^*, s_{fc}) in the water balance model.

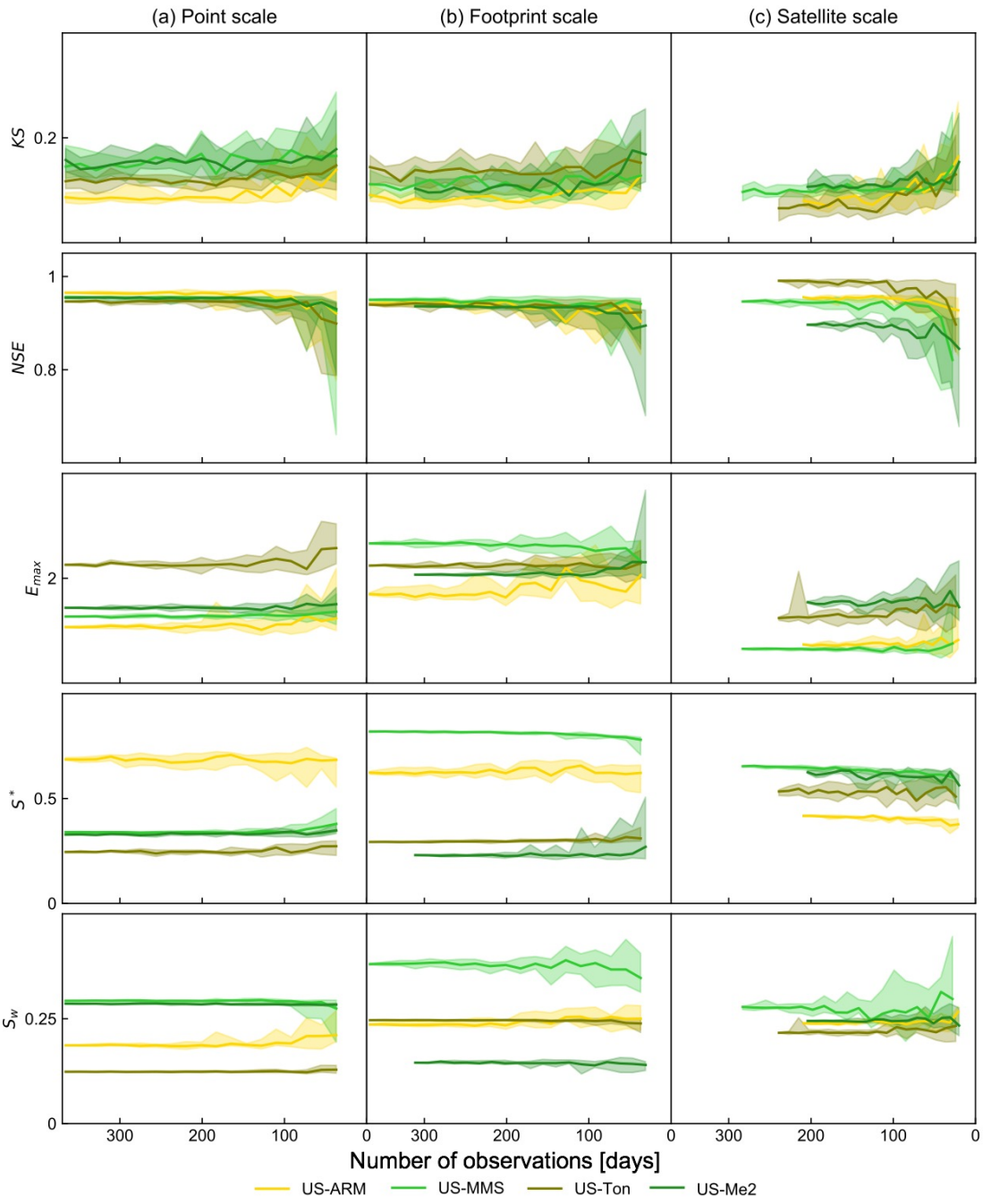

Figure 2.6 Goodness of fit and ecohydrological parameters inferred with decreasing number of soil saturation observations (annual model). For each subsample category, the median results of 10 repeats are plotted and results between the 90th and 10th percentiles are shaded. Colors correspond to the four sites in the legend. KS, Kolmogorov Smirnov statistic; NSE, quantile-level Nash Sutcliffe efficiency; E_{max}, maximum evapotranspiration in mm d^{-1}; s^*, point of incipient stomatal closure; s_w, wilting point.

2.10 Tables

Table 2.1 Selected Study sites

Site Name	ARM Southern Great Plains	Morgan Monroe State Forest	Tonzi Ranch	Metolius Mature Ponderosa Pine
FLUXNET2015 ID	US-ARM	US-MMS	US-Ton	US-ME2
COSMOS ID	15	27	32	38
Latitude	36.6058 (36.625)	39.3232 (39.375)	38.4316 (38.375)	44.4523 (44.375)
Longitude	-97.4888 (-97.375)	-86.4131 (-86.375)	-120.966 (-120.87)	-97.4888 (-97.375)
Elevation [m]	314	275	177	1253
Vegetation	Crops and grassland	Deciduous forest	Oak savanna	Ponderosa pine forest
Soil Texture	Loam	Loam	Loam	Sandy Loam
MAT [°C]	14.8	10.9	15.8	6.3
MAP [mm]	843	1032	559	523
α [mm day^{-1}]	21.0$^{(p, f)}$, 24.4$^{(s)}$	9.04$^{(p, f)}$, 11.8$^{(s)}$	9.3(p, f), 16.9(s)	8.1$^{(p, f)}$, 11.6$^{s)}$
α_w [mm day^{-1}]	21.4$^{(p, f)}$, 26.8$^{(s)}$	9.1$^{(p, f)}$, 11.9$^{(s)}$	8.7(p, f), 16.7(s)	7.9$^{(p, f)}$, 11.6$^{(s)}$
λ [day^{-1}]	0.05$^{(p, f)}$, 0.08$^{(s)}$	0.24$^{(p, f)}$, 0.20$^{(s)}$	0.22(p, f), 0.10(s)	0.24 $^{(p, f)}$, 0.21$^{(s)}$
λ_w [day^{-1}]	0.07$^{(p, f)}$, 0.08$^{(s)}$	0.27$^{(p, f)}$, 0.23$^{(s)}$	0.39(p, f), 0.17(s)	0.31$^{(p, f)}$, 0.27$^{(s)}$
t_d [days]	92	61	153	92
***n* [-]**	0.35$^{(p)}$, 0.34$^{(f)}$, 0.46$^{(s)}$	0.46$^{(p)}$, 0.66$^{(f)}$, 0.43$^{(s)}$	0.53$^{(p)}$, 0.39$^{(f)}$, 0.43$^{(s)}$	0.36$^{(p)}$, 0.59$^{(f)}$, 0.41$^{(s)}$
K_s [mm day^{-1}]	317	317	317	622
***b* [-]**	4.55	4.55	4.55	3.11
s_h [-]	0.06	0.06	0.06	0.09
s_{fc} [-]	0.81$^{(p)}$, 0.75$^{(f)}$, 0.44$^{(s)}$	0.93$^{(p)}$, 0.86$^{(f)}$, 0.69$^{(s)}$	0.75$^{(p)}$, 0.83$^{(f)}$, 0.69$^{(s)}$	0.94$^{(p)}$, 0.60$^{(f)}$, 0.72$^{(s)}$
s_{min} [-]	0.15$^{(p)}$, 0.19$^{(f)}$, 0.19 $^{(s)}$	0.28$^{(p)}$, 0.44$^{(f)}$, 0.30 $^{(s)}$	0.11$^{(p)}$, 0.22$^{(f)}$, 0.17 $^{(s)}$	0.27$^{(p)}$, 0.14$^{(f)}$, 0.23 $^{(s)}$
s_{max} [-]	1.0$^{(p)}$, 1.0$^{(f)}$, 0.67 $^{(s)}$	1.0 $^{(p)}$, 1.0 $^{(f)}$, 1.0 $^{(s)}$	1.0$^{(p)}$, 1.0$^{(f)}$, 0.80 $^{(s)}$	1.0$^{(p)}$, 1.0$^{(f)}$, 1.0$^{(s)}$
Mean *s* [-]	0.44$^{(p)}$, 0.42$^{(f)}$, 0.33 $^{(s)}$	0.71$^{(p)}$, 0.68$^{(f)}$, 0.59 $^{(s)}$	0.38$^{(p)}$, 0.49$^{(f)}$, 0.38 $^{(s)}$	0.64$^{(p)}$, 0.35$^{(f)}$, 0.50 $^{(s)}$
Standard deviation *s* [-]	0.21$^{(p)}$, 0.19$^{(f)}$, 0.11 $^{(s)}$	0.21$^{(p)}$, 0.11$^{(f)}$, 0.12 $^{(s)}$	0.25$^{(p)}$, 0.23$^{(f)}$, 0.17 $^{(s)}$	0.25 $^{(p)}$, 0.16$^{(f)}$, 0.18 $^{(s)}$

Latitude and longitude in parenthesis correspond the centroid of the satellite area associated with the site location; MAT, mean annual temperature from long-term FLUXNET2015 data; MAP, mean annual precipitation from long-term FLUXNET2015 data; soil texture taken from the HWSD; n, porosity; Ks, saturated soil hydraulic conductivity; b, pore size distribution index; sh, hydroscopic point; sfc, field capacity; α, observed average daily rainfall depth in 2012, the subscript w indicates that α was computed for only the wet season months; λ, observed average daily rainfall frequency in 2012, the subscript w indicates that λ was computed for only the wet season months;; td, number of days in the dry season; superscripts (p), (f), and (s) correspond to values used for the point-, footprint-, and satellite scale analysis. Citations for each FLUXNET2015 site: Sebastien Biraud (2002–) AmeriFlux US-ARM ARM Southern Great Plains site-Lamont, 10.17190/AMF/1246027; Kim Novick, Rich Phillips (1999–) AmeriFlux US-MMS Morgan Monroe State Forest, 10.17190/AMF/1246080; Bev Law (2002–) AmeriFlux US-Me2 Metolius mature ponderosa pine, 10.17190/AMF/1246076; Dennis Baldocchi (2001–) AmeriFlux US-Ton Tonzi Ranch, 10.17190/AMF/1245971

Table 2.2 Estimated ecohydrological parameters and goodness of fit of analytical soil saturation pdfs

Site name	Scale	N		NSE		KS		E_{max}		s^*		s_w	
		p	pwd	p	pwd	p	pwd	p	pwd	p	pwd	p	pwd
US-ARM	point	4	4	0.96	0.96	0.07	0.07	1.1 (11)	1.3 (14)	0.7 (8)	0.74 (5)	0.19 (4)	0.27 (7)
	footprint	3	3	0.94	0.94	0.08	0.06	1.7 (11)	2 (12)	0.62 (7)	0.61 (9)	0.24 (3)	0.29 (2)
	satellite	3	3	0.96	0.97	0.08	0.09	0.7 (13)	0.5 (13)	0.42 (4)	0.42 (4)	0.24 (3)	0.25 (2)
US-Ton	point	3	4	0.95	0.97	0.09	0.08	2.3 (4)	1.9 (10)	0.24 (6)	0.33 (7)	0.12 (1)	0.18 (6)
	footprint	3	3	0.94	0.98	0.13	0.08	2.2 (3)	1.8 (8)	0.29 (2)	0.4 (10)	0.25 (0)	0.26 (1)
	satellite	3	9	0.99	0.99	0.06	0.07	1.2 (15)	1 (13)	0.53 (12)	0.62 (6)	0.22 (3)	0.26 (3)
US-MMS	point	3	4	0.96	0.98	0.12	0.08	1.3 (3)	1.1 (6)	0.34 (3)	0.5 (8)	0.29 (0)	0.31 (2)
	footprint	3	3	0.95	0.95	0.13	0.08	2.7 (6)	4.5 (10)	0.82 (2)	0.79 (3)	0.38 (5)	0.59 (1)
	satellite	3	6	0.95	0.88	0.1	0.14	0.7 (8)	0.9 (10)	0.65 (4)	0.66 (3)	0.28 (9)	0.43 (2)
US-Me2	point	3	8	0.95	0.97	0.16	0.1	1.4 (3)	1.1 (7)	0.33 (3)	0.37 (8)	0.29 (0)	0.29 (1)
	footprint	3	6	0.94	0.94	0.09	0.1	2.1 (2)	2.9 (10)	0.23 (4)	0.45 (5)	0.15 (2)	0.2 (6)
	satellite	3	4	0.89	0.89	0.12	0.1	1.6 (12)	1.4 (15)	0.64 (8)	0.66 (8)	0.25 (3)	0.31 (4)

Values in parenthesis correspond to the coefficient of variation of the posterior parameter estimates in percentage. p, analytical model for the soil saturation pdf without seasons, p_{wd}, analytical model for the soil saturation pdf including wet and dry seasons; N, number of 20'000 simulation runs needed to obtain 3 converging results (see Sect. 2.3.2); NSE, quantile-level Nash Sutcliffe efficiency; KS, Kolmogorov Smirnov statistic; $\boldsymbol{E_{max}}$, maximum evapotranspiration in mm d^{-1} (the weighted average wet and dry season $\boldsymbol{E_{max}}$ is reported for the p_{wd} model) ; s^*, point of incipient stomatal closure; s_w, wilting point.

3 Global Variation in Thresholds of Soil Water Uptake

Maoya Bassiouni[1], Stephen P Good[1], Christopher J Still[2], and Chad W Higgins[1]

[1]Department of Biological and Ecological Engineering, Oregon State University, Corvallis, OR 97333, USA. [2]Department of Forest Ecosystems & Society, Oregon State University, Corvallis, OR 97333, USA

3.1 Abstract

Many contemporary models use empirical functions with constant soil water potentials to parameterize soil water stress. We infer global spatial patterns in soil water potentials at which no soil water uptake occurs; soil water potentials at which downregulation of uptake occurs; and maximum soil water uptake. We estimate thresholds, consistent with satellite surface soil moisture, through Bayesian inference using a stochastic water balance. Results improve global median Nash–Sutcliffe efficiency between empirical and theoretical soil moisture probability distributions from 0.46 using reference constants to 0.65 and 0.90 using median inferred thresholds per biome and spatially variable inferred thresholds. Spatially variable thresholds capture location-specific vegetation and climate characteristic and reflect diversity in biome-level water uptake strategies. Results demonstrate that satellite observations encode valuable ecophysiological information, critical to understanding ecosystem resilience to climate variability.

3.2 Plain language summary

Vegetation regulates a large fraction of the terrestrial water and carbon cycles, as it adapts to changing environmental conditions such as soil moisture availability, yet our ability to characterize diversity in vegetation soil water use behavior at large scales is limited. In this study, we analyze global satellite observations to estimate soil moisture thresholds that are commonly used to approximate when vegetation extracts water from the surface soil. We show that the newly found thresholds are more consistent with global patterns of soil moisture compared to using constant thresholds found in the literature. Spatially variable thresholds reflect landcover and climate characteristics and can be used to describe variability in biome-level water use strategies.

3.3 Introduction

Transpiration is the most important pathway by which water moves from the land back to the atmosphere (Good et al., 2015), and vegetation regulates terrestrial water and carbon cycles as it adapts to changing environmental conditions such as soil moisture availability. The driving force moving water from soils, through plant tissue, and to the atmosphere is the gradient in potential energy state of water. Soil water potentials bound water transport through plants: the soil moisture state when stomata are fully open and soil water uptake is at its maximum, and the soil moisture state when stomata are fully closed, after which soil water uptake is zero. These thresholds have been incorporated into soil water-stress functions associated with evapotranspiration and have been used in many hydrological (Laio et al., 2001; Westenbroek, 2018), agricultural (Hlavinka et al., 2011; Steduto et al., 2009) and earth system (Niu et al., 2011; Oleson et al., 2013) models. Our goal is to use satellite observations to provide biome-scale constraints on these critical parameters.

Contemporary applications routinely parameterize critical soil water potentials as constant potentials because spatially variable values, which account for diversity of plant responses to environmental stress, are generally unavailable. For example, the soil moisture threshold at which soil water uptake is zero, often termed wilting point, is commonly set to -1.5 MPa. This value was determined experimentally (Richards & Weaver, 1944) based on observations of leaf vigor; however, visible plant phenological changes, such as wilting, may not coincide with soil moisture thresholds that are most relevant to soil water balance, such as when roots stop extracting soil water. Empirical water-stress functions used in many biosphere models with reference constants are generally unable to realistically represent effects of soil moisture on stomatal conductance (Fatichi et al., 2016; Powell et al., 2013). Furthermore, soil moisture-limited productivity, occurring any time stomata are not fully open, represents a large and uncertain component of the simulated terrestrial carbon cycle (Trugman et al., 2018). Recent efforts have shown that soil water thresholds drive sensitivity of flux estimates in earth system models (Arsenault et al., 2018) and that calibrating wilting points to be consistent with observed spatial patterns in soil moisture improves simulations of gross primary production (Qiu et al., 2018).

Plant resilience and response to environmental stress is governed by complex and diverse plant hydraulic traits (Anderegg et al., 2016; Skelton et al., 2015), which are expected to vary depending on vegetation type, hydroclimatic conditions, ecosystem diversity, and scale. Plant hydraulic strategies vary along a continuum from drought-avoidant to drought-tolerant. Drought-avoidant plants favor water conservation with strict stomatal closure in response to drying soil conditions. Drought-tolerant plants continue to assimilate carbon and maintain high stomatal conductance even as soils dry (Fu & Meinzer, 2019). The relation between stomatal behavior and soil moisture may also be influenced by vapor pressure deficit, which implies that soil water uptake is lower than potential evapotranspiration in arid climates even at high soil moisture states (Li et al., 2018; Novick et al., 2016). Plants also adapt to rainfall stochasticity

and range between extensive and intensive water use strategies. Plants with extensive water use strategies, are usually deep-rooted and extract soil water over a larger range of soil moisture states, whereas intensive water users are usually shallow-rooted and respond quickly to short soil water pulses (Rodriguez-Iturbe et al., 2001). Simulations show that water and carbon fluxes are sensitive to diversity in plant traits (Pappas et al., 2016), but ecosystem-scale hydraulic behavior, resulting from coexistence of diverse species, is uncertain.

We address the need to distinguish spatial patterns of thresholds of soil water uptake using global satellite-based observations, which capture location-specific vegetation and climate characteristics. Remotely sensed observations have been used to identify broad spatial patterns of plant hydraulic behavior and response to water stress beyond the species level and across biogeographic regions (Feldman et al., 2018; Konings & Gentine, 2017); however, these efforts have been focused on vegetation canopy water content and do not fully capture complex processes associated with soil water uptake by plants. Thresholds of soil water uptake alone do not fully represent complex plant water use behaviors, however, large-scale estimates of thresholds of soil water uptake, consistent with soil moisture observations, may improve application of simple empirical soil water-stress functions still widely used in biosphere models.

Global soil moisture observations are available through NASA's Soil Moisture Active Passive (SMAP) mission (Entekhabi et al., 2010) and offer opportunities to diagnose satellite-scale ecohydrological processes (Feldman et al., 2018; McColl et al., 2017). Soil moisture observed from satellites tracks large-scale spatial and temporal variability of soil moisture and reflects variability in dominant land surface processes. The shape of local soil moisture probability distributions ($p(s)$) are constrained by ecohydrological characteristics, and a parsimonious theoretical model of $p(s)$ can be inverted to estimate ecohydrological thresholds (Bassiouni et al., 2018). This simple inverse modeling framework may not fully characterize complexity of plant hydraulic behavior; however, the framework overcomes some limitations of process-based models (Massoud et al., 2019) and satellite-scale data because it requires few parameters, does not require concurrent time series of hydroclimatic variables, is not affected by gaps in soil moisture observations (Bassiouni et al., 2018), and has relatively low computational cost. This inverse modeling approach only requires soil moisture observations, rainfall characteristics, and soil texture information and is consistent with the most commonly used soil water-stress frameworks. The model inversion results are therefore estimates of plant soil water uptake behavior and response to soil water stress, which are independent of vegetation data. Remote sensing-derived thresholds of soil water uptake may not be directly comparable to point-scale ground-level measurements because they reflect grid-scale processes encoded in satellite observations (Bassiouni et al., 2018), however, they may be more appropriate to describe vegetation processes relevant to large-scale models, or at least provide a new constraint on soil water-stress equations used in such models.

The focus of this study is to determine global values of ecohydrological thresholds that best fit empirical $p(s)$ derived from satellite soil moisture observations. Our goal is to estimate thresholds that are relevant to soil water-stress frameworks most commonly used to model evapotranspiration. We compare empirical $p(s)$ derived from satellite observations to theoretical $p(s)$ using both reference constants found in hydrologic literature and inferred spatially variable thresholds. We describe global variability in thresholds of soil water uptake by vegetation type and climate aridity. Finally, we summarize global trends in inferred ecohydrological characteristics and biome-scale plant water uptake strategies.

3.4 Data

We conduct all analysis at a spatial resolution of 36 km^2 (EASE-Grid 2.0) and over a 3-year period spanning April 2015 to March 2018. Surface soil moisture observations and climate variable estimates are available from NASA's SMAP mission (Entekhabi et al., 2010). We use global daily 36 km SMAP L3 (Version 5) radiometer soil moisture at about 5 cm depth (O'Neill et al., 2016). We only analyze observations flagged as recommended by the data product, which are not affected by water bodies, dense vegetation, frozen soil, and radio frequency interference. Thus, our analysis is mainly confined to temperate and tropical biomes that have less than 60 % woody vegetation, are dominated by shrub or herbaceous vegetation, or are sparsely vegetated and represent about 50 % of total global terrestrial surface. We use global 3-hourly 9 km SMAP L4 (Version 4) geophysical data (Reichle et al., 2017) to characterize average daily rainfall depth and frequency, average daily rate of potential evaporation (E_p) and aridity index (AI) at each grid cell over the 3-year study period. We use global soil hydraulic parameters at 5 cm soil depth available at a spatial resolution of 0.25° (Montzka et al., 2017) and re-gridded to 36 km EASE-Grid 2.0. We use the International Geosphere-Biosphere Programme (IGBP) land cover classification to characterize the biome of each grid cell (Kim, 2013).

3.5 Estimation of ecohydrological thresholds

We estimate ecohydrological thresholds for each grid cell with at least 365 daily SMAP L3 soil water content observations over the 3-year study period: soil saturation at the point of incipient stomatal closure (s^*) and associated soil water potential at which downregulation of surface soil water uptake occurs (Ψ_1); soil saturation at the wilting point (s_w) and associated soil water potential at which no surface soil water uptake occurs (Ψ_0); maximum rate surface soil water uptake or evapotranspiration (E_{max}); and rate of surface soil water uptake at the wilting point (E_w). We use the Mulalem-van Genuchten equation (Montzka et al., 2017) to convert between soil saturation and soil water potential and provide a more universal measure to compare soil water use strategies between locations. In the subsequent text, we

avoid terms ‘point of incipient stomatal closure’ and ‘wilting point’ because our focus is on soil moisture dynamics rather than canopy phenology.

We infer ecohydrological thresholds by inverting an analytical formulation of $p(s)$, derived from a commonly used stochastic soil water balance framework (Laio et al., 2001), within a Bayesian inference framework using SMAP data and a Metropolis-Hastings Markov chain Monte Carlo algorithm (Bassiouni et al., 2018). We assume that the 1-dimensional soil water balance at each grid cell can be modeled as a point and do not account for seasonality in stochastic rainfall characteristics. It is possible to perform the model inversion accounting for climate seasonality; however, the tradeoff for increased model complexity and thus computational time has been shown to not significantly improve goodness-of-fit and parameter identifiability (Bassiouni et al., 2018). We define the equation for $p(s)$ and all model parameters in Text S1. We determine that the model inversion converges when the Gelman-Rubin diagnostics (Gelman & Rubin, 1992) associated with all four unknown parameters are inferior to 1.1. We only analyze results, which have converged to reduce some but not all concerns of equifinality, where different parameter combinations emerge with high goodness-of-fit, while being less physically meaningful. We evaluate goodness-of-fit between empirical $p(s)$ and theoretical $p(s)$ using a quantile-level Nash–Sutcliffe efficiency (NSE) (Müller et al., 2014). We calculate NSE using both best-fit thresholds resulting from the model inversion (mean values of posteriori parameter estimates) and reference constants (Ψ_0 = -1.5 MPa; Ψ_1 = -0.033 MPa; $E_{max} = E_p$; $E_w = 0$).

3.6 Results and discussion

3.6.1 Global estimates of ecohydrological thresholds

Inferred thresholds Ψ_0, Ψ_1, and E_{max}/E_p (Figure 3.1a-c) are consistent with empirical $p(s)$ derived from SMAP surface soil moisture observations and are highly variable globally. We thus explore whether these patterns may reflect diversity in biome soil water uptake strategies and how they relate to vegetation type and climate.

Global median goodness-of-fit between empirical and theoretical $p(s)$, using quantile-level NSE is 0.90. Only locations for which NSE >0.5 are included in subsequent analyses. The coefficient of variation of posteriori parameter estimates is a measure of uncertainty we derive from the Bayesian inversion approach and median coefficients of variation are 2-, 5-, 7-, and 9-percent for s_w, s^*, E_{max}, and E_w, respectively. Ecohydrological thresholds for the most humid and most arid locations either do not converge or provide poor goodness-of-fit with empirical $p(s)$ (Figure 3.1d) likely because soil moisture observations at these locations do not span the full range of values between soil saturation and the point of no water uptake.

Inferred thresholds improve goodness-of-fit between observed and theoretical $p(s)$ (Figure 3.1e), compared to using reference constants. Global median NSE between empirical and theoretical $p(s)$ using these reference constants is 0.46. Modeled $p(s)$ using reference constants did not characterize observed $p(s)$ in many of the most arid regions of the world and characterized observed $p(s)$ best in North American grasslands and European croplands.

3.6.2 Variability in ecohydrological thresholds by vegetation type

We summarize ecohydrological thresholds using IGBP land cover classification to explore variability in water uptake strategies by biome (Figure 3.2). Global median NSE between empirical and theoretical $p(s)$ using median inferred thresholds for each IGBP class is 0.65. Median ecohydrological thresholds for each IGBP class inferred from global satellite soil moisture observations (Table 3.S1) may therefore be an improvement over reference constants, although variability in thresholds within each biome is large.

Median Ψ_0 is most negative for grasslands and open shrublands and least negative for woody savannas, savannas, and barren landscapes (Figure 3.2a). Grasslands and open shrublands extract water across a larger range of soil moisture states compared to savannas and woody savannas. This implies that temperate grasslands, which are usually dominated by C3 grasses, and open shrublands have the most extensive water uptake strategies, while savannas and woody savannas, which are dominated by C4 grasses, have more intensive water uptake strategies.

Median Ψ_1 is similar for all IGBP classes. It is most negative for grasslands, savannas, and barren landscapes and least negative for croplands (Figure 3.2b). Grasslands and savannas can withdraw soil water at a maximum rate at drier soil moisture states than do croplands. This implies that grasslands and savannas, whose ground layer is dominated by herbaceous vegetation, have a risky soil water uptake strategy compared to croplands which are often irrigated in temperate regions.

Median E_{max}/E_p is about 0.9 for grasslands and barren landscapes and about 0.5 for savannas and woody savannas (Figure 3.2c). Savannas and woody savannas have a more conservative water use strategy than grasslands and open shrublands, because the maximum rate of soil water uptake is relatively lower for savannas and woody savannas. Evapotranspiration is generally more coupled with atmospheric demand in aerodynamically smooth systems such as grasslands, whereas evapotranspiration is more coupled with stomatal conductance in aerodynamically rougher systems such as savannas and woody savannas, (Jarvis & Mcnaughton, 1986; Peng et al., 2019). In addition, C4 grasses, which are most abundant in savannas and woody savannas, tend to have higher water use efficiency compared to other plant functional types and often occur in hot and water-limited environments (Still et al., 2003).

While our results show that grasslands and open shrublands can extract moisture from drier soils than savannas and woody savannas, this does not imply that grasslands are less vulnerable to hydraulic failure than other biomes. Savannas and woody savannas are abundant in tropical hot environments and most often these are semi-arid or seasonally dry locations, whereas pure grasslands are more of a temperate and arctic phenomenon. Water potential in plant leaves coinciding with Ψ_0, which drives stomatal closure, may be much more negative for plants in savannas than in grasslands because the air is hotter and drier than in grasslands. Leaf-to-air vapor pressure gradient may be much larger in savannas than in grasslands although Ψ_0 is less negative. This may be a reason why grasslands are the biome for which inferred thresholds are closest to reference constants, which are based on observations made in temperate climates (Richards & Weaver, 1944).

Whole-plant transpiration is expected to stop when all soil layers in the rooting zone have dried past the critical soil water potential, and at this time surface soil moisture, sensed by SMAP, is generally much lower than deeper layers. This could be a reason why the canonical permanent wilting point value of -1.5 MPa, which is based on plant vigor when soil water uptake is zero in all layers, is more negative than our inferred Ψ_0 values. However, it is unknown whether root tissues stop uptake in their respective layers at similar soil moisture potentials. Prior satellite estimates of soil moisture thresholds at which vegetation water content decreases correspond to more negative soil water potentials than those found in this study (Feldman et al., 2018). Soil moisture thresholds estimated here are associated with plant stomatal control only in so far as they influence surface soil water uptake and may not capture physiological behavior of the entire plant.

3.6.3 Relation between ecohydrological thresholds and aridity

Variability of ecohydrological thresholds within each IGBP class may reflect soil water uptake strategy responses or adaptations to local environmental conditions. Stomatal conductance generally decreases exponentially with increasing vapor pressure deficit (Oren et al., 1999) and research shows that atmospheric water stress affects plant stomatal control and reduces evapotranspiration even when soil moisture is not limited (Novick et al., 2016). Aridity index (*AI*), defined as the ratio of potential evaporation to total annual precipitation, is used in this study to investigate general spatial patterns in water uptake strategies with climate.

Trends between $|\Psi_0|$ and *AI* are positive for woody savannas and crop and natural vegetation mosaic; negative for barren landscapes, crops and open shrublands; about null for savannas and grasslands; and overall strongest for woody savannas (Figure 3.2d, Table 3.S2). Woody savannas and crop and natural vegetation mosaic increase the range of soil moisture states for which they extract water from surface soil as climate conditions become more arid. This implies that water uptake strategies for biomes with

up to 60% woody vegetation (Kim, 2013) tend to be more extensive as aridity increases, which is consistent with deeper rooting patterns and switching uptake to deeper soil water reserves in woody plants (Holdo & Nippert, 2015).

Trends between $|\Psi_1|$ and *AI* are negative for savannas, woody savannas, and grasslands; positive for open shrublands, croplands and crop and natural vegetation mosaic; and overall strongest for savannas (Figure 3.2e, Table 3.S2). Grasslands, savannas, and woody savannas decrease the range of soil moisture states at which they uptake water at a maximum rate as climate conditions become more arid. This implies that water uptake strategies for biomes dominated by herbaceous vegetation tend to adapt and become less risky as aridity increases, whereas open shrublands, croplands, and crop and natural vegetation mosaic tend to be riskier. Such patterns are consistent with anisohydric behavior, which is more common in arid shrublands and croplands (Fu & Meinzer, 2019; Konings & Gentine, 2017).

Trends between E_{max}/E_p and *AI* are negative for all biomes except for grasslands and strongest for open shrublands (Figure 3.2f, Table 3.S2). Grasslands are the only biome in which vegetation consistently uptakes soil water at a rate close to potential evaporation even in arid climates. When conditions are energy versus water limited ($AI < 1$) grasslands tend to increase E_{max}/E_p. Such patterns for grasslands reflect behavior of aerodynamically uncoupled land covers (Jarvis & Mcnaughton, 1986).

3.6.4 Trends in soil water uptake and stress with aridity

The combined effect of each of the ecohydrological thresholds adaptation to aridity may result in an overall expansion or reduction in vegetation capacity to uptake soil water. Plants make tradeoffs between carbon assimilation and water conservation (Skelton et al., 2015) and need to balance soil water uptake and stress. We thus combine these contrasting dynamics in a soil water uptake index that is normalized by precipitation and weighted by stress (ε) (Text S2) (Manfreda et al., 2017) to evaluate soil water uptake responses to aridity for each biome. A biome's water uptake strategy may expand or reduce vegetation soil water uptake with increased stress. Trends between ε and *AI* represents biome resilience to water-limited conditions.

Soil moisture stress increases with increasing *AI* across all biomes. This trend is greater for humid biomes than dry biomes, steepest for croplands and least steep for open shrublands (Figure 3.S1a, Table 3.S2). Normalized soil water uptake also increases with increasing *AI* across all biomes, as a larger fraction of incoming precipitation is partitioned into evapotranspiration. This trend is steepest for woody savannas and savannas and least steep for croplands (Figure 3.S1b, Table 3.S2). Trends between ε and *AI* are positive for woody savannas, savannas, open shrublands, and crop and natural vegetation mosaic; negative for bare soils and croplands; and positive for humid grasslands but negative for dry grasslands (Figure 3.3a, Table 3.S2).

Patterns in soil water uptake are considerably different when reference constants are used instead of inferred thresholds (Figure 3.3a). Reference constants are unable to realistically characterize soil water uptake because soil water uptake exceeds available water at $AI > 5$ (Figure 3.S1b). Median ε is about 0.5 for $AI < 4$ and increases steeply at $AI > 4$. This is a direct consequence of inconsistency of reference constants with empirical $p(s)$ (Figure 3.1e). Empirical water-stress functions used in many biosphere models with reference constants are also unable to realistically represent effects of soil moisture on stomatal conductance (Fatichi et al., 2016; Powell et al., 2013). Many leaf-level stomatal conductance models, which do not adequately account for stomatal sensitivity to declining soil water potential, are also biased toward over predicting stomatal conductance during dry conditions (Anderegg et al., 2017).

3.6.5 Global biome water uptake strategies

The geographic distribution of plant species is largely driven by vegetation sensitivity to drought (Engelbrecht et al., 2007). Theory suggests that plants become more water efficient as water becomes scarce (Troch et al., 2009). Plant species with trait plasticity produce phenotypes adapted outside their optimal environments (Sultan, 2000), and can withstand a larger range of climates, but sometimes also trade off overall lower efficiency compared to specialized plants in their optimal climate.

We quantify ecohydrological adaptation ($\partial X/\partial AI$) of a biome as the relative variation of each ecohydrological threshold (X) associated with a relative variation in aridity. A positive ecohydrological adaptation indicates that the absolute value of ecohydrological thresholds increases with aridity. This corresponds to an increase in vegetation capacity to uptake soil water as conditions become less favorable to soil water uptake. We quantify ecohydrological resilience ($\partial\varepsilon/\partial AI$) as the relative variation of ε, associated with a relative variation in AI. A positive ecohydrological resilience indicates that a greater fraction of available water, weighted by stress, is extracted from surface soil as climatic conditions become more arid. We relate ecohydrological adaptation with ecohydrological resilience to compare and interpret inferred ecosystem water uptake strategies (Figure 3.3b).

Our results indicate that woody savannas and savannas have the most resilient water uptake strategies. Woody savannas and savannas may be more effective at taking up soil water in arid conditions compared to other biomes because the combination of individual ecohydrological threshold adaptations with AI results in an overall expansion of plant capacity to uptake surface soil water. In contrast, our results show that ecohydrological thresholds associated with grasslands dominated by C3 grasses are less variable with climate, and grasslands are overall less resilient to water stress. Plant species, which are specialized at using resources in a particular climate, can experience greater stress in climatic conditions outside their optimal range (Sultan, 2000). Ecohydrological resilience is negative for croplands and barren landscapes, suggesting water uptake strategies that do not withstand increasingly arid conditions and

compromise their capacity to uptake surface soil moisture. Our results indicate that water uptake strategies in arid locations are generally more drought resilient. This is consistent with species-level studies of plant isohydricity (Fu & Meinzer, 2019; Li et al., 2018), although this trend is more uncertain in previous global studies (Konings & Gentine, 2017).

We compare vegetation sensitivity to water availability at the biome-level based on *AI,* although spatial distribution of species-level drought sensitivity within a biome and between ecosystems in a biome may vary significantly. We acknowledge that *AI* only captures a small portion of spatial variability in ecohydrological thresholds and there are many other factors that affect thresholds which are often also correlated with *AI.* The non-parametric approach we apply to calculate ecohydrological adaptation and resilience (Text S3) assumes that effects of such factors within a biome or cross-sectional sample is constant. Additional exploration of ecohydrological thresholds can be done when a longer time series of SMAP data is available. For example, pooling data both in space and in time with additional climate and land surface characteristics may provide causal inferences about vegetation drought sensitivity and disentangle variability both within and between each location instead of broadly by biome.

3.7 Conclusions

We provide ecohydrological thresholds consistent with observed probability distributions of satellite soil moisture and a parsimonious soil water balance model. Inferred thresholds integrate grid-scale surface soil water uptake dynamics from satellite soil moisture observations, capture location-specific land cover and climate characteristics, and reflect diversity in water uptake strategies among major global biomes. Critical soil water potentials derived from soil moisture states may be more applicable to water balance equations than those correlated with observable plant phenological change. Our results improve commonly used empirical relations between soil moisture stress and soil water uptake at large scales compared to using reference constants. Further research is needed to apply ecohydrological thresholds inferred from satellite observations in hydrological and earth system models and to evaluate their performance. Critical soil water potentials estimated in this study are associated with surface soil moisture dynamics, and their relation to total biome evapotranspiration or soil water uptake in the full rooting zone remains uncertain. Further research is necessary to determine whether critical soil water potentials inferred from surface soil moisture are different than those associated with deeper soil layers. Our approach provides a novel framework for connecting plant physiological behavior with soil-water dynamics that can enhance understanding of vegetation resilience under varying climatic conditions.

3.8 Data and code

Results, datasets, and code are publicly available: Global maps of ecohydrological parameters (http://doi.org/10.5281/zenodo.3351623); SMAP (https://doi.org/10.5067/ZX7YX2Y2LHEB, https://doi.org/10.5067/KPJNN2GI1DQR, https://doi.org/10.5067/KGLC3UH4TMAQ); soil hydraulic parameters (https://doi.pangaea.de/10.1594/PANGAEA.870605); inverse modelling of soil saturation probability distributions (https://doi.org/10.5281/zenodo.1257718); data processing scripts (https://doi.org/10.5281/zenodo.3235820).

3.9 Acknowledgments

We acknowledge support from the NSF Graduate Research Fellowship (1314109-DGE), NASA (NNX16AN13G), and XSEDE allocation DEB160018, which is supported by NSF (ACI-1548562).

3.10 References

Anderegg, W. R. L., Klein, T., Bartlett, M., Sack, L., Pellegrini, A. F. A., Choat, B., & Jansen, S. (2016). Meta-analysis reveals that hydraulic traits explain cross-species patterns of drought-induced tree mortality across the globe. Proceedings of the National Academy of Sciences, 113(18), 5024–5029. https://doi.org/10.1073/pnas.1525678113

Anderegg, W. R. L., Wolf, A., Arango-Velez, A., Choat, B., Chmura, D. J., Jansen, S., et al. (2017). Plant water potential improves prediction of empirical stomatal models. PLOS ONE, 12(10), e0185481. https://doi.org/10.1371/journal.pone.0185481

Arsenault, K. R., Nearing, G. S., Wang, S., Yatheendradas, S., & Peters-Lidard, C. D. (2018). Parameter Sensitivity of the Noah-MP Land Surface Model with Dynamic Vegetation. Journal of Hydrometeorology, 19(5), 815–830. https://doi.org/10.1175/jhm-d-17-0205.1

Bassiouni, M., Higgins, C. W., Still, C. J., & Good, S. P. (2018). Probabilistic inference of ecohydrological parameters using observations from point to satellite scales. Hydrology and Earth System Sciences, 22(6), 3229–3243. https://doi.org/10.5194/hess-22-3229-2018

Engelbrecht, B. M. J., Comita, L. S., Condit, R., Kursar, T. A., Tyree, M. T., Turner, B. L., & Hubbell, S. P. (2007). Drought sensitivity shapes species distribution patterns in tropical forests. Nature, 447(7140), 80–82. https://doi.org/10.1038/nature05747

Entekhabi, D., Njoku, E. G., O'Neill, P. E., Kellogg, K. H., Crow, W. T., Edelstein, W. N., et al. (2010). The Soil Moisture Active Passive (SMAP) Mission. Proceedings of the IEEE, 98(5), 704–716. https://doi.org/10.1109/JPROC.2010.2043918

Fatichi, S., Pappas, C., & Ivanov, V. Y. (2016). Modeling plant-water interactions: an ecohydrological overview from the cell to the global scale: Modeling plant-water interactions. Wiley Interdisciplinary Reviews: Water, 3(3), 327–368. https://doi.org/10.1002/wat2.1125

Feldman, A. F., Short Gianotti, D. J., Konings, A. G., McColl, K. A., Akbar, R., Salvucci, G. D., & Entekhabi, D. (2018). Moisture pulse-reserve in the soil-plant continuum observed across biomes. Nature Plants, 4(12), 1026–1033. https://doi.org/10.1038/s41477-018-0304-9

Fu, X., & Meinzer, F. C. (2019). Metrics and proxies for stringency of regulation of plant water status (iso/anisohydry): a global data set reveals coordination and trade-offs among water transport traits. Tree Physiology, 39(1), 122–134. https://doi.org/10.1093/treephys/tpy087

Gelman, A., & Rubin, D. B. (1992). Inference from iterative simulation using multiple sequences. Statistical Science, 457–472.

Good, S. P., Noone, D., & Bowen, G. (2015). Hydrologic connectivity constrains partitioning of global terrestrial water fluxes. Science, 349(6244), 175–177.

Hlavinka, P., Trnka, M., Balek, J., Semerádová, D., Hayes, M., Svoboda, M., et al. (2011). Development and evaluation of the SoilClim model for water balance and soil climate estimates. Agricultural Water Management, 98(8), 1249–1261. https://doi.org/10.1016/j.agwat.2011.03.011

Holdo, R. M., & Nippert, J. B. (2015). Transpiration dynamics support resource partitioning in African savanna trees and grasses. Ecology, 96(6), 1466–1472. https://doi.org/10.1890/14-1986.1

Jarvis, P. G., & Mcnaughton, K. G. (1986). Stornatal Control of Transpiration: Scaling Up from Leaf' to Region, 49.

Kim, S. (2013). Ancillary Data Report: Landcover Classification. Pasadena, CA: Jet Propulsion.

Konings, A. G., & Gentine, P. (2017). Global variations in ecosystem-scale isohydricity. Global Change Biology, 23(2), 891–905. https://doi.org/10.1111/gcb.13389

Laio, F., Porporato, A., Ridolfi, L., & Rodriguez-Iturbe, I. (2001). Plants in water-controlled ecosystems: active role in hydrologic processes and response to water stress: II. Probabilistic soil moisture dynamics. Advances in Water Resources, 24(7), 707–723.

Li, X., Blackman, C. J., Choat, B., Duursma, R. A., Rymer, P. D., Medlyn, B. E., & Tissue, D. T. (2018). Tree hydraulic traits are coordinated and strongly linked to climate-of-origin across a rainfall gradient: Hydraulic traits coordination and link to climate. Plant, Cell & Environment, 41(3), 646–660. https://doi.org/10.1111/pce.13129

Manfreda, S., Caylor, K. K., & Good, S. P. (2017). An ecohydrological framework to explain shifts in vegetation organization across climatological gradients: Vegetation pattern in dry environments. Ecohydrology, 10(3), e1809. https://doi.org/10.1002/eco.1809

Massoud, E. C., Purdy, A. J., Christoffersen, B. O., Santiago, L. S., & Xu, C. (2019). Bayesian inference of hydraulic properties in and around a white fir using a process-based ecohydrologic model. Environmental Modelling & Software, 115, 76–85. https://doi.org/10.1016/j.envsoft.2019.01.022

McColl, K. A., Wang, W., Peng, B., Akbar, R., Short Gianotti, D. J., Lu, H., et al. (2017). Global characterization of surface soil moisture drydowns: Geophysical Research Letters, 44(8), 3682–3690. https://doi.org/10.1002/2017GL072819

Montzka, C., Herbst, M., Weihermüller, L., Verhoef, A., & Vereecken, H. (2017). A global data set of soil hydraulic properties and sub-grid variability of soil water retention and hydraulic conductivity curves. Earth System Science Data, 9(2), 529–543.

Müller, M. F., Dralle, D. N., & Thompson, S. E. (2014). Analytical model for flow duration curves in seasonally dry climates. Water Resources Research, 50(7), 5510–5531.

Niu, G.-Y., Yang, Z.-L., Mitchell, K. E., Chen, F., Ek, M. B., Barlage, M., et al. (2011). The community Noah land surface model with multiparameterization options (Noah-MP): 1. Model description and evaluation with local-scale measurements. Journal of Geophysical Research, 116(D12). https://doi.org/10.1029/2010JD015139

Novick, K. A., Ficklin, D. L., Stoy, P. C., Williams, C. A., Bohrer, G., Oishi, A. C., et al. (2016). The increasing importance of atmospheric demand for ecosystem water and carbon fluxes. Nature Climate Change, 6(11), 1023–1027. https://doi.org/10.1038/nclimate3114

Oleson, K. W., Lawrence, D. M., Bonan, G. B., Drewniak, B., Huang, M., Levis, S., et al. (2013). Technical Description of version 4.5 of the Community Land Model (CLM), 434.

O'Neill, P. E., Chan, S. K., Njoku, E. G., Jackson, T., & Bindlish, R. (2016). SMAP L3 Radiometer Global Daily 36 km EASE-Grid Soil Moisture, Version 5, Boulder, Colorado USA, NASA National Snow and Ice Data Center Distributed Active Archive Center.

Oren, R., Sperry, J. S., Katul, G. G., Pataki, D. E., Ewers, B. E., Phillips, N., & Schäfer, K. V. R. (1999). Survey and synthesis of intra- and interspecific variation in stomatal sensitivity to vapour pressure deficit: Intra- and interspecific variation in stomatal sensitivity to vapour pressure deficit. Plant, Cell & Environment, 22(12), 1515–1526. https://doi.org/10.1046/j.1365-3040.1999.00513.x

Pappas, C., Fatichi, S., & Burlando, P. (2016). Modeling terrestrial carbon and water dynamics across climatic gradients: does plant trait diversity matter? New Phytologist, 209(1), 137–151. https://doi.org/10.1111/nph.13590

Peng, L., Zeng, Z., Wei, Z., Chen, A., Wood, E. F., & Sheffield, J. (2019). Determinants of the ratio of actual to potential evapotranspiration. Global Change Biology, 25(4), 1326–1343. https://doi.org/10.1111/gcb.14577

Powell, T. L., Galbraith, D. R., Christoffersen, B. O., Harper, A., Imbuzeiro, H. M. A., Rowland, L., et al. (2013). Confronting model predictions of carbon fluxes with measurements of Amazon forests subjected to experimental drought. New Phytologist, 200(2), 350–365. https://doi.org/10.1111/nph.12390

Qiu, B., Xue, Y., Fisher, J. B., Guo, W., Berry, J. A., & Zhang, Y. (2018). Satellite Chlorophyll Fluorescence and Soil Moisture Observations Lead to Advances in the Predictive Understanding of Global Terrestrial Coupled Carbon-Water Cycles. Global Biogeochemical Cycles, 32(3), 360–375. https://doi.org/10.1002/2017GB005744

Reichle, R. H., De Lannoy, G. J., Koster, R. D., Crow, W. T., Kimball J. S., Liu, Q. (2017). SMAP L4 Radiometer Global 3-hourly 9 km EASE-Grid Surface and Root Zone Soil Moisture Geophysical Data, Version 4, Boulder, Colorado USA, NASA National Snow and Ice Data Center Distributed Active Archive Center.

Richards, L. A., & Weaver, L. R. (1944). Moisture retention by some irrigated soils as related to soil moisture tension. Journal of Agricultural Research, 69(6), 215–235.

Rodriguez-Iturbe, I., Porporato, A., Laio, F., & Ridolfi, L. (2001). Intensive or extensive use of soil moisture: plant strategies to cope with stochastic water availability. Geophysical Research Letters, 28(23), 4495–4497.

Skelton, R. P., West, A. G., & Dawson, T. E. (2015). Predicting plant vulnerability to drought in biodiverse regions using functional traits. Proceedings of the National Academy of Sciences, 112(18), 5744–5749. https://doi.org/10.1073/pnas.1503376112

Steduto, P., Hsiao, T. C., Raes, D., & Fereres, E. (2009). AquaCrop—The FAO Crop Model to Simulate Yield Response to Water: I. Concepts and Underlying Principles. Agronomy Journal, 101(3), 426. https://doi.org/10.2134/agronj2008.0139s

Still, C. J., Berry, J. A., Collatz, G. J., & DeFries, R. S. (2003). Global distribution of C3 and C4 vegetation: carbon cycle implications. Global Biogeochemical Cycles, 17(1), 6-1-6–14.

Sultan, S. E. (2000). Phenotypic plasticity for plant development, function and life history. Trends in Plant Science, 5(12), 537–542. https://doi.org/10.1016/S1360-1385(00)01797-0

Troch, P. A., Martinez, G. F., Pauwels, V. R. N., Durcik, M., Sivapalan, M., Harman, C., et al. (2009). Climate and vegetation water use efficiency at catchment scales. Hydrological Processes, 23(16), 2409–2414. https://doi.org/10.1002/hyp.7358

Trugman, A. T., Medvigy, D., Mankin, J. S., & Anderegg, W. R. L. (2018). Soil Moisture Stress as a Major Driver of Carbon Cycle Uncertainty. Geophysical Research Letters, 45(13), 6495–6503. https://doi.org/10.1029/2018GL078131

Westenbroek. (2018). SWB Version 2.0—A Soil-Water-Balance Code for Estimating Net Infiltration and Other Water-Budget Components (Techniques and Methods).

3.11 Figures

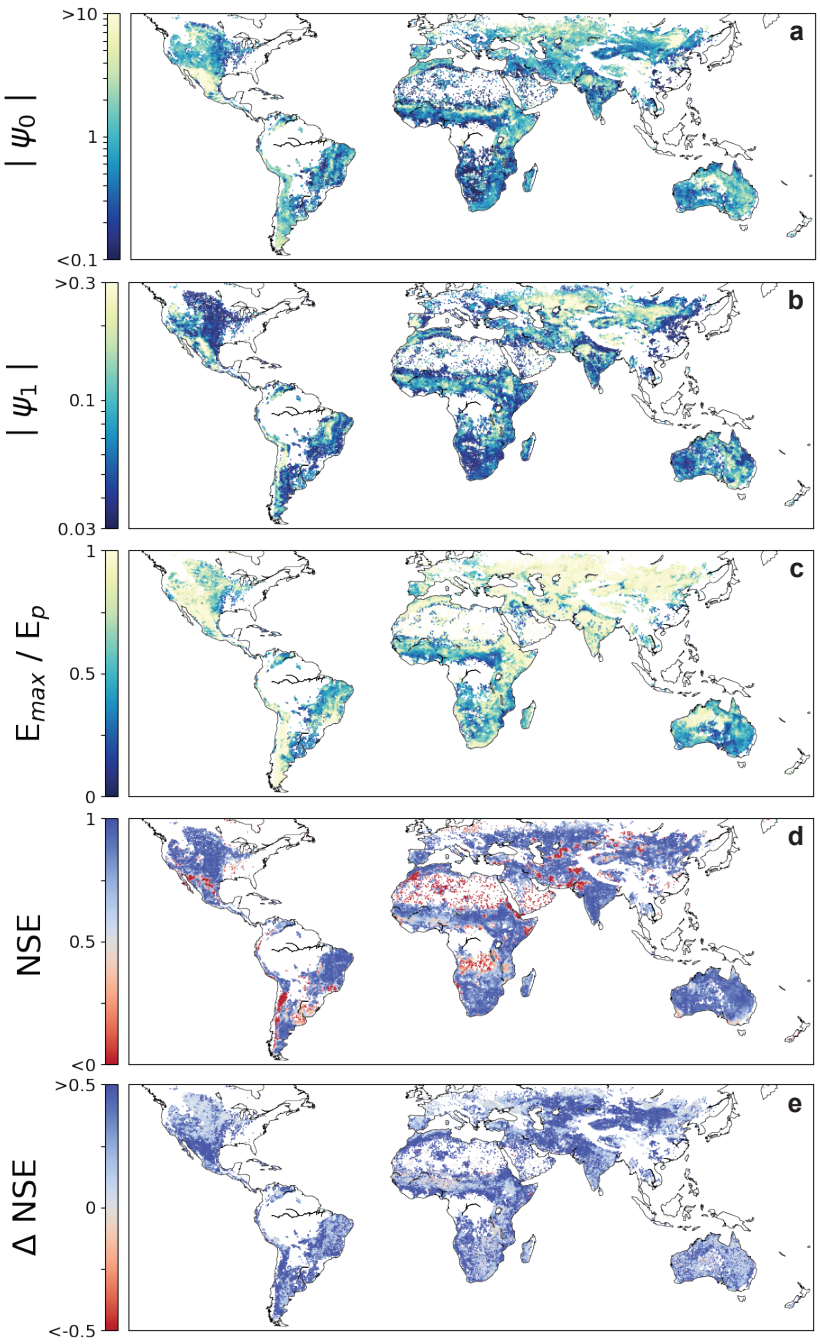

Figure 3.1 Global ecohydrological thresholds, which best fit empirical p(s) derived from satellite observations. (a) |Ψ0|, soil water potential at no uptake, MPa. (b) |Ψ1| soil water potential at uptake downregulation, MPa. (c) Emax/Ep, normalized maximum rate of soil water uptake. (d) NSE of theoretical versus empirical p(s). (e) Difference in NSE between using inferred thresholds and reference constants. Locations with insufficient observations or non-converging results are white.

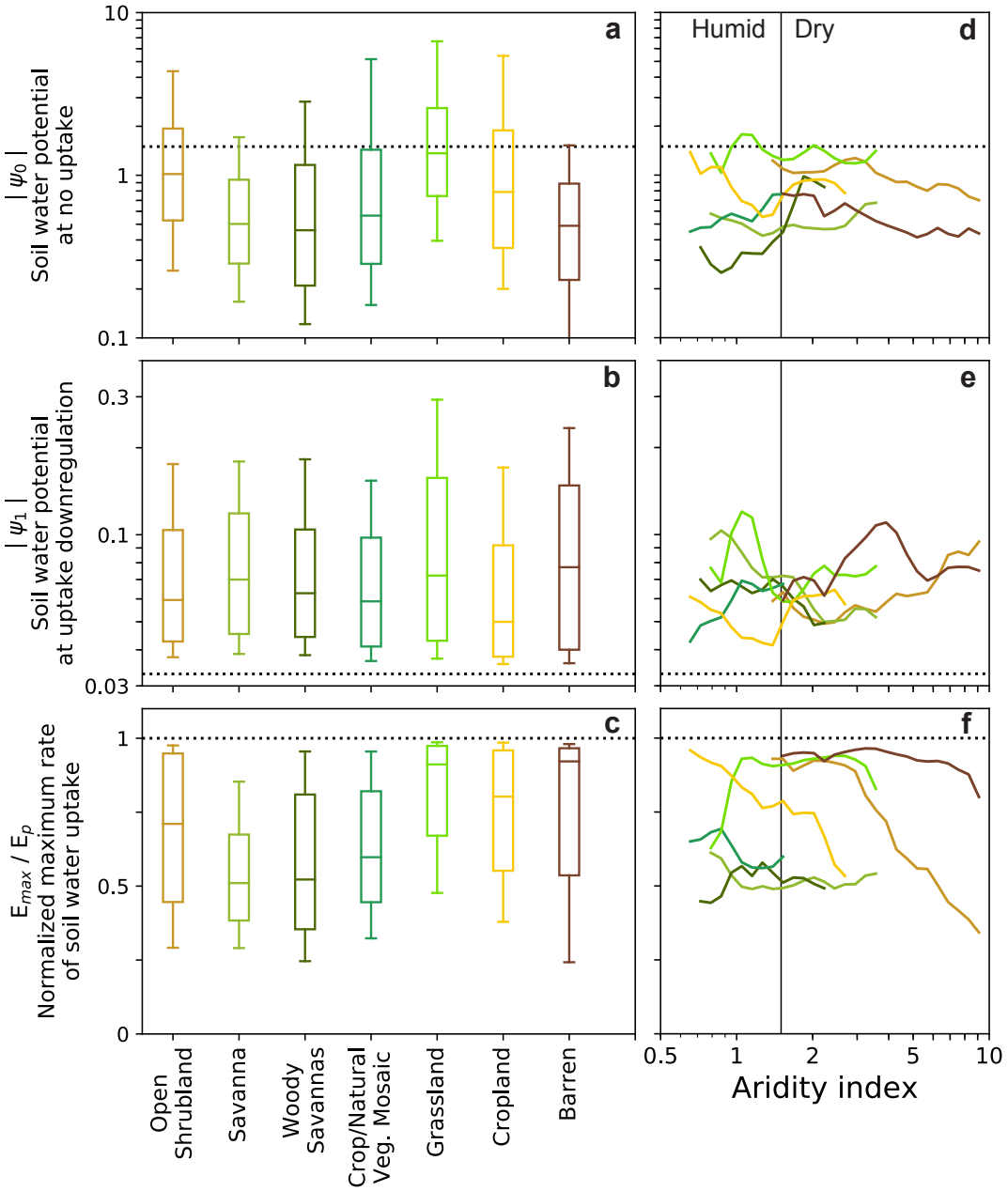

Figure 3.2 Ecohydrological thresholds by vegetation type and climate. (a-c) Boxes represent interquartile range, horizontal line represents median, and whiskers represent 10th and 90th percentiles. See Table 3.S1 for values and sample sizes. (d-f) Median relation between ecohydrological thresholds and aridity index.

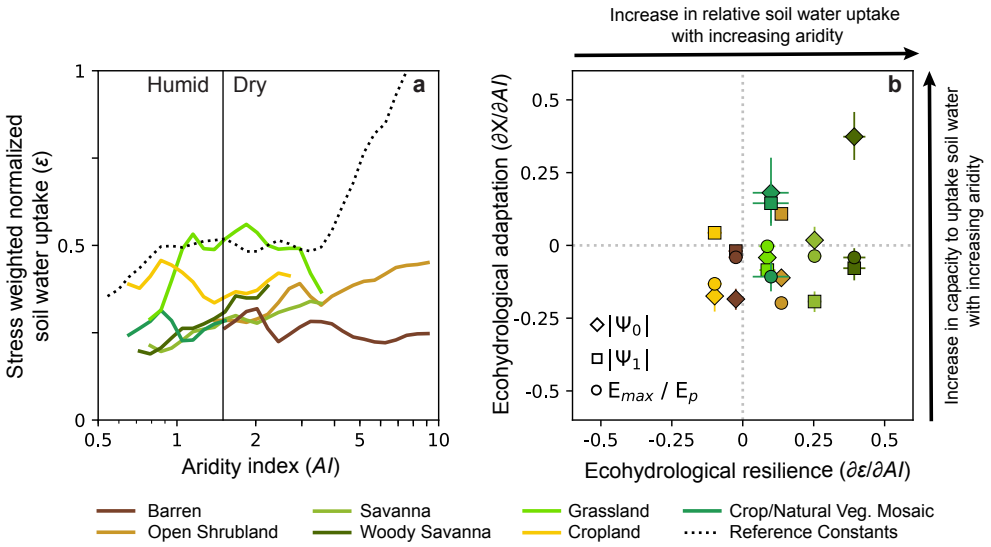

Figure 3.3 Vegetation capacity to uptake soil moisture in water-limited conditions. (a) Median relation between stress-weighted normalized soil water uptake (ε) and aridity index (AI). All global locations are represented with the dotted black line using reference constants. (b) Ecohydrological adaptation (∂X/∂AI) versus ecohydrological resilience (∂ε/∂AI). See Table 3.S2 for values. Vertical and horizontal lines on markers represent 95% confidence intervals for each axis.

3.12 Supplementary material

3.12.1 Supplementary text

Text S1

The theoretical probability distribution of soil saturation, $p(s)$ (Laio et al., 2001), used in this study is given by

$$p(s) = \begin{cases} 0, & 0 < s \le s_h, \\ \frac{C}{\eta_w}\left(\frac{s-s_h}{s_w-s_h}\right)^{\frac{\lambda(s_w-s_h)}{\eta_w}-1} e^{-\gamma s}, & s_h < s \le s_w, \\ \frac{C}{\eta_w}\left[1+\left(\frac{\eta}{\eta_w}-1\right)\left(\frac{s-s_w}{s^*-s_w}\right)\right]^{\frac{\lambda(s^*-s_w)}{\eta-\eta_w}-1} e^{-\gamma s}, & s_w < s \le s^*, \\ \frac{C}{\eta} e^{-\gamma s+\frac{\lambda}{\eta}(s-s^*)} \frac{\eta}{\eta_w}^{\frac{\lambda(s^*-s_w)}{\eta-\eta_w}}, & s^* < s \le s_{fc}, \\ \frac{C}{\eta} e^{-(\beta+\gamma)s+\beta s_{fc}} \left(\frac{\eta e^{\beta s}}{(\eta-m)e^{\beta s_{fc}}+me^{\beta s}}\right)^{\frac{\lambda}{\beta(\eta-m)}+1} \frac{\eta}{\eta_w}^{\frac{\lambda(s^*-s_w)}{\eta-\eta_w}} e^{\frac{\lambda}{\eta}\left(s_{fc}-s^*\right)}, & s_{fc} < s \le 1, \end{cases} \quad \text{(i)}$$

where

$\frac{1}{\gamma} = \frac{\alpha}{nZ}$;

$\eta_w = \frac{E_w}{nZ}$;

$\eta = \frac{E_{max}}{nZ}$;

$m = \frac{K_S}{nZ(e^{\beta\left(1-s_{fc}\right)}-1)}$;

$\beta = 2b-4$;

Z [mm]; soil layer depth is equal to the average SMAP sensing depth of 50 mm;

n [-], soil porosity is the maximum value between soil water content at saturation from (Montzka et al., 2017) and the maximum observed SMAP soil water content;

s [-], soil saturation ($0 \le s \le 1$) is computed by dividing SMAP soil water content observations by n;

α [mm day $^{-1}$], average daily rainfall depth is calculated from L4 SMAP precipitation concurrent with the study period (Rodriguez-Iturbe et al., 1984b) ;

λ [day $^{-1}$], average daily rainfall frequency is calculated from L4 SMAP precipitation concurrent with the study period (Rodriguez-Iturbe et al., 1984b);

s_h [-], hygroscopic point is the minimum value between and the residual soil saturation from (Montzka et al., 2017) and minimum observed SMAP saturation offset by 0.01 so that $p(s_h) = 0$ remains true;

s_w [-], wilting point is unknown and determined through inverse modelling and the reference constant value used is equal to soil saturation at 1.5 MPa pressure head (Rawls et al., 1982);

s^* [-], point of incipient stomatal closure is unknown and determined through inverse modelling and the reference constant value used is equal to soil saturation at 0.033 MPa pressure head (Laio et al., 2001);

s_{fc} [-], field capacity is calculated as soil saturation at 0.033 MPa pressure head (Rawls et al., 1982);

E_{max} [mm day^{-1}], maximum daily rate of evapotranspiration is unknown and determined through inverse modelling and within the range [0.1 E_p, E_p] and the reference constant value used is E_p, potential evaporation (Priestley & Taylor, 1972a);

E_w [mm day^{-1}], daily rate of evaporation at the wilting point is unknown and determined through inverse modelling and within the range [0, 0.1 E_p] and the reference constant value used is 0;

K_s [mm day^{-1}], saturated soil hydraulic conductivity from (Montzka et al., 2017);

b [-], empirical soil water retention curve parameter (Clapp & Hornberger, 1978; Montzka et al., 2017) ;

C [-], constant obtained numerically to ensure the integral of $p(s) = 1$.

Global maps of parameters values for Eq. (i) and estimates of unknown ecohydrological thresholds determined from inverse modelling, including convergence, uncertainty, and goodness-of-fit diagnostics are reported at http://doi.org/10.5281/zenodo.3351623. We define all variables available in this dataset in Table 3.S3. Datasets used to determine parameters are referenced above and described in the main text.

Text S2

We calculate an average stress-weighted, normalized soil water uptake (ε) defined as (Manfreda et al., 2017):

$$\varepsilon = \frac{\overline{\mathrm{ET}}}{\alpha\lambda}\,(1-\bar{\xi}) \tag{1}$$

where $\frac{\overline{\mathrm{ET}}}{\alpha\lambda}$, the theoretical average normalized soil water uptake for each grid cell is calculated using three years of daily soil saturation observations from SMAP L3 and the simplified soil moisture loss curve, defined as (Laio et al., 2001):

$$ET(s) = \begin{cases} 0, & 0 < s \le s_h, \\ \left(\frac{s_w - s}{s_w - s_h}\right) E_w, & s_h < s \le s_w, \\ \left(\frac{s^* - s}{s^* - s_w}\right)(E_{max} - E_w) + E_w, & s_w < s \le s^*, \\ E_{max}, & s^* < s \le 1. \end{cases} \tag{2}$$

and $\bar{\xi}$, the theoretical average soil moisture stress index for each grid cell, is calculated using three years of daily soil saturation observations from SMAP L3 and the relation between plant water stress and soil saturation, defined as (Porporato et al., 2001):

$$\xi(s) = \begin{cases} 1, & 0 < s \le s_w, \\ \left(\frac{s^* - s}{s^* - s_w}\right)^2, & s_w < s \le s^*, \\ 0, & s^* < s \le 1. \end{cases} \tag{3}$$

Text S3

We calculate the sensitivity of the absolute value of each ecohydrological threshold ($X = |\Psi_0|$, $|\Psi_1|$, E_{max}/E_p) to *AI* to quantify ecohydrological adaptation ($\partial X/\partial AI$) and the sensitivity of ε to the *AI* to quantify ecohydrological resilience ($\partial\varepsilon/\partial AI$) for each IGBP land cover class separately. We approximate these sensitivities with the non-parametric Thiel-Sen estimator (Theil, 1992). We first standardize each variable within each IGBP class by subtracting and dividing by the median value. We then calculate the Thiel-Sen estimator as the median of the slopes determined by all pairs of points. Ecohydrological adaptation represents the relative variation of an ecohydrological threshold associated with a relative variation in the *AI*, and ecohydrological resilience represents the relative variation of the fraction of available water uptake weighted by stress, associated with a relative variation in *AI*. For example, $\partial|\Psi_0|/\partial AI$ = - 0.1, corresponds to a 10% decrease from the median $|\Psi_0|$ value for a unit change from the

median *AI*. Sensitivities for each ecohydrological variable to *AI* are reported in Table 3.S2. These sensitivities represent the slopes in Figures 3.2d-f, 3.3a, and 3.S1 and the marker values in Figure 3b.

References

Clapp, R. B., & Hornberger, G. M. (1978). Empirical equations for some soil hydraulic properties. Water Resources Research, 14(4), 601–604.

Laio, F., Porporato, A., Ridolfi, L., & Rodriguez-Iturbe, I. (2001). Plants in water-controlled ecosystems: active role in hydrologic processes and response to water stress: II. Probabilistic soil moisture dynamics. Advances in Water Resources, 24(7), 707–723.

Manfreda, S., Caylor, K. K., & Good, S. P. (2017). An ecohydrological framework to explain shifts in vegetation organization across climatological gradients: Vegetation pattern in dry environments. Ecohydrology, 10(3), e1809. https://doi.org/10.1002/eco.1809

Montzka, C., Herbst, M., Weihermüller, L., Verhoef, A., & Vereecken, H. (2017). A global data set of soil hydraulic properties and sub-grid variability of soil water retention and hydraulic conductivity curves. Earth System Science Data, 9(2), 529–543.

Porporato, A., Laio, F., Ridol, L., & Rodriguez-Iturbe, I. (2001). Plants in water-controlled ecosystems: active role in hydrologic processes and response to water stress III. Vegetation water stress. Advances in Water Resources, 20.

Priestley, C. H. B., & Taylor, R. J. (1972). On the Assessment of Surface Heat Flux and Evaporation Using Large-Scale Parameters. Monthly Weather Review, 100(2), 81–92. https://doi.org/10.1175/1520-0493(1972)100<0081:OTAOSH>2.3.CO;2

Rawls, W. J., Brakensiek, D. L., & Saxtonn, K. E. (1982). Estimation of soil water properties. Transactions of the ASAE, 25(5), 1316–1320.

Rodriguez-Iturbe, I., Gupta, V. K., & Waymire, E. (1984). Scale considerations in the modeling of temporal rainfall. Water Resources Research, 20(11), 1611–1619.

Theil, H. (1992). A Rank-Invariant Method of Linear and Polynomial Regression Analysis. In B. Raj & J. Koerts (Eds.), Henri Theil's Contributions to Economics and Econometrics (Vol. 23, pp. 345–381). Dordrecht: Springer Netherlands. https://doi.org/10.1007/978-94-011-2546-8_20

3.12.2 Supplementary figures

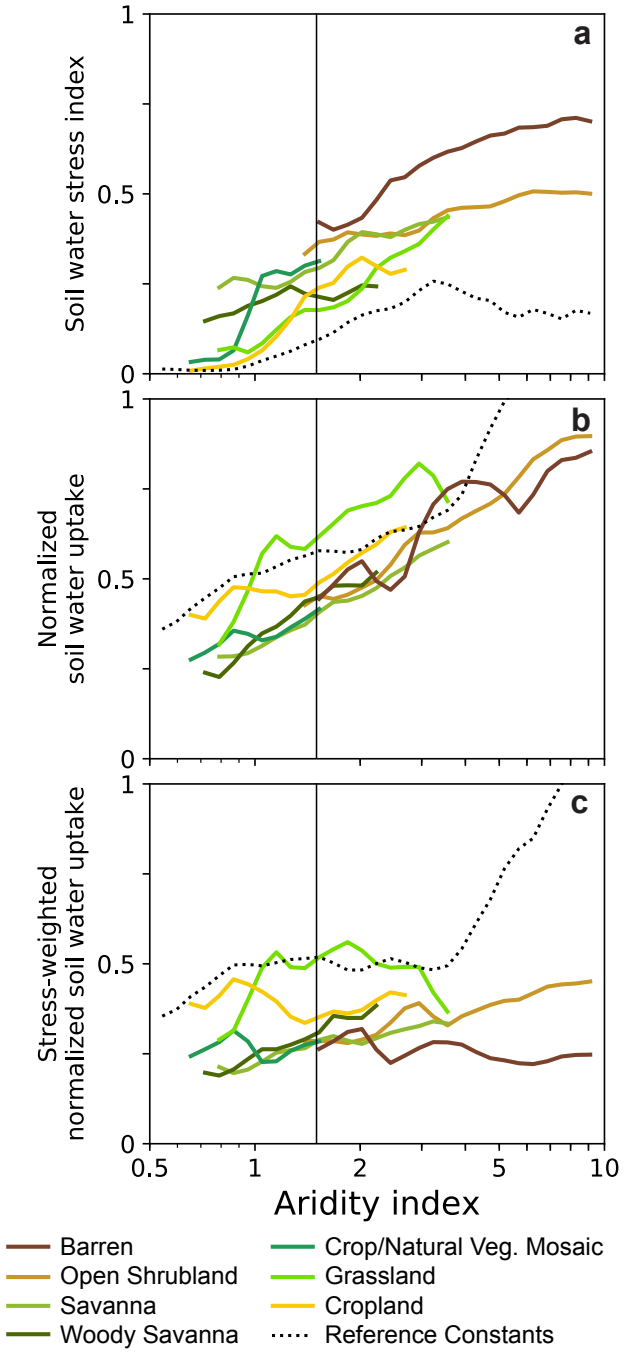

Figure 3.S1 Trends in indices of soil water stress and soil water uptake with aridity by land cover. The moving median is visualized using 50 log spaced bins between aridity index values of 0.5 and 10. All global locations are represented in the dotted black line using reference constants.

3.12.3 Supplementary tables

Table 3.S1 Median ecohydrological thresholds inferred from satellite soil moisture by land cover

	Open Shrubland	Savanna	Woody Savanna	Crop/Natural Veg. Mosaic	Grassland	Cropland	Barren Landscape
$\|\Psi_0\|$	1.02	0.50	0.46	0.56	1.36	0.79	0.49
$\|\Psi_1\|$	0.06	0.07	0.06	0.06	0.07	0.05	0.08
E_{max} / E_p	0.71	0.51	0.52	0.60	0.91	0.80	0.92
n	6638	5391	2094	1925	7315	5225	4015

$|\Psi_0|$, soil water potential at which no surface soil water uptake occurs, absolute value in MPa; $|\Psi_1|$, soil water potential at which downregulation of surface soil water uptake occurs, absolute value in MPa; E_{max}/E_p, maximum rate of surface soil water uptake normalized by potential evaporation; *n,* sample size.

Table 3.S2 Variability of ecohydrological parameters with aridity by land cover

	Open Shrubland	Savanna	Woody Savanna	Crop/Natural Veg. Mosaic	Grassland	Cropland	Barren Landscape
$\partial\|\Psi 0\|/\partial$AI	-0.11	0.02	0.37	0.18	-0.04	-0.17	-0.18
$\partial\|\Psi 1\|/\partial$AI	0.11	-0.19	-0.08	0.14	-0.08	0.04	-0.02
$\partial \frac{E_{max}}{E_p}/\partial$AI	-0.2	-0.04	-0.04	-0.11	-0.0	-0.13	-0.04
$\partial\bar{\xi}/\partial$AI	0.15	0.39	0.37	1.09	0.91	1.58	0.16
$\partial\frac{\overline{ET}}{\alpha\lambda}/\partial$AI	0.31	0.45	0.48	0.38	0.31	0.19	0.25
$\partial\varepsilon/\partial$AI	0.14	0.25	0.39	0.1	0.09	-0.1	-0.02

$\partial X/\partial AI$ are approximated by the non-parametric Thiel-Sen estimator. *X* takes the values of $|\Psi_0|$, soil water potential at which no surface soil water uptake occurs, absolute value in MPa; $|\Psi_1|$, soil water potential at which downregulation of surface soil water uptake occurs, absolute value in MPa; E_{max}/E_p, maximum rate of surface soil water uptake normalized by potential evaporation; $\bar{\xi}$, soil moistures stress index; $\frac{\overline{ET}}{\alpha\lambda}$, normalized soil water uptake; ε , stress-weighted normalized soil water uptake. Numbers in bold indicate a p-value lower than 0.05.

Table 3.S3 Description of variables available in "Global dataset of ecohydrological parameters inferred from satellite observations" (http://doi.org/10.5281/zenodo.3351623)

latitude	degrees	latitude of grid centroid
longitude	degrees	longitude of grid centroid
len_s_obs	unitless	number of soil moisture observations in L3 SMAP 04/ 2015 to 03/2018 used in analysis
aridity_index	unitless	ratio of average potential evapotranspiration to rainfall
max_s	unitless	maximum soil saturation value in L3 SMAP 04/ 2015 to 03/2018
min_s	unitless	minimum soil saturation value in L3 SMAP 04/ 2015 to 03/2018
mean_s	unitless	mean soil saturation value in L3 SMAP 04/ 2015 to 03/2018
std_s	unitless	standard deviation of observed soil saturation values in L3 SMAP 04/ 2015 to 03/2018
alpha_MvG	unitless	empirical parameter used in the Mulalem-van Genuchten equation
n_MvG	unitless	empirical parameter used in the Mulalem-van Genuchten equation
Z	mm	soil depth
n	unitless	soil porosity
b	unitless	empirical parameter used in the Clapp and Hornberger soil water retention curve equation
Ks	mm/day	saturated soil hydraulic conductivity
s_fc	unitless	soil saturation at field capacity
s_h	unitless	soil saturation at the hygroscopic point
s_1.5MPa	unitless	soil saturation at 1.5 MPa soil water potential
s_0.033MPa	unitless	soil saturation at 0.033 MPa soil water potential
rf_alpha	mm/day	average daily rainfall depth
rf_lambda	unitless	average daily rainfall frequency
E_p	mm/day	average daily potential evapotranspiration
s_star	unitless	soil saturation at the point of incipient stomatal closure, mean of posterior estimates
s_wilt	unitless	soil saturation at the wilting point, mean of posterior estimates
f_max	unitless	ratio of maximum soil water uptake to E_p, mean of posterior estimates
f_w	unitless	ratio of soil water uptake at the wilting point to E_p, mean of posterior estimates
psi_0	MPa	soil water potential at the point of no soil water uptake
psi_1	MPa	soil water potential at the point of downregulation of soil water uptake
s_wilt_grd	unitless	Gelman-Rubin diagnostic for s_wilt
s_star_grd	unitless	Gelman-Rubin diagnostic for s_star
f_max_grd	unitless	Gelman-Rubin diagnostic for f_max
f_w_grd	unitless	Gelman-Rubin diagnostic for f_w
s_wilt_std	unitless	standard deviation of posterior estimates of s_wilt
s_star_std	unitless	standard deviation of posterior estimates of s_star
f_max_std	unitless	standard deviation of posterior estimates of f_max
f_w_std	unitless	standard deviation of posterior estimates of f_w
efficiency	unitless	efficiency of Metropolis-Hastings Markov chain Monte Carlo algorithm
NSE_pdf	unitless	quantile level Nash Sutcliffe efficiency between theoretical and empirical soil saturation probability distribution using inferred thresholds
NSE_pdf_rc	unitless	quantile level Nash Sutcliffe efficiency between theoretical and empirical soil saturation probability distribution using constant reference thresholds
stress_index	unitless	soil moisture stress index estimated using inferred thresholds
stress_index_rc	unitless	soil moisture stress index estimated using constant reference thresholds
norm_wu	unitless	soil water use normalized by rainfall estimated using inferred thresholds
norm_wu_rc	unitless	soil water use normalized by rainfall estimated using constant reference thresholds
swnwu	unitless	stress weighted normalized water use estimated using inferred thresholds
swnwu_rc	unitless	stress weighted normalized water use estimated using constant reference thresholds
vegcls	unitless	IGBP land cover class

4 Disentangling Soil Moisture Limits on Evapotranspiration

4.1 Abstract

Theoretical descriptions of the variability of soil moisture such as the energy spectrum and probability distribution parameterize interactions between climate type, soil pedology, and vegetation physiology. We quantify the relation between soil moisture and evapotranspiration by calibrating these theoretical equations to soil moisture observations and by partitioning mutual information from soil moisture and vapor pressure deficit about evapotranspiration at 71 FLUXNET2015 sites. The ecohydrological metrics developed in this study are able to capture patterns in atmospheric versus soil moisture stress on transpiration at forested and non-forested sites.

4.2 Introduction

The variability of evapotranspiration (*ET*) relative to the potential atmospheric moisture demand (E_p) driven by radiation and temperature is controlled by a variety of land-surface characteristics and estimates of empirical factors ET/E_p derived from observations and models are widely divergent (Peng et al., 2019). Understanding the variability in *ET* and in particular the relation between soil moisture and vegetation stress is key to quantifying feedbacks between hydrology and climate (Fisher et al., 2017). Numerous studies have explored empirical relations between *ET*, soil moisture and vegetation stress (Porporato et al., 2001; Katul et al., 2012; Novick et al., 2016; Peng et al., 2019; Purdy et al., 2018) yet these relations remain difficult to untangle because ecohydrological variables are highly correlated. Simple metrics for these relations, which are based on observations are necessary to evaluate earth systems models.

Soil moisture integrates processes of the water cycle and the variability in soil moisture reflects interactions between climate type, soil pedology, and vegetation physiology (Rodriguez-Iturbe, 2000). Theoretical descriptions of the variability of soil moisture such as the energy spectrum (Katul et al., 2007) and probability distribution functions (Laio et al., 2001) parameterize these dynamics and are simpler models to calibrate than water balance differential equations in numerical models. In particular, confronting theoretical and observed descriptions of soil moisture variability provides a framework to quantify the relation between soil moisture and *ET,* while overcoming some limitations of more direct correlation approaches. Non-linear dynamics in complex environmental systems can also be analyzed independently of model form using information theoretical metrics (Goodwell & Kumar, 2017b; Ruddell & Kumar, 2009). Diagnosis of mutual information between hydrological and meteorological variables can reveal controls on the variability of *ET* and information partitioning can disentangle information from correlated variables.

The objective of this study is to quantify the relation between soil moisture and *ET* using observations from 71 sites in a range of biomes. We estimate the shape of the relation between soil moisture and *ET* based on theoretical descriptions of the energy spectrum and probability distributions of soil moisture and compare them to information theoretical metrics to disentangle moisture controls on *ET*. We define the theoretical models and information metrics and identify patterns in atmospheric versus soil moisture stress on transpiration at forested and non-forested sites captured by each approach.

4.3 Data

We use daily data from the FLUXNET2015 Tier one data product (http://fluxnet.fluxdata.org/data/fluxnet2015-dataset/, last access: October 2016) that has standardized processing, quality control

and gap filling (Reichstein et al., 2005). We only analyze daily values with a quality flag > 0.5 ensuring that at least 50-percent of the half-hourly values in a day are observed and only good quality half-hourly gap-filled data are used. We select sites, which have continuous and concurrent high-quality daily values of volumetric water content (θ), latent heat flux (LE), sensible heat flux (H), precipitation (P), air temperature (T) and vapor pressure deficit (δ_e) during at least one growing season. We calculate daily values of potential evaporation (E_p) (Priestley & Taylor, 1972b) from observed available surface energy flux (Q_n) and T. We estimate Q_n as the sum of eddy-covariance measurements of LE and H instead of the difference between net radiation and ground heat flux because LE and H measurements are more consistently available at FLUXNET2015 sites.

We only analyze growing season data, when vegetation is most active, and define the growing season for the northern hemisphere as June–August and for the southern hemisphere as December–February (Anderegg et al., 2019), although site-specific growing seasons may be variable and extend beyond the selected 90-day periods. We do not select any wetland sites because soil water dynamics at wetland sites are influenced by groundwater and do not meet our model assumptions. We also visually inspect soil moisture time series to exclude sites with possible ground water effects on soil moisture dynamics. We identify possible groundwater effects on soil moisture by persistent soil moisture values close to saturation during the selected growing seasons. A range of biomes are represented in 71 selected sites (Table 4.S1). We determine the physical soil characteristics of each site using each site's latitude and longitude and a global dataset of soil hydraulic parameters (Montzka et al., 2017). We assume that all soil moisture measurements are at a depth Z of 10 cm. We estimate the soil porosity (n) as the maximum observed θ during the selected growing seasons and divide θ timeseries by porosity to obtain time series of soil saturation (s).

4.4 Methods

4.4.1 Analytical model for the energy density spectrum of soil moisture

The energy density spectrum of soil moisture describes the relative distribution of a soil moisture time series with frequency. We assume that at the daily time scale and selected FLUXNET2015 sites, the soil water balance is dominated by precipitation forcing (P) and, ET losses, because the occurrence of daily soil moisture values at saturation are rare. We assume rainfall interception, runoff and soil water losses due to drainage are negligible. Thus, a simple analytical model of the soil moisture energy density spectrum (ρ_θ) is derived based on Katul et al. (2007). We define the soil water balance of a soil column with depth, Z and at time, t as:

$$Zn\frac{ds(t)}{dt} = P(t) - ET(t) \quad (1)$$

We assume that soil moisture losses due to *ET* are bound between two models. The first is moisture-limited, denoted with subscript $_W$ and the second is energy-limited, denoted with subscript $_R$. The combination of these models encompasses possible non-linear relations between *ET* and soil moisture that account for a range of soil moisture states at which *ET* is not moisture limited. In the moisture-limiting model, $ET(t)$ decreases linearly with $s(t)$ from a maximum value and soil moisture losses are:

$$[ET(t)]_w = E_{max}s(t) \tag{2}$$

In the energy-limited model, $ET(t)$ is equal to $E_p(t)$ and soil moisture losses are defined as

$$[ET(t)]_R = E_p(t) \tag{3}$$

We recast Eq (1) using Eq (2) and Eq (3) separately and then convert from the temporal domain (t) to the frequency domain (f) using the Fourier transform ($\hat{x}(f)$), defined for an arbitrary timeseries $x(t)$ as:

$$\hat{x}(f) = \int_{-\infty}^{+\infty} x(t)e^{ift}dt \tag{4}$$

The two soil water balance models in frequency domain are

$$-if[\hat{s}(f)]_W = \frac{\widehat{P}}{nZ}(f) - \beta\hat{s}(f) \tag{5}$$

and

$$-if[\hat{s}(f)]_R = \frac{\widehat{P}}{nZ}(f) - \frac{\widehat{E_p}}{nZ}(f) \tag{6}$$

where $\beta^{-1} = \frac{nZ}{E_{max}}$ [days] is the soil water memory or soil moisture decay time scale (Katul et al., 2007) and we approximate E_{max} as the growing season average E_p. We rearrange Eq (5) and Eq (6) as

$$[\hat{s}(f)]_W = \frac{\beta+if}{\beta^2+f^2}\frac{\widehat{P}}{nZ}(f) \tag{7}$$

and

$$[\hat{s}(f)]_R = -\frac{1}{if}\frac{\widehat{P-E_0}}{nZ}(f) \tag{8}$$

and apply the general definition for the energy spectrum ($\phi_x(f)$) of an arbitrary signal $\hat{x}(f)$

$$\phi_x(f) = |\hat{x}(f)|^2 = x_{real}(f)^2 + x_{imag}(f)^2 \tag{9}$$

where x_{real} and x_{imag} are the real and imaginary parts of $\hat{x}(f)$. We simplify $[\phi_s(f)]_W$ and $[\phi_s(f)]_R$ and define the energy spectrum of soil moisture as

$$[\phi_s(f)]_W = \frac{1}{(nZ)^2} \frac{\phi_P(f)}{\beta^2+f^2} \tag{10}$$

and

$$[\phi_s(f)]_R = \frac{1}{(nZ)^2} \frac{\phi_{P-E_p}(f)}{f^2} \tag{11}$$

Finally, we combine the two models Eq (10) and Eq (11) with a non-dimensional coefficient, α, that can take values between 0 and 1 and measures the degree of non-linearity of the relation between *ET* and soil moisture (Figure 4.1b). The model for $\rho_s(f)$ for the energy density spectrum, which corresponds to the fraction of the total variance contributed by each frequency, is thus defined as a function of the energy density spectrum of *P* and the energy density spectrum of ($P - E_p$)

$$\rho_s(f) = C\left(\alpha \frac{\rho_{P-E_p}(f)}{f^2} + (1-\alpha)\frac{\rho_P(f)}{\beta^2+f^2} +\right) \tag{12}$$

where C [days^{-2}] is a coefficient that ensures that the sum of $\rho_s(f)$ over the range of frequencies is equal to 1.

We subtract the mean from time series of *s*, *P*, *P*-E_p for each selected growing season. We estimate individual power spectrums for each normalized time series using discrete fast Fourier transform then divide by the power spectrum sum to obtain power spectrum densities. We average the individual growing season power spectrum densities to estimate $\rho_s(f)$, $\rho_P(f)$ and, $\rho_{P-E_p}(f)$ (Figure 4.1c). We then estimate α from $\rho_s(f)$, $\rho_P(f)$ and, $\rho_{P-E_p}(f)$ as the best fit of Eq (12) (Figure 4.1c).

We use α to describe the shape of the relation between soil moisture controls and *ET*. For α=0, the most drought avoidant vegetation water use strategy, *ET* is moisture limited over all soil moisture states; for α = 1, drought tolerant vegetation water use strategy, *ET* is independent of soil moisture; and for 0<α<1 soil moisture losses are controlled by both energy and moisture limitations.

4.4.2 Piece-wise soil moisture loss function

Soil moisture losses are often parameterized by a piece-wise function of soil saturation (Figure 4.1b) (Laio et al., 2001). The rate of leakage due to gravity is maximum (K_S) when the soil is saturated (s=1), and decays exponentially to zero at field capacity (s_{fc}); *ET* is maximum (E_{max}) until the point of incipient

stomatal closure (s^*), when plants start to down-regulate transpiration; *ET* decreases linearly from E_{max} to 0 at the wilting point (s_w). The piece-wise soil moisture function ($\chi(s)$) is defined as

$$\chi(s) = \begin{cases} K_s \frac{e^{(2b+4)(s-s_{fc})} - 1}{e^{(2b+4)(1-s_{fc})} - 1} + E_{max} & s_{fc} < s \leq 1, \\ E_{max}, & s^* < s \leq s_{fc}, \\ \left(\frac{s - s_w}{s^* - s_w}\right) E_{max}, & s_w < s \leq s^*, \\ 0 & 0 < s \leq s_w. \end{cases} \quad (13)$$

where *b* is a parameter of the soil water retention curve (Clapp & Hornberger, 1978).

A theoretical equation of the soil moisture probability distribution function can be derived by forcing the soil water balance with rainfall described by a stochastic process, assuming infiltration excess runoff, using the piece-wise soil water loss curve (Eq. 14), and integrating over steady state conditions (Laio et al., 2001). Given a rainfall average daily depth and frequency, the shape of soil moisture probability distributions is constrained by parameter of the loss function (Eq 14). We determine soil water retention parameters (K_s and *b*) using site-specific soil texture information (Montzka et al., 2017), approximate s_{fc} as the 90th percentile of soil moisture peaks and s_w as the minimum observed soil moisture value during the selected growing seasons. We estimate the two remaining unknown thresholds of the soil moisture loss curve (s^* and E_{max}), which depend on vegetation type, that best fit the empirical soil moisture probability distribution of soil moisture observed during the selected growing seasons (Figure 4.1d) using a Bayesian inference framework (Bassiouni et al., 2018).

We describe the shape of the relation between *ET* and soil moisture by γ, the area below the inferred relation between *ET* and soil moisture relative to the potential area, if *ET* is constant and equal to E_p

$$\gamma = \frac{E_{max}}{E_p} \frac{1 - 0.5(s^* + s_w)}{1 - s_w} \quad (14)$$

The shape parameter γ, is thus an index of the relative strength of soil moisture controls on *ET* and the point at which vegetation responds to stress and regulates transpiration. Vegetation is least sensitive to stress for $\gamma=0$, which indicates that stomata are fully open and transpiration is maximum for all soil. moisture states. Vegetation is most intolerant to stress for $\gamma=0$, which indicates that stomata are completely closed and transpiration is 0 at all soil moisture states. The linear combination of Eq (2) and Eq (3), which neglects soil losses from leakage due to gravity, is a simple approximation of the piece-wise soil moisture loss function (Eq (14)). The shape parameters α and γ should co-vary and reflect similar controls of soil moisture on *ET* and vegetation water use strategies.

4.4.3 Partitioning information about *ET*

The shape parameters (α and γ) may indirectly account for vegetation stress from low atmospheric moisture. Thus a shape parameter for a same vegetation type can be different in an aridity versus a humid climate. We examine the relative controls of moisture in the soil and atmosphere on *ET* through the partitioning of multi-variate mutual information from θ and δ_e about ET/E_p (ET_n). We focus our analysis on effects of moisture in the air and the soil on *ET* because ET_n is a non-dimensional quantity that already accounts for variability in available energy that drives *ET*. We thus indirectly analyze dynamics the water gradient or potential between the soil, through the plant and into the atmosphere that drives *ET*.

Definition of information metrics

Uncertainty in a discrete variable X with a probability density function $p(x)$ is quantified by information theory as the Shannon's entropy ($H(X)$), measured in bits and defined as (Shannon, 1948)

$$H(X) = -\sum_{x \in X} p(x) log_2 p(x) \tag{15}$$

The multi-variate case or joint entropy for discrete variables X and Y with a joint probability density function $p(x, y)$ is defined as

$$H(X,Y) = -\sum_{x \in X} \sum_{y \in Y} p(x,y) log_2 p(x,y) \tag{16}$$

Mutual information ($I(\theta; ET_n)$ and $I(\delta_e; ET_n)$), relates shared information between two variables (Cover & Thomas, 2012) and quantifies the reduction in uncertainty of a variable (ET_n) given knowledge of another variable (θ or δ_e). In other words, the knowledge we gain about ET_n from measuring θ or δ_e. Additionally, the total multi-variate mutual information ($I(\theta, \delta_e; ET_n)$) quantifies the total reduction in uncertainty of ET_n given knowledge of variables θ and δ_e together and conditional mutual information ($I(\theta; ET_n| \delta_e)$) quantifies the reduction in uncertainty of ET_n given knowledge of θ beyond the reduction of uncertainty due to knowledge of δ_e. The definitions of mutual information metrics are based on Shannon's entropy (Cover & Thomas, 2012) which can also be derived intuitively from Venn diagrams (Figure 4.2a-c):

$$I(\theta; ET_n) = H(\theta) + H(ET_n) - H(\theta, ET_n), \tag{17}$$

$$I(\theta, \delta_e; ET_n) = H(\theta, \delta_e) + H(ET_n) - H(\theta, \delta_e, ET_n), \text{ and} \tag{18}$$

$$\begin{aligned} I(\theta; ET_n|\delta_e) &= I(\theta, \delta_e; ET_n) - I(\delta_e; ET_n) \\ &= H(\theta, \delta_e) + H(ET_n, \delta_e) - H(\delta_e) - H(\theta, \delta_e, ET_n) \end{aligned} \tag{19}$$

We remove outliers, rescale and discretize ecohydrological variables before calculating information metrics (Goodwell & Kumar, 2017a). We remove outliers in ET_n by setting $ET_n < 0$ to 0 and $ET_n > ET_{n,max} = p_{75} + 1.5(p_{75} - p_{25})$ to $ET_{n,max}$ where p_{75} and p_{25} are the 75-th and 25-th percentiles of ET_n. We rescale θ, δ_e, and ET_n between 0 and 1, by dividing each variable by its maximum value in each site's record. We discretize rescaled observations of θ, δ_e, and ET_n in 10 evenly spaced bins between 0 and 1 to estimate 1-, 2-, 3-dimensional probability density functions necessary to calculate Shannon entropy and joint entropy. We apply a shuffled surrogates method (Goodwell & Kumar, 2017a; Ruddell & Kumar, 2009) to test statistical significance of $I(\theta,\delta_e; ET_n)$. We shuffle θ, δ_e, and ET_n to destroy existing correlations between variables and recompute $I(\theta,\delta_e;ET_n)$ 1000 times. We consider $I(\theta,\delta_e;ET_n)$ statistically significant if it is greater than the shuffled iterations at >99% confidence level.

Partitioning total multi-variate mutual information

We partition total information $I(\theta,\delta_e;ET_n)$ into non-negative quantities (Barrett, 2015; Goodwell & Kumar, 2017a; Williams & Beer, 2010) as follows:

$$I(\theta, \delta_e; ET_n) = S(ET_n; \theta, \delta_e) + U(ET_n; \theta) + U(ET_n; \delta_e) + R(ET_n; \theta, \delta_e) \quad (20)$$

The synergistic component (S) quantifies information shared only when θ and δ_e influence ET_n together. The unique components (U_θ and $U_{\delta e}$) quantify information provided about ET_n by θ and δ_e, respectively by themselves. The redundant component (R) quantifies overlapping information provided about ET_n by θ and δ_e together. The relative magnitudes of U_θ and $U_{\delta e}$ can be a measure of the relative control from each variable on ET. We estimate total, synergistic, unique, and redundant information about ET_n from θ and δ_e for each site with the following equations, which can also be derived intuitively from Venn diagrams (Figure 4.2d-e).

$$I(\theta; ET_n) = U(ET_n; \theta) + R(ET_n; \theta, \delta_e), \quad (21)$$

$$I(\delta_e; ET_n) = U(ET_n; \delta_e) + R(ET_n; \theta, \delta_e), \text{ and} \quad (22)$$

$$I(\theta; \delta_e; ET_n) = I(\theta; ET_n|\delta_e) - I(\theta, ET_n) = I(\delta_e; ET_n|\theta) - I(\delta_e, ET_n)$$
$$= S(ET_n; \theta, \delta_e) - R(ET_n; \theta, \delta_e) \quad (23)$$

We estimate redundancy as the rescaled redundancy (R_s) developed by (Goodwell & Kumar, 2017a) and defined as

$$\frac{R_s - R_{min}}{R_{MMI} - R_{min}} = \frac{I(\theta;\delta_e)}{\min[H(\theta),H(\delta_e)]} \quad (24)$$

where $R_{min} = \max[0, -I(\theta; \delta_e; ET_n)]$, and $R_{MMI} = \min[I(\theta; ET_n), I(\delta_e; ET_n)]$.

4.5 Results and discussion

4.5.1 Shape parameters of the relation between soil moisture and *ET*

The analytical model for the energy spectrum of soil moisture is applicable to observations at all 71 selected FLUXNET2015 sites. The frequency-level Nash Sutcliffe efficiency (NSE) between observed and modeled energy spectrum of soil moisture ranges between 0.38 and 0.98 and the median NSE is 0.82. The best fit α is on average greater at forested than non-forested sites (Figure 4.3a) and indicates that the relation between soil moisture and *ET* is more nonlinear, where soil water losses are close to potential even as soil moisture becomes limiting. The relation between soil moisture and *ET* is on average the most linear (α approaching 0) for woody savanna and closed shrubland sites and soil moisture controls on *ET* are on average stronger at non-forested sites. The aridity index, defined as the average annual ratio E_p/P is not correlated with α, indicating that α does not generally reflect the energy versus moisture limitations on the soil water balance and may be more related to site-specific vegetation behavior.

The analytical model for soil moisture probability distribution was consistent with 68 of the selected FLUXNET2015 sites and the model inversion approach did not converge for 3 sites. The quantile-level NSE between observed and modeled soil moisture probability distributions ranges between 0.13 and 0.99 and the median NSE is 0.95. The best fit γ is generally higher for grassland and evergreen needle leaf forest sites (Figure 4.3b) indicating that soil water losses are close to potential for the largest range of soil moisture states. The Spearman's correlation coefficient between γ and the aridity index is -0.59 (p-value<0.01) for non-forested sites, indicating that as conditions become more arid, soil moisture controls on *ET* increase and *ET* is more down regulated from stress. There is no significant relation between the aridity index and γ for forested sites indicating that the relation between soil moisture and *ET* may not be sensitive to climate aridity.

4.5.2 Soil and atmospheric moisture controls on *ET* inferred from information partitioning

Total multi-variate mutual information from θ and δ_e about ET_n, $I(\theta, \delta_e; ET_n)$ is statistically significant at 61 out of the 71 study sites and partitioning of total information reveals patterns between soil and atmospheric controls on *ET* with the aridity index (Figure 4.4). Sites for which $I(\theta,\delta_e;ET_n)$ is not

statistically significant include sites with limited periods of record (only 1 to 2 growing seasons for 8 of the 10 sites).

Less than half of the uncertainty in ET_n can be reduced by measurements of θ and δ_e. The median value of $I(\theta,\delta_e;ET_n)$ relative to $H(ET_n)$ is 0.3 for forested sites and 0.4 for non-forested sites. A relatively greater amount of uncertainty in ET_n can be attributed to δ_e compared to θ at forested sites, while δ_e and θ contributions are about equal at non-forested sites. The median value of U_θ and $U_{\delta e}$ relative to $I(\theta,\delta_e;ET_n)$ is 0.21 and 0.5 for forested sites, respectively and 0.33 and 0.34 for non-forested sites. The fraction of synergistic information relative to redundant information from θ and δ_e about ET_n is generally greater for forested sites than non-forested sites. The median value of S and R relative to $I(\theta,\delta_e;ET_n)$ is 0.23 and 0.09 for forested sites, respectively and 0.18 and 0.06 for non-forested sites. These results are consistent with our expectation that woody vegetation controls its stomatal as a result of stress from atmospheric moisture demand, while having access to soil moisture in a deeper rooting zone. In contrast, information from δ_e and θ are more redundant for herbaceous vegetation, which typically has access to soil moisture from a shallower rooting zone that is more consistent with the θ measurement depth.

Overall the information shared between from θ, δ_e, and ET_n increases with increasing aridity index. The Spearman's correlation coefficient between $I(\theta,\delta_e;ET_n)$, $I(\theta;ET_n)$, and $I(\delta_e;ET_n)$, and the aridity index at each site is 0.5, 0.69, and 0.4, respectively with p-value<0.01. These results are consistent with our expectation that soil and atmospheric moisture controls on *ET* are greatest in more arid climates. As the aridity index of a site increases U_θ increases, while $U_{\delta e}$ decreases and R increases while S decreases. The Spearman's correlation coefficient between U_θ, $U_{\delta e}$, S, and R, and the aridity index at each site is 0.47, -0.38, -0.41, and 0.62, respectively with p-value<0.01. These results are consistent with our expectation that vegetation stress is greater in more arid climates and controls on *ET* from θ and δ_e become more redundant, while in less arid climates soil moisture stress is lower and controls on *ET* may be more attributed to δ_e.

4.5.3 Vegetation controls on *ET* captured by soil moisture metrics

We compare shape parameters (α and γ) of the relation between soil moisture and *ET* and relate them to information partitioning metrics to identify controls on *ET* captured by each approach (Figure 4.5). We summarize forested and non-forests sites separately because aerodynamic roughness effects of canopy height is known to affect the ratio of actual to potential *ET* (Peng et al., 2019) and our focus is more on effects of vegetation conductance due to water stress.

The relation between α and γ is weak but reflects some consistency between the two approaches. The Spearman's correlation coefficient between α and γ is 0.26. The degree of non-linearity in the relation between soil moisture and *ET*, quantified by α is not sensitive to climate aridity. The more complex

shape of the relation between soil moisture and ET captured by γ reflects more diverse ecohydrological behavior. However, γ is inferred using a more complex multi-parameter calibration method and may be more affected by the range of soil moisture observations values and therefore the metric can be influenced by climate aridity.

At non-forested sites, the Spearman's correlation coefficient between γ and U_θ is -0.32. Unique information from θ about ET_n reflects the magnitude of soil moisture controls on ET. Greater U_θ reflects greater vegetation stress from soil moisture and results in a smaller γ or smaller range of soil moisture state at which vegetation transpires. At forested sites the Spearman's correlation coefficient between α and $U_{\delta e}$ is -046 and the Spearman's correlation coefficient between γ and S is -0.33. These results indicate that the shape of the relation between soil moisture and ET at forested sites may be more influenced by effects of stress from δ_e and θ together rather than θ alone. No other correlations between α and γ and information partitioning metrics are statistically significant. Our metrics α and γ capture plant water use strategies which are more controlled by moisture stress in the atmosphere at forested sites and soil moisture stress at non-forested sites.

4.6 Conclusions

This study develops and compares ecohydrological metrics to quantify the relation between soil moisture and ET based on theoretical equations for the variability of soil moisture. Detecting patterns from limited data is a major challenge in ecohydrology and we use information partitioning to untangle atmospheric versus soil moisture stress on ET at forested and non-forested sites. Proposed ecohydrological metrics describing the relation between soil moisture and evapotranspiration in different biomes can be used to diagnose the functional error of earth system models and is key to quantifying feedbacks between hydrology and climate.

4.7 Data

All datasets are available from public sources: hydrometeorological observations (http://fluxnet.fluxdata.org/data/fluxnet2015-dataset/); soil hydraulic parameters (https://doi.pangaea.de/10.1594/PANGAEA.870605).

4.8 Acknowledgements

This material is based upon work supported by the National Science Foundation Graduate Research Fellowship under Grant No. 1314109-DGE. This work used data acquired and shared by the FLUXNET community, including these networks: AmeriFlux, AfriFlux, AsiaFlux, CarboAfrica, CarboEuropeIP, CarboItaly, CarboMont, ChinaFlux, Fluxnet-Canada, GreenGrass, ICOS, KoFlux, LBA, NECC, OzFlux-TERN, TCOS-Siberia, and USCCC. The FLUXNET eddy covariance data processing and harmonization was carried out by the European Fluxes Database Cluster, AmeriFlux Management Project, and Fluxdata project of FLUXNET, with the support of CDIAC and ICOS Ecosystem Thematic Center and the OzFlux, ChinaFlux and AsiaFlux offices.

4.9 References

Anderegg, W. R. L., Trugman, A. T., Bowling, D. R., Salvucci, G., & Tuttle, S. E. (2019). Plant functional traits and climate influence drought intensification and land–atmosphere feedbacks. Proceedings of the National Academy of Sciences, 116(28), 14071–14076. https://doi.org/10.1073/pnas.1904747116

Barrett, A. B. (2015). Exploration of synergistic and redundant information sharing in static and dynamical Gaussian systems. Physical Review E, 91(5). https://doi.org/10.1103/PhysRevE.91.052802

Bassiouni, M., Higgins, C. W., Still, C. J., & Good, S. P. (2018). Probabilistic inference of ecohydrological parameters using observations from point to satellite scales. Hydrology and Earth System Sciences, 22(6), 3229–3243. https://doi.org/10.5194/hess-22-3229-2018

Clapp, R. B., & Hornberger, G. M. (1978). Empirical equations for some soil hydraulic properties. Water Resources Research, 14(4), 601–604.

Cover, T. M., & Thomas, J. A. (2012). Elements of information theory. John Wiley & Sons.

Fisher, J. B., Melton, F., Middleton, E., Hain, C., Anderson, M., Allen, R., et al. (2017). The future of evapotranspiration: Global requirements for ecosystem functioning, carbon and climate feedbacks, agricultural management, and water resources: THE FUTURE OF EVAPOTRANSPIRATION. Water Resources Research, 53(4), 2618–2626. https://doi.org/10.1002/2016WR020175

Goodwell, A. E., & Kumar, P. (2017a). Temporal information partitioning: Characterizing synergy, uniqueness, and redundancy in interacting environmental variables: SYNERGY, UNIQUENESS, AND REDUNDANCY. Water Resources Research, 53(7), 5920–5942. https://doi.org/10.1002/2016WR020216

Goodwell, A. E., & Kumar, P. (2017b). Temporal Information Partitioning Networks (TIPNets): A process network approach to infer ecohydrologic shifts: INFORMATION PARTITIONING NETWORKS. Water Resources Research, 53(7), 5899–5919. https://doi.org/10.1002/2016WR020218

Katul, G. G., Porporato, A., Daly, E., Oishi, A. C., Kim, H.-S., Stoy, P. C., et al. (2007). On the spectrum of soil moisture from hourly to interannual scales: SPECTRUM OF SOIL MOISTURE CONTENT. Water Resources Research, 43(5). https://doi.org/10.1029/2006WR005356

Katul, G. G., Oren, R., Manzoni, S., Higgins, C., & Parlange, M. B. (2012). Evapotranspiration: A process driving mass transport and energy exchange in the soil-plant-atmosphere-climate system: EVAPOTRANSPIRATION AND CLIMATE. Reviews of Geophysics, 50(3). https://doi.org/10.1029/2011RG000366

Laio, F., Porporato, A., Ridolfi, L., & Rodriguez-Iturbe, I. (2001). Plants in water-controlled ecosystems: active role in hydrologic processes and response to water stress: II. Probabilistic soil moisture dynamics. Advances in Water Resources, 24(7), 707–723.

Montzka, C., Herbst, M., Weihermüller, L., Verhoef, A., & Vereecken, H. (2017). A global data set of soil hydraulic properties and sub-grid variability of soil water retention and hydraulic conductivity curves. Earth System Science Data, 9(2), 529–543.

Novick, K. A., Ficklin, D. L., Stoy, P. C., Williams, C. A., Bohrer, G., Oishi, A. C., et al. (2016). The increasing importance of atmospheric demand for ecosystem water and carbon fluxes. Nature Climate Change, 6(11), 1023–1027. https://doi.org/10.1038/nclimate3114

Peng, L., Zeng, Z., Wei, Z., Chen, A., Wood, E. F., & Sheffield, J. (2019). Determinants of the ratio of actual to potential evapotranspiration. Global Change Biology, 25(4), 1326–1343. https://doi.org/10.1111/gcb.14577

Porporato, A., Laio, F., Ridol, L., & Rodriguez-Iturbe, I. (2001). Plants in water-controlled ecosystems: active role in hydrologic processes and response to water stress III. Vegetation water stress. Advances in Water Resources, 20.

Priestley, C. H. B., & Taylor, R. J. (1972). On the Assessment of Surface Heat Flux and Evaporation Using Large-Scale Parameters. Monthly Weather Review, 100(2), 81–92. https://doi.org/10.1175/1520-0493(1972)100<0081:OTAOSH>2.3.CO;2

Purdy, A. J., Fisher, J. B., Goulden, M. L., Colliander, A., Halverson, G., Tu, K., & Famiglietti, J. S. (2018). SMAP soil moisture improves global evapotranspiration. Remote Sensing of Environment, 219, 1–14. https://doi.org/10.1016/j.rse.2018.09.023

Reichstein, M., Falge, E., Baldocchi, D., Papale, D., Aubinet, M., Berbigier, P., et al. (2005). On the separation of net ecosystem exchange into assimilation and ecosystem respiration: review and improved algorithm. Global Change Biology, 11(9), 1424–1439. https://doi.org/10.1111/j.1365-2486.2005.001002.x

Rodriguez-Iturbe, I. (2000). Ecohydrology: A hydrologic perspective of climate-soil-vegetation dynamies. Water Resources Research, 36(1), 3–9. https://doi.org/10.1029/1999WR900210

Ruddell, B. L., & Kumar, P. (2009). Ecohydrologic process networks: 1. Identification: ECOHYDROLOGIC PROCESS NETWORKS, 1. Water Resources Research, 45(3). https://doi.org/10.1029/2008WR007279

Shannon, C. E. (1948). A mathematical theory of communication. Bell System Technical Journal, 27(3), 379–423.

Williams, P. L., & Beer, R. D. (2010). Nonnegative Decomposition of Multivariate Information. ArXiv:1004.2515 [Math-Ph, Physics:Physics, q-Bio]. Retrieved from http://arxiv.org/abs/1004.2515

4.10 Figures

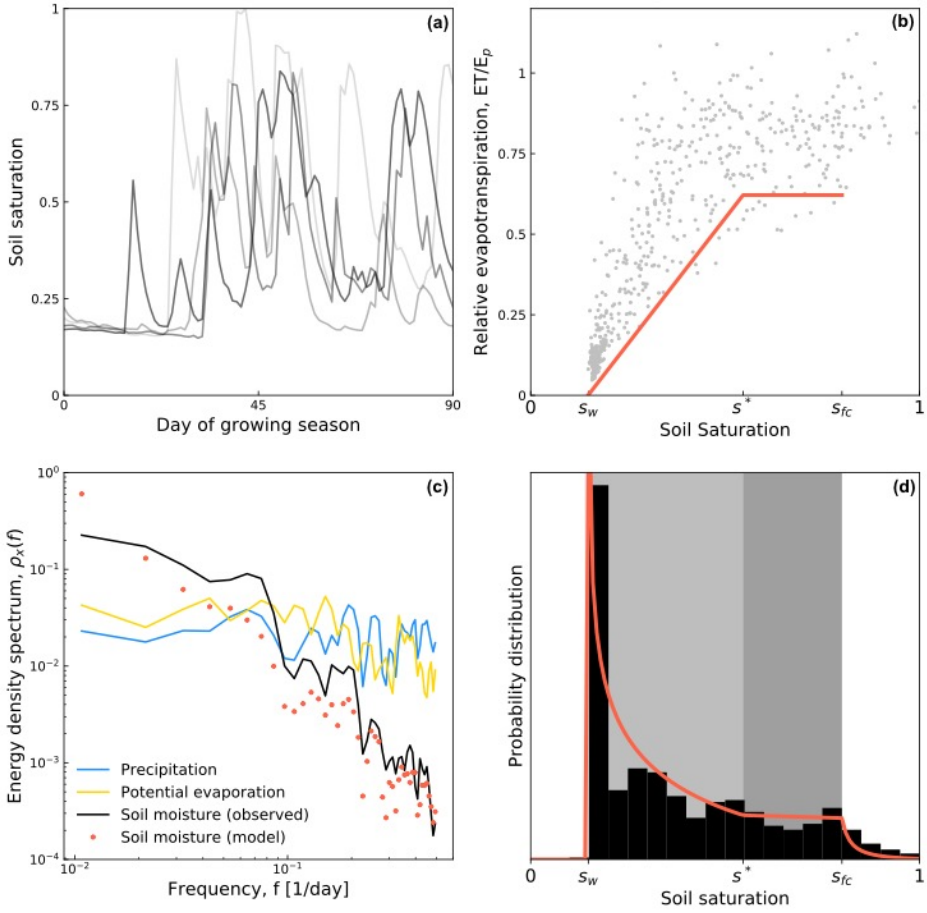

Figure 4.1 Ecohydrological dynamics of the semi-desert Santa Rita experimental range grassland site (US-SRG) (a) Timeseries of growing season soil saturation. (b) Observed (grey markers) and theoretical (red line) relation between relative evapotranspiration and soil saturation. The theoretical relation is inferred from the probability distribution of soil moisture. (c) Energy density power spectrum of precipitation, potential evaporation, and observed and modelled soil moisture. (d) Observed (black histogram) and theoretical (red line) probability distribution of soil saturation.

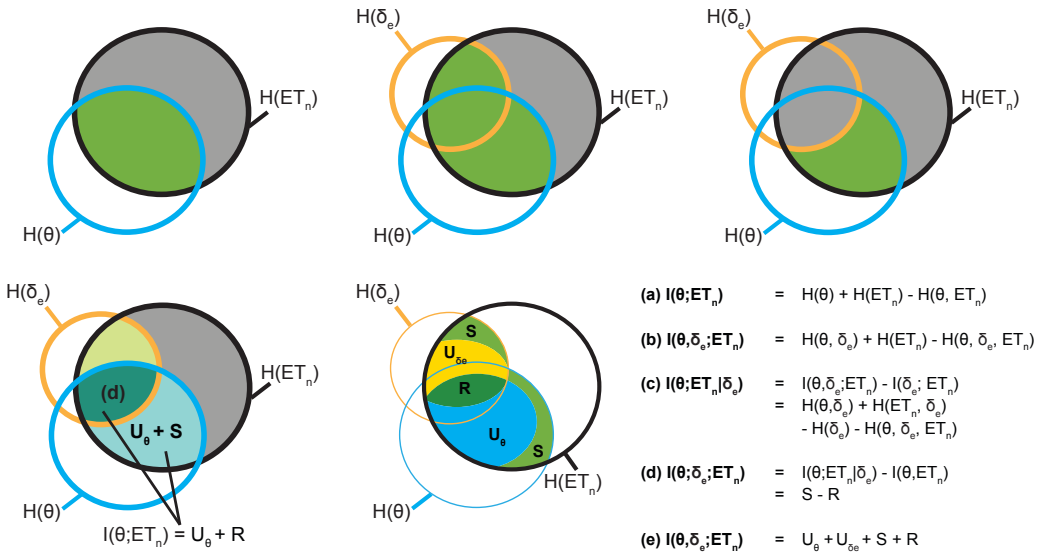

Figure 4.2 Visual derivation of information theory metrics (a) $I(\theta;ET_n)$ mutual information; (b) $I(\theta,\delta_e;ET_n)$ total multi-variate mutual information; (c) $I(\theta;ET_n|\delta_e)$ conditional mutual information; (d) $I(\theta;\delta_e;ET_n)$ interaction information; (e) total information partitioning.

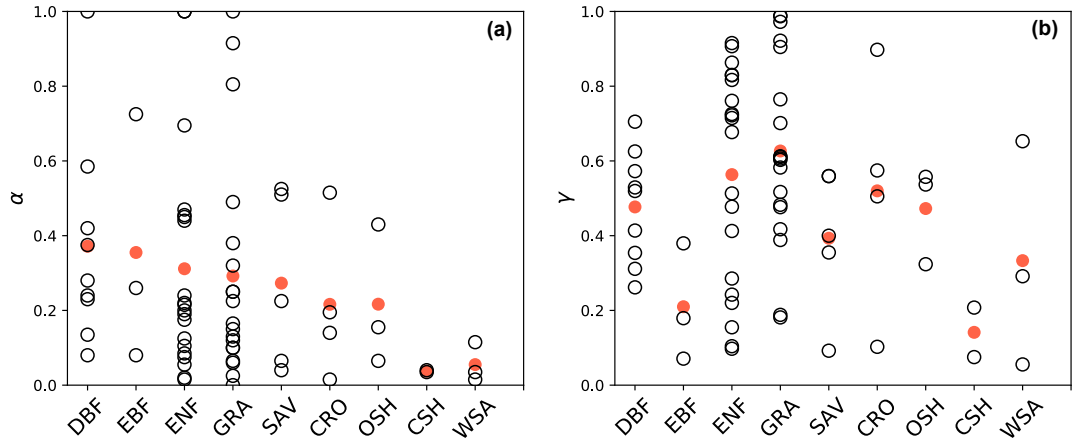

Figure 4.3 Shape parameters of the relation between soil moisture and evapotranspiration based on (a) the energy density spectrum (b) The probability distribution of soil moisture at a range of biomes. (CRO, cropland; GRA, grassland; SAV, savanna; WSA, woody savanna; OSH, open shrubland; CSH, closed shrubland; MF, mixed forest; DBF, deciduous broadleaf forest; EBF, evergreen broadleaf forest; ENF, evergreen needleleaf forest)

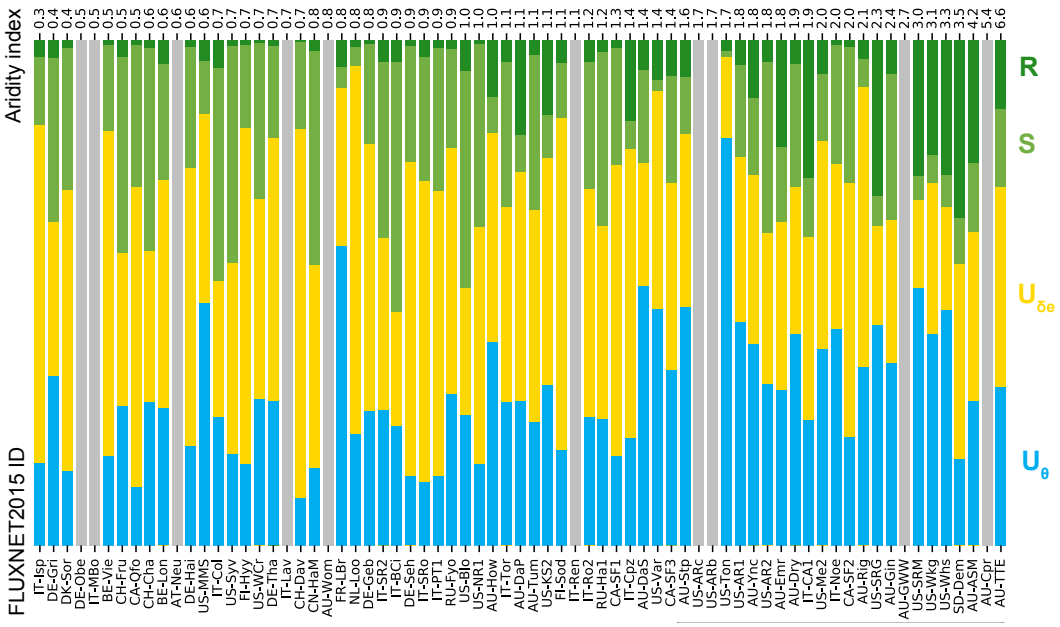

Figure 4.4 Partitioning of total multi-variate mutual information from soil moisture and vapor pressure deficit about relative evapotranspiration ($I(\theta,\delta_e;ET_n)$) at 71 FLUXNET2015 sites ordered left to right from least arid to most arid. Information is partitioned into unique information from soil moisture (U_θ), unique information from vapor pressure deficit ($U_{\delta e}$), synergistic information (S) and redundant information (R). Sites with non-significant total information are masked in grey.

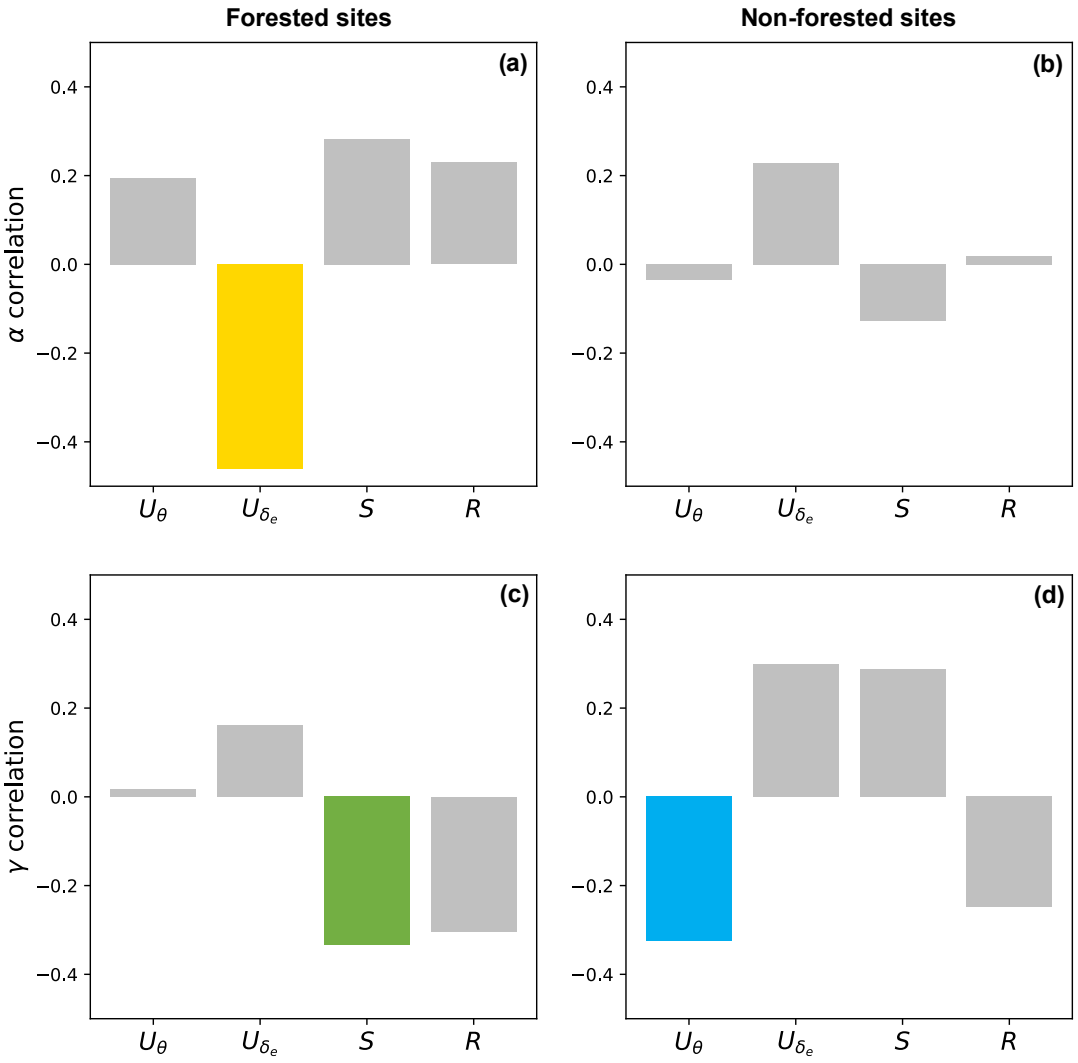

Figure 4.5 Correlation between information partitioning and shape parameters of the relation between soil moisture and evapotranspiration based on (a-b) the energy spectrum and (c-d) the probability distribution of soil moisture. Bar plots represent the spearman's correlation coefficient and are colored only if p-value<0.1.

Table 4.S1 Selected FLUXNET21015 sites

Site ID	Biome	Latitude	Longitude	Data years	Citation
AT-Neu	GRA	47.117	11.318	2004, 2006, 2007, 2008, 2010, 2012	Georg Wohlfahrt, Albin Hammerle, Lukas Hörtnagl, Alois Haslwanter (2002-2012) FLUXNET2015 AT-Neu Neustift, 10.18140/FLX/1440121
AU-ASM	ENF	-22.283	133.249	2011, 2012, 2013	James Cleverly, Derek Eamus (2010-2014) FLUXNET2015 AU-ASM Alice Springs, 10.18140/FLX/1440194
AU-Cpr	SAV	-34.002	140.589	2012, 2013	Wayne Meyer, Peter Cale, Georgia Koerber, Cacilia Ewenz, Qiaoqi Sun (2010-2014) FLUXNET2015 AU-Cpr Calperum, 10.18140/FLX/1440195
AU-DaP	GRA	-14.063	131.318	2009, 2010, 2012, 2013	Jason Beringer, Lindsay Hutley (2007-2013) FLUXNET2015 AU-DaP Daly River Savanna, 10.18140/FLX/1440123
AU-DaS	SAV	-14.159	131.388	2011, 2012, 2013	Jason Beringer, Prof. Lindsay Hutley (2008-2014) FLUXNET2015 AU-DaS Daly River Cleared, 10.18140/FLX/1440122
AU-Dry	SAV	-15.259	132.371	2012, 2013	Jason Beringer, Lindsay Hutley (2008-2014) FLUXNET2015 AU-Dry Dry River, 10.18140/FLX/1440197
AU-Emr	GRA	-23.859	148.475	2012, 2013	Ivan Schroder, Steve Zegelin, Tehani Palu, Andrew Feitz (2011-2013) FLUXNET2015 AU-Emr Emerald, 10.18140/FLX/1440198
AU-Gin	WSA	-31.376	115.714	2011, 2012	Craig Macfarlane, Patricia Lambert, John Byrne, Chris Johnstone, Natalie Smart (2011-2014) FLUXNET2015 AU-Gin Gingin, 10.18140/FLX/1440199
AU-GWW	SAV	-30.191	120.654	2013, 2014	Craig Macfarlane, Suzanne Prober, Georg Wiehl (2013-2014) FLUXNET2015 AU-GWW Great Western Woodlands, Western Australia, Australia, 10.18140/FLX/1440200
AU-How	WSA	-12.494	131.152	2009, 2010, 2011, 2012	Jason Beringer, Lindsay Hutley (2001-2014) FLUXNET2015 AU-How Howard Springs, 10.18140/FLX/1440125
AU-Rig	GRA	-36.650	145.576	2012, 2013, 2014	Jason Beringer, Jason Beringer, Shaun Cunningham, Patrick Baker, Timothy Cavagnaro, Ralph MacNally, Ross Thompson, Ian McHugh (2011-2014) FLUXNET2015 AU-Rig Riggs Creek, 10.18140/FLX/1440202
AU-Stp	GRA	-17.151	133.350	2010, 2012, 2013	Jason Beringer, Lindsay Hutley (2008-2014) FLUXNET2015 AU-Stp Sturt Plains, 10.18140/FLX/1440204
AU-TTE	OSH	-22.287	133.640	2012, 2013	James Cleverly, Derek Eamus (2012-2014) FLUXNET2015 AU-TTE Ti Tree East, 10.18140/FLX/1440205
AU-Tum	EBF	-35.657	148.152	2003, 2004, 2008, 2009, 2010, 2013, 2014	William Woodgate, Eva van Gorsel, Ray Leuning (2001-2014) FLUXNET2015 AU-Tum Tumbarumba, 10.18140/FLX/1440126
AU-Wom	EBF	-37.422	144.094	2011, 2012	Stefan Arndt, Nina Hinko-Najera, Anne Griebel (2010-2014) FLUXNET2015 AU-Wom Wombat, 10.18140/FLX/1440207
AU-Ync	GRA	-34.989	146.291	2013, 2014	Jason Beringer, Jeffery Walker (2012-2014) FLUXNET2015 AU-Ync Jaxa, 10.18140/FLX/1440208
BE-Lon	CRO	50.552	4.746	2012, 2014	Anne De Ligne, Tanguy Manise, Christine Moureaux, Marc Aubinet, Bernard Heinesch

Site ID	Biome	Latitude	Longitude	Data years	Citation
BE-Lon	CRO	50.552	4.746	2004, 2005, 2006, 2007, 2008, 2009, 2010, 2011, 2012, 2013, 2014	(2004-2014) FLUXNET2015 BE-Lon Lonzee, 10.18140/FLX/1440129
BE-Vie	MF	50.305	5.998	2000, 2011, 2014	Anne De Ligne, Tanguy Manise, Bernard Heinesch, Marc Aubinet, Caroline Vincke (1996-2014) FLUXNET2015 BE-Vie Vielsalm, 10.18140/FLX/1440130
CA-Qfo	ENF	49.693	-74.342	2009, 2006, 2007	Hank A. Margolis (2003-2010) FLUXNET2015 CA-Qfo Quebec - Eastern Boreal, Mature Black Spruce, 10.18140/FLX/1440045
CA-SF1	ENF	54.485	-105.818	2005, 2006	Brian Amiro (2003-2006) FLUXNET2015 CA-SF1 Saskatchewan - Western Boreal, forest burned in 1977, 10.18140/FLX/1440046
CA-SF2	ENF	54.254	-105.878	2002, 2003, 2004	Brian Amiro (2001-2005) FLUXNET2015 CA-SF2 Saskatchewan - Western Boreal, forest burned in 1989, 10.18140/FLX/1440047
CA-SF3	OSH	54.092	-106.005	2001, 2004	Brian Amiro (2001-2006) FLUXNET2015 CA-SF3 Saskatchewan - Western Boreal, forest burned in 1998, 10.18140/FLX/1440048
CH-Cha	GRA	47.210	8.410	2007, 2008, 2011, 2012, 2013, 2014	Kathrin Fuchs, Lutz Merbold, Nina Buchmann, Werner Eugster, Matthias Zeeman, Lukas Hörtnagl (2005-2014) FLUXNET2015 CH-Cha Chamau, 10.18140/FLX/1440131
CH-Dav	ENF	46.815	9.856	2007, 2008, 2009, 2010, 2011, 2012, 2013	Lukas Hörtnagl, Werner Eugster, Lutz Merbold, Nina Buchmann, Sophia Etzold, Rudolf Haesler, Matthias Haeni (1997-2014) FLUXNET2015 CH-Dav Davos, 10.18140/FLX/1440132
CH-Fru	GRA	47.116	8.538	2006, 2007, 2008, 2010, 2011, 2012, 2013, 2014	Kathrin Fuchs, Lutz Merbold, Nina Buchmann, Werner Eugster, Matthias Zeeman, Lukas Hörtnagl (2005-2014) FLUXNET2015 CH-Fru Früebüel , 10.18140/FLX/1440133
CN-HaM	GRA	37.370	101.180	2002, 2003	Yanhong Tang, Tomomichi Kato, Mingyuan Du (2002-2004) FLUXNET2015 CN-HaM Haibei Alpine Tibet site, 10.18140/FLX/1440190
DE-Geb	CRO	51.100	10.914	2001, 2002, 2004, 2005, 2006, 2007, 2009, 2010, 2011, 2012, 2013, 2014	Christian Brümmer, Antje M. Lucas-Moffat, Mathias Herbst, Olaf Kolle (2001-2014) FLUXNET2015 DE-Geb Gebesee, 10.18140/FLX/1440146
DE-Gri	GRA	50.950	13.513	2009, 2010, 2011, 2013	Christian Bernhofer, Thomas Grünwald, Uta Moderow, Markus Hehn, Uwe Eichelmann, Heiko Prasse (2004-2014) FLUXNET2015 DE-Gri Grillenburg, 10.18140/FLX/1440147
DE-Hai	DBF	51.079	10.453	2000, 2001, 2002, 2004, 2005, 2006, 2007, 2008, 2009	Alexander Knohl, Frank Tiedemann, Olaf Kolle, Ernst-Detlef Schulze, Werner Kutsch, Mathias Herbst, Lukas Siebicke (2000-2012) FLUXNET2015 DE-Hai Hainich, 10.18140/FLX/1440148
DE-Obe	ENF	50.784	13.720	2011, 2013	Christian Bernhofer, Thomas Grünwald, Uta Moderow, Markus Hehn, Uwe Eichelmann, Heiko Prasse (2008-

Site ID	Biome	Latitude	Longitude	Data years	Citation
DE-Obe	ENF	50.787	13.721	2008, 2014	2014) FLUXNET2015 DE-Obe Oberbärenburg, 10.18140/FLX/1440151
DE-Seh	CRO	50.871	6.450	2008, 2007	Karl Schneider, Marius Schmidt (2007-2010) FLUXNET2015 DE-Seh Selhausen, 10.18140/FLX/1440217
DE-Tha	ENF	50.964	13.567	2003, 2006, 2007, 2008, 2009, 2011, 2012, 2013	Christian Bernhofer, Thomas Grünwald, Uta Moderow, Markus Hehn, Uwe Eichelmann, Heiko Prasse (1996-2014) FLUXNET2015 DE-Tha Tharandt, 10.18140/FLX/1440152
DK-Sor	DBF	55.486	11.645	2001, 2003, 2004, 2014, 2006	Andreas Ibrom, Kim Pilegaard (1996-2014) FLUXNET2015 DK-Sor Soroe, 10.18140/FLX/1440155
FI-Hyy	ENF	61.848	24.295	2003, 2005, 2006, 2007, 2008, 2010, 2011, 2012, 2013	Ivan Mammarella, Petri Keronen, Pasi Kolari, Samuli Launiainen, Jukka Pumpanen, Üllar Rannik, Erkki Siivola, Janne Levula, Toivo Pohja, Timo Vesala (1996-2014) FLUXNET2015 FI-Hyy Hyytiala, 10.18140/FLX/1440158
FI-Sod	ENF	67.362	26.638	2008	Mika Aurela, Juha-Pekka Tuovinen, Juha Hatakka, Annalea Lohila, Timo Mäkelä, Juuso Rainne, Tuomas Lauria (2001-2014) FLUXNET2015 FI-Sod Sodankyla, 10.18140/FLX/1440160
FR-LBr	ENF	44.717	-0.769	2005, 2007	Paul Berbigier, Denis Loustau (1996-2008) FLUXNET2015 FR-LBr Le Bray, 10.18140/FLX/1440163
IT-BCi	CRO	40.524	14.957	2008	Vincenzo Magliulo, Paul Di Tommasi, Daniela Famulari, Daniele Gasbarra, Luca Vitale, Antonio Manco (2004-2014) FLUXNET2015 IT-BCi Borgo Cioffi, 10.18140/FLX/1440166
IT-CA1	DBF	42.380	12.027	2012	Simone Sabbatini, Nicola Arriga, Dario Papale (2011-2014) FLUXNET2015 IT-CA1 Castel d'Asso1, 10.18140/FLX/1440230
IT-Col	DBF	41.849	13.588	2012, 2013	Giorgio Matteucci (1996-2014) FLUXNET2015 IT-Col Collelongo, 10.18140/FLX/1440167
IT-Cpz	EBF	41.705	12.376	2005, 2007	Riccardo Valentini, Sabina Dore, Francesco Mazzenga, Simone Sabbatini, Paolo Stefani, Giampiero Tirone, Dario Papale (1997-2009) FLUXNET2015 IT-Cpz Castelporziano, 10.18140/FLX/1440168
IT-Isp	DBF	45.813	8.634	2013, 2014	Carsten Gruening, Ignacio Goded, Alessandro Cescatti, Olga Pokorska (2013-2014) FLUXNET2015 IT-Isp Ispra ABC-IS, 10.18140/FLX/1440234
IT-Lav	ENF	45.956	11.281	2008, 2014	Damiano Gianelle, Roberto Zampedri, Mauro Cavagna, Matteo Sottocornola (2003-2014) FLUXNET2015 IT-Lav Lavarone, 10.18140/FLX/1440169
IT-MBo	GRA	46.015	11.046	2005, 2006, 2007	Damiano Gianelle, Mauro Cavagna, Roberto Zampedri, Barbara Marcolla (2003-2013) FLUXNET2015 IT-MBo Monte Bondone, 10.18140/FLX/1440170
IT-Noe	CSH	40.606	8.152	2004, 2005, 2014	Donatella Spano, Pierpaolo Duce, Serena Marras, Costantino Sirca, Angelo Arca, Pierpaolo Zara, Andrea Ventura (2004-2014) FLUXNET2015 IT-Noe Arca di Noe - Le Prigionette, 10.18140/FLX/1440171

Site ID	Biome	Latitude	Longitude	Data years	Citation
IT-PT1	DBF	45.201	9.061	2002, 2004	Alessandro Cescatti (2002-2004) FLUXNET2015 IT-PT1 Parco Ticino forest, 10.18140/FLX/1440172
IT-Ren	ENF	46.587	11.434	2011	(1998-2013) FLUXNET2015 IT-Ren Renon, Dario Papale, Nicola Arriga, Luca Belelli, Claudia Consalvo, Sabina Dore, Giovanni Manca, Francesco Mazzenga, Simone Sabbatini, Paolo Stefani, Giampiero Tirone, Riccardo Valentini (2002-2012) FLUXNET2015 IT-Ro2 Roccarespampani 2, 10.18140/FLX/1440175
IT-Ro2	DBF	42.390	11.921	2002, 2010, 2006, 2007	
IT-SR2	ENF	43.732	10.291	2013, 2014	Carsten Gruening, Ignacio Goded, Alessandro Cescatti, Olga Pokorska (2013-2014) FLUXNET2015 IT-SR2 San Rossore 2, 10.18140/FLX/1440236
IT-SRo	ENF	43.728	10.284	2003, 2007	Carsten Gruening, Ignacio Goded, Alessandro Cescatti, Giovanni Manca, Guenther Seufert (1999-2012) FLUXNET2015 IT-SRo San Rossore, 10.18140/FLX/1440176
IT-Tor	GRA	45.844	7.578	2011, 2012	Edoardo Cremonese, Marta Galvagno, Umberto Morra di Cella, Mirco Migliavacca (2008-2014) FLUXNET2015 IT-Tor Torgnon, 10.18140/FLX/1440237
NL-Loo	ENF	52.167	5.744	2003, 2004, 2005, 2006, 2007, 2009, 2010, 2012	Eddy Moors, Jan Elbers (1996-2014) FLUXNET2015 NL-Loo Loobos, 10.18140/FLX/1440178
RU-Fyo	ENF	56.462	32.922	2009, 2012	Andrej Varlagin, Julia Kurbatova, Natalia Vygodskaya (1998-2014) FLUXNET2015 RU-Fyo Fyodorovskoye, 10.18140/FLX/1440183
RU-Ha1	GRA	54.725	90.002	2003, 2004	Luca Belelli, Dario Papale, Riccardo Valentini (2002-2004) FLUXNET2015 RU-Ha1 Hakasia steppe, 10.18140/FLX/1440184
SD-Dem	SAV	13.283	30.478	2009	Jonas Ardö, Bashir Awad El Tahir, Hatim Abdalla M. ElKhidir (2005-2009) FLUXNET2015 SD-Dem Demokeya, 10.18140/FLX/1440186
US-AR1	GRA	36.427	-99.420	2009, 2010, 2011	Dave Billesbach, James Bradford, Margaret Torn (2009-2012) FLUXNET2015 US-AR1 ARM USDA UNL OSU Woodward Switchgrass 1, 10.18140/FLX/1440103
US-AR2	GRA	36.636	-99.598	2010, 2011	Dave Billesbach, James Bradford, Margaret Torn (2009-2012) FLUXNET2015 US-AR2 ARM USDA UNL OSU Woodward Switchgrass 2, 10.18140/FLX/1440104
US-ARb	GRA	35.550	-98.040	2006	Margaret Torn (2005-2006) FLUXNET2015 US-ARb ARM Southern Great Plains burn site- Lamont, 10.18140/FLX/1440064
US-ARc	GRA	35.547	-98.040	2005, 2006	Margaret Torn (2005-2006) FLUXNET2015 US-ARc ARM Southern Great Plains control site- Lamont, 10.18140/FLX/1440065
US-Blo	ENF	38.895	-120.633	2000	Allen Goldstein (1997-2007) FLUXNET2015 US-Blo Blodgett Forest, 10.18140/FLX/1440068
US-KS2	CSH	28.609	-80.672	2004, 2005, 2006	Bert Drake, Ross Hinkle (2003-2006) FLUXNET2015 US-KS2 Kennedy

Site ID	Biome	Latitude	Longitude	Data years	Citation
					Space Center (scrub oak), 10.18140/FLX/1440075
US-Me2	ENF	44.452	-121.557	2002, 2003, 2004, 2005, 2006, 2010, 2011, 2012, 2013	Bev Law (2002-2014) FLUXNET2015 US-Me2 Metolius mature ponderosa pine, 10.18140/FLX/1440079
US-MMS	DBF	39.323	-86.413	2005, 2007, 2008, 2012, 2013, 2014	Kim Novick, Rich Phillips (1999-2014) FLUXNET2015 US-MMS Morgan Monroe State Forest, 10.18140/FLX/1440083
US-NR1	ENF	40.033	-105.546	2003, 2005, 2006, 2007, 2008, 2010, 2011, 2012, 2013, 2014	Andrew A. Turnipseed, David R. Bowling, Peter D. Blanken, Russel K. Monson, Sean P. Burns (1998-2014) FLUXNET2015 US-NR1 Niwot Ridge Forest (LTER NWT1), 10.18140/FLX/1440087
US-SRG	GRA	31.789	-110.828	2008, 2009, 2011, 2012, 2013, 2014	Russell Scott (2008-2014) FLUXNET2015 US-SRG Santa Rita Grassland, 10.18140/FLX/1440114
US-SRM	WSA	31.821	-110.866	2004, 2005, 2007, 2008, 2009, 2010, 2011, 2012, 2014	Russell Scott (2004-2014) FLUXNET2015 US-SRM Santa Rita Mesquite, 10.18140/FLX/1440090
US-Syv	MF	46.242	-89.348	2002, 2003, 2006	Ankur Desai (2001-2014) FLUXNET2015 US-Syv Sylvania Wilderness Area, 10.18140/FLX/1440091
US-Ton	WSA	38.432	-120.966	2003, 2005, 2006, 2009, 2010, 2011, 2013	Dennis Baldocchi (2001-2014) FLUXNET2015 US-Ton Tonzi Ranch, 10.18140/FLX/1440092
US-Var	GRA	38.413	-120.951	2001, 2013, 2005, 2009	Dennis Baldocchi (2000-2014) FLUXNET2015 US-Var Vaira Ranch-Ione, 10.18140/FLX/1440094
US-WCr	DBF	45.806	-90.080	2000, 2001, 2005, 2006, 2011, 2012, 2013, 2014	Ankur Desai (1999-2014) FLUXNET2015 US-WCr Willow Creek, 10.18140/FLX/1440095
US-Whs	OSH	31.744	-110.052	2009, 2010, 2011, 2013, 2014	Russ Scott (2007-2014) FLUXNET2015 US-Whs Walnut Gulch Lucky Hills Shrub, 10.18140/FLX/1440097
US-Wkg	GRA	31.737	-109.942	2004, 2005, 2006, 2007, 2008, 2009, 2010, 2011, 2012, 2013, 2014	Russell Scott (2004-2014) FLUXNET2015 US-Wkg Walnut Gulch Kendall Grasslands, 10.18140/FLX/1440096

CRO, cropland; GRA, grassland; OSH, open shrubland; CSH, closed shrubland; SAV, savanna; WSA, woody savanna; MF, mixed forest; DBF, deciduous broad leaf forest; EBF, evergreen broadleaf forest, ENF, evergreen need leaf forest.

5 General Conclusions

Calibrating ecohydrological parameters is increasingly challenging as models become more structurally complex to match our understanding of earth system processes (Pitman, 2003). Satellites are now comparable to “flux towers in the sky” (Schimel et al., 2019) and provide opportunities to confront global hydrological observations to commonly used equations and parameterize them at the grid scale to reflect more realistic ecohydrological interactions. This dissertation developed methods to extract information encoded in soil moisture observations and estimate ecohydrological parameters that describe plant water use strategies. While it seems obvious that the variability of soil moisture reflects vegetation water use and patterns that were inferred in this study are not surprising, this work is important because it provides a framework that is simple enough to apply to satellite data and quantify ecosystem-scale variables that cannot be measured directly. Results are consistent with observed hydrological patterns and using different statistical approaches, but they are not exempt from problems of equifinality. Results have yet to be put to test in a more complex numerical model and evaluate if they can contribute to getting “the right answers for the rights reasons” (Kirchner, 2006).

6 Bibliography

Anderegg, W. R. L., Klein, T., Bartlett, M., Sack, L., Pellegrini, A. F. A., Choat, B., & Jansen, S. (2016). Meta-analysis reveals that hydraulic traits explain cross-species patterns of drought-induced tree mortality across the globe. Proceedings of the National Academy of Sciences, 113(18), 5024–5029. https://doi.org/10.1073/pnas.1525678113

Anderegg, W. R. L., Wolf, A., Arango-Velez, A., Choat, B., Chmura, D. J., Jansen, S., et al. (2017). Plant water potential improves prediction of empirical stomatal models. PLOS ONE, 12(10), e0185481. https://doi.org/10.1371/journal.pone.0185481

Anderegg, W. R. L., Trugman, A. T., Bowling, D. R., Salvucci, G., & Tuttle, S. E. (2019). Plant functional traits and climate influence drought intensification and land–atmosphere feedbacks. Proceedings of the National Academy of Sciences, 116(28), 14071–14076. https://doi.org/10.1073/pnas.1904747116

Arsenault, K. R., Nearing, G. S., Wang, S., Yatheendradas, S., & Peters-Lidard, C. D. (2018). Parameter Sensitivity of the Noah-MP Land Surface Model with Dynamic Vegetation. Journal of Hydrometeorology, 19(5), 815–830. https://doi.org/10.1175/jhm-d-17-0205.1

Baldocchi, D., Falge, E., Gu, L., Olson, R., Hollinger, D., Running, S., et al. (2001). FLUXNET: A new tool to study the temporal and spatial variability of ecosystem–scale carbon dioxide, water vapor, and energy flux densities. Bulletin of the American Meteorological Society, 82(11), 2415–2434.

Baldwin, D., Manfreda, S., Keller, K., & Smithwick, E. A. H. (2017). Predicting root zone soil moisture with soil properties and satellite near-surface moisture data across the conterminous United States. Journal of Hydrology, 546, 393–404. https://doi.org/10.1016/j.jhydrol.2017.01.020

Barrett, A. B. (2015). Exploration of synergistic and redundant information sharing in static and dynamical Gaussian systems. Physical Review E, 91(5). https://doi.org/10.1103/PhysRevE.91.052802

Bassiouni, M., Higgins, C. W., Still, C. J., & Good, S. P. (2018). Probabilistic inference of ecohydrological parameters using observations from point to satellite scales. Hydrology and Earth System Sciences, 22(6), 3229–3243. https://doi.org/10.5194/hess-22-3229-2018

Brooks, R., & Corey, T. (1964). HYDRAU uc Properties Of Porous Media. Hydrology Papers, Colorado State University.

Caylor, K. K., D'Odorico, P., & Rodriguez-Iturbe, I. (2006). On the ecohydrology of structurally heterogeneous semiarid landscapes. Water Resources Research, 42(7). https://doi.org/10.1029/2005WR004683

Chen, X., Rubin, Y., Ma, S., & Baldocchi, D. (2008). Observations and stochastic modeling of soil moisture control on evapotranspiration in a Californian oak savanna: SOIL MOISTURE CONTROL ON ET. Water Resources Research, 44(8). https://doi.org/10.1029/2007WR006646

Clapp, R. B., & Hornberger, G. M. (1978). Empirical equations for some soil hydraulic properties. Water Resources Research, 14(4), 601–604.

Cover, T. M., & Thomas, J. A. (2012). Elements of information theory. John Wiley & Sons.

Dorigo, W. A., Gruber, A., De Jeu, R. A. M., Wagner, W., Stacke, T., Loew, A., et al. (2015). Evaluation of the ESA CCI soil moisture product using ground-based observations. Remote Sensing of Environment, 162, 380–395. https://doi.org/10.1016/j.rse.2014.07.023

Dralle, D. N., & Thompson, S. E. (2016). A minimal probabilistic model for soil moisture in seasonally dry climates. Water Resources Research, 52(2), 1507–1517.

Dralle, D. N., Karst, N. J., & Thompson, S. E. (2016). Dry season streamflow persistence in seasonal climates. Water Resources Research, 52(1), 90–107. https://doi.org/10.1002/2015WR017752

Engelbrecht, B. M. J., Comita, L. S., Condit, R., Kursar, T. A., Tyree, M. T., Turner, B. L., & Hubbell, S. P. (2007). Drought sensitivity shapes species distribution patterns in tropical forests. Nature, 447(7140), 80–82. https://doi.org/10.1038/nature05747

Entekhabi, D., Njoku, E. G., O'Neill, P. E., Kellogg, K. H., Crow, W. T., Edelstein, W. N., et al. (2010). The Soil Moisture Active Passive (SMAP) Mission. Proceedings of the IEEE, 98(5), 704–716. https://doi.org/10.1109/JPROC.2010.2043918

Fatichi, S., Pappas, C., & Ivanov, V. Y. (2016). Modeling plant-water interactions: an ecohydrological overview from the cell to the global scale: Modeling plant-water interactions. Wiley Interdisciplinary Reviews: Water, 3(3), 327–368. https://doi.org/10.1002/wat2.1125

Feldman, A. F., Short Gianotti, D. J., Konings, A. G., McColl, K. A., Akbar, R., Salvucci, G. D., & Entekhabi, D. (2018). Moisture pulse-reserve in the soil-plant continuum observed across biomes. Nature Plants, 4(12), 1026–1033. https://doi.org/10.1038/s41477-018-0304-9

Feng, X., Dawson, T. E., Ackerly, D. D., Santiago, L. S., & Thompson, S. E. (2017). Reconciling seasonal hydraulic risk and plant water use through probabilistic soil-plant dynamics. Global Change Biology, 23(9), 3758–3769. https://doi.org/10.1111/gcb.13640

Fisher, J. B., Melton, F., Middleton, E., Hain, C., Anderson, M., Allen, R., et al. (2017). The future of evapotranspiration: Global requirements for ecosystem functioning, carbon and climate feedbacks, agricultural management, and water resources: THE FUTURE OF EVAPOTRANSPIRATION. Water Resources Research, 53(4), 2618–2626. https://doi.org/10.1002/2016WR020175

Friedlingstein, P., Meinshausen, M., Arora, V. K., Jones, C. D., Anav, A., Liddicoat, S. K., & Knutti, R. (2014). Uncertainties in CMIP5 Climate Projections due to Carbon Cycle Feedbacks. Journal of Climate, 27(2), 511–526. https://doi.org/10.1175/JCLI-D-12-00579.1

Fu, X., & Meinzer, F. C. (2019). Metrics and proxies for stringency of regulation of plant water status (iso/anisohydry): a global data set reveals coordination and trade-offs among water transport traits. Tree Physiology, 39(1), 122–134. https://doi.org/10.1093/treephys/tpy087

Gelman, A., & Rubin, D. B. (1992). Inference from iterative simulation using multiple sequences. Statistical Science, 457–472.

Good, S. P., Soderberg, K., Guan, K., King, E. G., Scanlon, T. M., & Caylor, K. K. (2014). δ 2 H isotopic flux partitioning of evapotranspiration over a grass field following a water pulse and subsequent dry down. Water Resources Research, 50(2), 1410–1432. https://doi.org/10.1002/2013WR014333

Good, S. P., Noone, D., & Bowen, G. (2015). Hydrologic connectivity constrains partitioning of global terrestrial water fluxes. Science, 349(6244), 175–177.

Good, S. P., Moore, G. W., & Miralles, D. G. (2017). A mesic maximum in biological water use demarcates biome sensitivity to aridity shifts. Nature Ecology & Evolution, 1(12), 1883.

Goodwell, A. E., & Kumar, P. (2017a). Temporal information partitioning: Characterizing synergy, uniqueness, and redundancy in interacting environmental variables: SYNERGY, UNIQUENESS, AND REDUNDANCY. Water Resources Research, 53(7), 5920–5942. https://doi.org/10.1002/2016WR020216

Goodwell, A. E., & Kumar, P. (2017b). Temporal Information Partitioning Networks (TIPNets): A process network approach to infer ecohydrologic shifts: INFORMATION PARTITIONING NETWORKS. Water Resources Research, 53(7), 5899–5919. https://doi.org/10.1002/2016WR020218

Hastings, W. K. (1970). Monte Carlo Sampling Methods Using Markov Chains and Their Applications. Biometrika, 57(1), 97. https://doi.org/10.2307/2334940

Hlavinka, P., Trnka, M., Balek, J., Semerádová, D., Hayes, M., Svoboda, M., et al. (2011). Development and evaluation of the SoilClim model for water balance and soil climate estimates. Agricultural Water Management, 98(8), 1249–1261. https://doi.org/10.1016/j.agwat.2011.03.011

Holdo, R. M., & Nippert, J. B. (2015). Transpiration dynamics support resource partitioning in African savanna trees and grasses. Ecology, 96(6), 1466–1472. https://doi.org/10.1890/14-1986.1

Huffman, G. J., Bolvin, D. T., Nelkin, E. J., Wolff, D. B., Adler, R. F., Gu, G., et al. (2007). The TRMM Multisatellite Precipitation Analysis (TMPA): Quasi-Global, Multiyear, Combined-Sensor Precipitation Estimates at Fine Scales. Journal of Hydrometeorology, 8(1), 38–55. https://doi.org/10.1175/JHM560.1

Jarvis, P. G., & Mcnaughton, K. G. (1986). Stornatal Control of Transpiration: Scaling Up from Leaf' to Region, 49.

Katul, G. G., Porporato, A., Daly, E., Oishi, A. C., Kim, H.-S., Stoy, P. C., et al. (2007). On the spectrum of soil moisture from hourly to interannual scales: SPECTRUM OF SOIL MOISTURE CONTENT. Water Resources Research, 43(5). https://doi.org/10.1029/2006WR005356

Katul, G. G., Oren, R., Manzoni, S., Higgins, C., & Parlange, M. B. (2012). Evapotranspiration: A process driving mass transport and energy exchange in the soil-plant-atmosphere-climate system: EVAPOTRANSPIRATION AND CLIMATE. Reviews of Geophysics, 50(3). https://doi.org/10.1029/2011RG000366

Kim, S. (2013). Ancillary Data Report: Landcover Classification. Pasadena, CA: Jet Propulsion.

King, E. G., & Caylor, K. K. (2011). Ecohydrology in practice: strengths, conveniences, and opportunities. Ecohydrology, 4(4), 608–612. https://doi.org/10.1002/eco.248

Kirchner, J. W. (2006). Getting the right answers for the right reasons: Linking measurements, analyses, and models to advance the science of hydrology. Water Resources Research, 42(3).

Köhli, M., Schrön, M., Zreda, M., Schmidt, U., Dietrich, P., & Zacharias, S. (2015). Footprint characteristics revised for field-scale soil moisture monitoring with cosmic-ray neutrons. Water Resources Research, 51(7), 5772–5790. https://doi.org/10.1002/2015WR017169

Konings, A. G., & Gentine, P. (2017). Global variations in ecosystem-scale isohydricity. Global Change Biology, 23(2), 891–905. https://doi.org/10.1111/gcb.13389

Laio, F., Porporato, A., Ridolfi, L., & Rodriguez-Iturbe, I. (2001). Plants in water-controlled ecosystems: active role in hydrologic processes and response to water stress: II. Probabilistic soil moisture dynamics. Advances in Water Resources, 24(7), 707–723.

Laio, F., Porporato, A., Fernandez-Illescas, C. P., & Rodriguez-Iturbe, I. (2001). Plants in water-controlled ecosystems: active role in hydrologic processes and response to water stress: IV. Discussion of real cases. Advances in Water Resources, 24(7), 745–762.

Laio, F., D'Odorico, P., & Ridolfi, L. (2006). An analytical model to relate the vertical root distribution to climate and soil properties: VERTICAL ROOT DISTRIBUTION. Geophysical Research Letters, 33(18), n/a-n/a. https://doi.org/10.1029/2006GL027331

Li, X., Blackman, C. J., Choat, B., Duursma, R. A., Rymer, P. D., Medlyn, B. E., & Tissue, D. T. (2018). Tree hydraulic traits are coordinated and strongly linked to climate-of-origin across a rainfall gradient: Hydraulic traits coordination and link to climate. Plant, Cell & Environment, 41(3), 646–660. https://doi.org/10.1111/pce.13129

Li, Y., Guan, K., Gentine, P., Konings, A. G., Meinzer, F. C., Kimball, J. S., et al. (2017). Estimating global ecosystem iso/anisohydry using active and passive microwave satellite data: Estimate global ecosystem iso/anisohydry. Journal of Geophysical Research: Biogeosciences. https://doi.org/10.1002/2017JG003958

Liu, Y. Y., Parinussa, R. M., Dorigo, W. A., De Jeu, R. A. M., Wagner, W., van Dijk, A. I. J. M., et al. (2011). Developing an improved soil moisture dataset by blending passive and active microwave

satellite-based retrievals. Hydrology and Earth System Sciences, 15(2), 425–436. https://doi.org/10.5194/hess-15-425-2011

Liu, Y. Y., Dorigo, W. A., Parinussa, R. M., de Jeu, R. A. M., Wagner, W., McCabe, M. F., et al. (2012). Trend-preserving blending of passive and active microwave soil moisture retrievals. Remote Sensing of Environment, 123, 280–297. https://doi.org/10.1016/j.rse.2012.03.014

Manfreda, S., Caylor, K. K., & Good, S. P. (2017). An ecohydrological framework to explain shifts in vegetation organization across climatological gradients: Vegetation pattern in dry environments. Ecohydrology, 10(3), e1809. https://doi.org/10.1002/eco.1809

Manzoni, S., Vico, G., Katul, G., Palmroth, S., & Porporato, A. (2014). Optimal plant water-use strategies under stochastic rainfall. Water Resources Research, 50(7), 5379–5394. https://doi.org/10.1002/2014WR015375

Massoud, E. C., Purdy, A. J., Christoffersen, B. O., Santiago, L. S., & Xu, C. (2019). Bayesian inference of hydraulic properties in and around a white fir using a process-based ecohydrologic model. Environmental Modelling & Software, 115, 76–85. https://doi.org/10.1016/j.envsoft.2019.01.022

McColl, K. A., Wang, W., Peng, B., Akbar, R., Short Gianotti, D. J., Lu, H., et al. (2017). Global characterization of surface soil moisture drydowns: Geophysical Research Letters, 44(8), 3682–3690. https://doi.org/10.1002/2017GL072819

Metropolis, N., Rosenbluth, A. W., Rosenbluth, M. N., Teller, A. H., & Teller, E. (1953). Equation of State Calculations by Fast Computing Machines. The Journal of Chemical Physics, 21(6), 1087–1092. https://doi.org/10.1063/1.1699114

Miller, G. R., Baldocchi, D. D., Law, B. E., & Meyers, T. (2007). An analysis of soil moisture dynamics using multi-year data from a network of micrometeorological observation sites. Advances in Water Resources, 30(5), 1065–1081. https://doi.org/10.1016/j.advwatres.2006.10.002

Montzka, C., Herbst, M., Weihermüller, L., Verhoef, A., & Vereecken, H. (2017). A global data set of soil hydraulic properties and sub-grid variability of soil water retention and hydraulic conductivity curves. Earth System Science Data, 9(2), 529–543.

Müller, M. F., Dralle, D. N., & Thompson, S. E. (2014). Analytical model for flow duration curves in seasonally dry climates. Water Resources Research, 50(7), 5510–5531.

Niu, G.-Y., Yang, Z.-L., Mitchell, K. E., Chen, F., Ek, M. B., Barlage, M., et al. (2011). The community Noah land surface model with multiparameterization options (Noah-MP): 1. Model description and evaluation with local-scale measurements. Journal of Geophysical Research, 116(D12). https://doi.org/10.1029/2010JD015139

Novick, K. A., Ficklin, D. L., Stoy, P. C., Williams, C. A., Bohrer, G., Oishi, A. C., et al. (2016). The increasing importance of atmospheric demand for ecosystem water and carbon fluxes. Nature Climate Change, 6(11), 1023–1027. https://doi.org/10.1038/nclimate3114

Oleson, K. W., Lawrence, D. M., Bonan, G. B., Drewniak, B., Huang, M., Levis, S., et al. (2013). Technical Description of version 4.5 of the Community Land Model (CLM), 434.

O'Neill, P. E., Chan, S. K., Njoku, E. G., Jackson, T., & Bindlish, R. (2016). SMAP L3 Radiometer Global Daily 36 km EASE-Grid Soil Moisture, Version 4, Boulder, Colorado USA, NASA National Snow and Ice Data Center Distributed Active Archive Center.

Oren, R., Sperry, J. S., Katul, G. G., Pataki, D. E., Ewers, B. E., Phillips, N., & Schäfer, K. V. R. (1999). Survey and synthesis of intra- and interspecific variation in stomatal sensitivity to vapour pressure deficit: Intra- and interspecific variation in stomatal sensitivity to vapour pressure deficit. Plant, Cell & Environment, 22(12), 1515–1526. https://doi.org/10.1046/j.1365-3040.1999.00513.x

Pappas, C., Fatichi, S., & Burlando, P. (2016). Modeling terrestrial carbon and water dynamics across climatic gradients: does plant trait diversity matter? New Phytologist, 209(1), 137–151. https://doi.org/10.1111/nph.13590

Peng, L., Zeng, Z., Wei, Z., Chen, A., Wood, E. F., & Sheffield, J. (2019). Determinants of the ratio of actual to potential evapotranspiration. Global Change Biology, 25(4), 1326–1343. https://doi.org/10.1111/gcb.14577

Pitman, A. J. (2003). The evolution of, and revolution in, land surface schemes designed for climate models. International Journal of Climatology, 23(5), 479–510. https://doi.org/10.1002/joc.893

Porporato, A, Laio, F., Ridol, L., & Rodriguez-Iturbe, I. (2001). Plants in water-controlled ecosystems: active role in hydrologic processes and response to water stress III. Vegetation water stress. Advances in Water Resources, 20.

Porporato, A, Daly, E., & Rodriguez-Iturbe, I. (2004). Soil water balance and ecosystem response to climate change. The American Naturalist, 164(5), 625–632.

Powell, T. L., Galbraith, D. R., Christoffersen, B. O., Harper, A., Imbuzeiro, H. M. A., Rowland, L., et al. (2013). Confronting model predictions of carbon fluxes with measurements of Amazon forests subjected to experimental drought. New Phytologist, 200(2), 350–365. https://doi.org/10.1111/nph.12390

Priestley, C. H. B., & Taylor, R. J. (1972). On the Assessment of Surface Heat Flux and Evaporation Using Large-Scale Parameters. Monthly Weather Review, 100(2), 81–92. https://doi.org/10.1175/1520-0493(1972)100<0081:OTAOSH>2.3.CO;2

Purdy, A. J., Fisher, J. B., Goulden, M. L., Colliander, A., Halverson, G., Tu, K., & Famiglietti, J. S. (2018). SMAP soil moisture improves global evapotranspiration. Remote Sensing of Environment, 219, 1–14. https://doi.org/10.1016/j.rse.2018.09.023

Qiu, B., Xue, Y., Fisher, J. B., Guo, W., Berry, J. A., & Zhang, Y. (2018). Satellite Chlorophyll Fluorescence and Soil Moisture Observations Lead to Advances in the Predictive Understanding of Global Terrestrial Coupled Carbon-Water Cycles. Global Biogeochemical Cycles, 32(3), 360–375. https://doi.org/10.1002/2017GB005744

Rawls, W. J., Brakensiek, D. L., & Saxtonn, K. E. (1982). Estimation of soil water properties. Transactions of the ASAE, 25(5), 1316–1320.

Reichle, R. H., De Lannoy, G. J., Liu, Q., Ardizzone, J. V., Colliander, A., Conaty, A., et al. (2017). Assessment of the SMAP level-4 surface and root-zone soil moisture product using in situ measurements. Journal of Hydrometeorology, 18(10), 2621–2645.

Reichstein, M., Falge, E., Baldocchi, D., Papale, D., Aubinet, M., Berbigier, P., et al. (2005). On the separation of net ecosystem exchange into assimilation and ecosystem respiration: review and improved algorithm. Global Change Biology, 11(9), 1424–1439. https://doi.org/10.1111/j.1365-2486.2005.001002.x

Richards, L. A., & Weaver, L. R. (1944). Moisture retention by some irrigated soils as related to soil moisture tension. Journal of Agricultural Research, 69(6), 215–235.

Roberts, G. O., & Rosenthal, J. S. (n.d.). Optimal Scaling for Various Metropolis–Hastings Algorithms.

Rodriguez-Iturbe, I. (2000). Ecohydrology: A hydrologic perspective of climate-soil-vegetation dynamics. Water Resources Research, 36(1), 3–9. https://doi.org/10.1029/1999WR900210

Rodríguez-Iturbe, I., & Porporato, A. (2007). Ecohydrology of water-controlled ecosystems: soil moisture and plant dynamics. Cambridge University Press.

Rodriguez-Iturbe, I., Gupta, V. K., & Waymire, E. (1984). Scale considerations in the modeling of temporal rainfall. Water Resources Research, 20(11), 1611–1619. https://doi.org/10.1029/WR020i011p01611

Rodriguez-Iturbe, I., Porporato, A., Ridolfi, L., Isham, V., & Coxi, D. R. (1999). Probabilistic modelling of water balance at a point: the role of climate, soil and vegetation. In Proceedings of the Royal Society of London A: Mathematical, Physical and Engineering Sciences (Vol. 455, pp. 3789–3805). The Royal Society.

Rodriguez-Iturbe, I., Porporato, A., Laio, F., & Ridolfi, L. (2001). Intensive or extensive use of soil moisture: plant strategies to cope with stochastic water availability. Geophysical Research Letters, 28(23), 4495–4497.

Ruddell, B. L., & Kumar, P. (2009). Ecohydrologic process networks: 1. Identification: ECOHYDROLOGIC PROCESS NETWORKS, 1. Water Resources Research, 45(3). https://doi.org/10.1029/2008WR007279

Saleem, J. A., & Salvucci, G. D. (2002). Comparison of soil wetness indices for inducing functional similarity of hydrologic response across sites in Illinois. Journal of Hydrometeorology, 3(1), 80–91.

Salvucci, G. D. (2001). Estimating the moisture dependence of root zone water loss using conditionally averaged precipitation. Water Resources Research, 37(5), 1357–1365.

Schimel, D., Schneider, F., JPL Carbon and Ecosystem Participants, Bloom, A., Bowman, K., Cawse-Nicholson, K., et al. (2019). Flux towers in the sky: global ecology from space. New Phytologist. https://doi.org/10.1111/nph.15934

Shannon, C. E. (1948). A mathematical theory of communication. Bell System Technical Journal, 27(3), 379–423.

Skelton, R. P., West, A. G., & Dawson, T. E. (2015). Predicting plant vulnerability to drought in biodiverse regions using functional traits. Proceedings of the National Academy of Sciences, 112(18), 5744–5749. https://doi.org/10.1073/pnas.1503376112

Steduto, P., Hsiao, T. C., Raes, D., & Fereres, E. (2009). AquaCrop—The FAO Crop Model to Simulate Yield Response to Water: I. Concepts and Underlying Principles. Agronomy Journal, 101(3), 426. https://doi.org/10.2134/agronj2008.0139s

Still, C. J., Berry, J. A., Collatz, G. J., & DeFries, R. S. (2003). Global distribution of C3 and C4 vegetation: carbon cycle implications. Global Biogeochemical Cycles, 17(1), 6-1-6–14.

Sultan, S. E. (2000). Phenotypic plasticity for plant development, function and life history. Trends in Plant Science, 5(12), 537–542. https://doi.org/10.1016/S1360-1385(00)01797-0

Suweis, S., Rinaldo, A., Van der Zee, S. E. A. T. M., Daly, E., Maritan, A., & Porporato, A. (2010). Stochastic modeling of soil salinity. Geophysical Research Letters, 37(7), n/a-n/a. https://doi.org/10.1029/2010GL042495

Teuling, A. J., Seneviratne, S. I., Williams, C., & Troch, P. A. (2006). Observed timescales of evapotranspiration response to soil moisture. Geophysical Research Letters, 33(23). https://doi.org/10.1029/2006GL028178

Theil, H. (1992). A Rank-Invariant Method of Linear and Polynomial Regression Analysis. In B. Raj & J. Koerts (Eds.), Henri Theil's Contributions to Economics and Econometrics (Vol. 23, pp. 345–381). Dordrecht: Springer Netherlands. https://doi.org/10.1007/978-94-011-2546-8_20

Thompson, S., Levin, S., & Rodriguez-Iturbe, I. (2013). Linking Plant Disease Risk and Precipitation Drivers: A Dynamical Systems Framework. The American Naturalist, 181(1), E1–E16. https://doi.org/10.1086/668572

Troch, P. A., Martinez, G. F., Pauwels, V. R. N., Durcik, M., Sivapalan, M., Harman, C., et al. (2009). Climate and vegetation water use efficiency at catchment scales. Hydrological Processes, 23(16), 2409–2414. https://doi.org/10.1002/hyp.7358

Trugman, A. T., Medvigy, D., Mankin, J. S., & Anderegg, W. R. L. (2018). Soil Moisture Stress as a Major Driver of Carbon Cycle Uncertainty. Geophysical Research Letters, 45(13), 6495–6503. https://doi.org/10.1029/2018GL078131

Tuttle, S. E., & Salvucci, G. D. (2014). A new approach for validating satellite estimates of soil moisture using large-scale precipitation: Comparing AMSR-E products. Remote Sensing of Environment, 142, 207–222. https://doi.org/10.1016/j.rse.2013.12.002

Volo, T. J., Vivoni, E. R., Martin, C. A., Earl, S., & Ruddell, B. L. (2014). Modelling soil moisture, water partitioning, and plant water stress under irrigated conditions in desert urban areas. Ecohydrology, n/a-n/a. https://doi.org/10.1002/eco.1457

Wagner, W., Dorigo, W., de Jeu, R., Fernandez, D., Benveniste, J., Haas, E., & Ertl, M. (2012). Fusion of active and passive microwave observations to create an essential climate variable data record on soil moisture. ISPRS Annals of the Photogrammetry, Remote Sensing and Spatial Information Sciences (ISPRS Annals), 7, 315–321.

Wang, T., Franz, T. E., Yue, W., Szilagyi, J., Zlotnik, V. A., You, J., et al. (2016). Feasibility analysis of using inverse modeling for estimating natural groundwater recharge from a large-scale soil moisture monitoring network. Journal of Hydrology, 533, 250–265. https://doi.org/10.1016/j.jhydrol.2015.12.019

Westenbroek. (2018). SWB Version 2.0—A Soil-Water-Balance Code for Estimating Net Infiltration and Other Water-Budget Components (Techniques and Methods).

Whitney, K. M., Vivoni, E. R., Duniway, M. C., Bradford, J. B., Reed, S. C., & Belnap, J. (2017). Ecohydrological role of biological soil crusts across a gradient in levels of development. Ecohydrology, 10(7), e1875. https://doi.org/10.1002/eco.1875

Williams, P. L., & Beer, R. D. (2010). Nonnegative Decomposition of Multivariate Information. ArXiv:1004.2515 [Math-Ph, Physics:Physics, q-Bio]. Retrieved from http://arxiv.org/abs/1004.2515

Xu, C., McDowell, N. G., Sevanto, S., & Fisher, R. A. (2013). Our limited ability to predict vegetation dynamics under water stress. New Phytologist, 200(2), 298–300. https://doi.org/10.1111/nph.12450

Xu, T., White, L., Hui, D., & Luo, Y. (2006). Probabilistic inversion of a terrestrial ecosystem model: Analysis of uncertainty in parameter estimation and model prediction. Global Biogeochemical Cycles, 20(2), n/a-n/a. https://doi.org/10.1029/2005GB002468